Aus dem Pathologischen Institut der Ludwig-Maximilians-Universität München
Direktor: Prof. Dr. med. Thomas Kirchner
Arbeitsgruppe Experimentelle und Molekulare Pathologie
Leiter: Prof. Dr. rer. nat. Heiko Hermeking

Genetic analysis of *Mir34a* in mouse models of colorectal cancer

Dissertation zum Erwerb des Doktorgrades der
Naturwissenschaften (Dr. rer. nat.) an der Medizinischen Fakultät der
Ludwig-Maximilians-Universität München

vorgelegt von
Meryem Gülfem Öner-Ziegler
aus Balıkesir, Türkei
2018

Gedruckt mit der Genehmigung der Medizinischen Fakultät
der Ludwig-Maximilians-Universität München

Betreuer: Prof. Dr. rer. nat. Heiko Hermeking

Zweitgutachterin: Priv. Doz. Dr. Anna Friedl

Dekan: Prof. Dr. med. dent. Reinhard Hickel

Tag der mündlichen Prüfung: 26.03.2019

Science is the most reliable guide for civilization,
for life, for success in the world.
M. Kemal Atatürk

To my family

Eidesstattliche Versicherung

Meryem Gülfem Öner-Ziegler

Ich erkläre hiermit an Eides statt, dass ich die vorliegende Dissertation mit dem Thema “Genetic analysis of *Mir34a* in mouse models of colorectal cancer” selbständig verfasst, mich außer der angegebenen keiner weiteren Hilfsmittel bedient und alle Erkenntnisse, die aus dem Schrifttum ganz oder annähernd übernommen sind, als solche kenntlich gemacht und nach ihrer Herkunft unter Bezeichnung der Fundstelle einzeln nachgewiesen habe.
Ich erkläre des Weiteren, dass die hier vorgelegte Dissertation nicht in gleicher oder in ähnlicher Form bei einer anderen Stelle zur Erlangung eines akademischen Grades eingereicht wurde.

Ort, Datum: München, 26/03/2019 Unterschrift: Meryem Gülfem Öner-Ziegler

Publications

The results of this thesis have been published in the following articles:

Original articles:

* Equal contribution

Öner MG, Rokavec M, Kaller M, Bouznad N, Horst D, Kirchner T and Hermeking H: Combined Inactivation of TP53 and MIR34A Promotes Colorectal Cancer Development and Progression via Increasing Levels of IL6R and PAI1. **Gastroenterology**. 2018 Aug 9.

pii: S0016-5085(18)34868-6. doi: 10.1053/j.gastro.2018.08.011.

Rokavec M*, **Öner MG***, Li H*, Jackstadt R*, Jiang L, Lodygin D, Kaller M, Horst D, Ziegler PK, Schwitalla S, Slotta-Huspenina J, Bader FG, Greten FR, Hermeking H. IL-6R/STAT3/miR-34a feedback loop promotes EMT-mediated colorectal cancer invasion and metastasis. **Journal of Clinical Investigations**. 2014 Apr; 124(4):1853-67. doi: 10.1172/JCI73531.

Reviews:

Rokavec M, **Öner MG**, Hermeking H. lnflammation-induced epigenetic switches in cancer. **Cellular and Molecular Life Sciences**. 2016 Jan; 73(1):23-39.

In addition, I contributed to following articles, which are not further described here:

Ziegler PK, Bollrath J, Pallangyo CK, Matsutani T, Canli Ö, De Oliveira T, Diamanti MA, Müller N, Gamrekelashvili J, Putoczki T, Horst D, Mankan AK, **Öner MG**, Müller S, Müller-Höcker J, Kirchner T, Slotta-Huspenina J, Taketo MM, Reinheckel T, Dröse S, Larner AC, Wels WS, Ernst M, Greten TF, Arkan MC, Korn T, Wirth D, Greten FR. Mitophagy in Intestinal Epithelial Cells Triggers Adaptive Immunity during Tumorigenesis. **Cell**. 2018 Jun 28;174(1):88-101.e16. doi: 10.1016/j.cell.2018.05.028.

Cheng CY, Hwang CI, Corney DC, Flesken-Nikitin A, Jiang L, **Öner GM**, Munroe RJ, Schimenti JC, Hermeking H, and Nikitin AY. MiR-34 Cooperates with p53 in Suppression of Prostate Cancer by Joint Regulation of Stem Cell Compartment. **Cell Reports**. 2014 Mar 27;6(6):1000-1007. doi: 10.1016/j.celrep.2014.02.023.

Table of Contents

Abbreviations

Abbreviation	Description
ABC	Avidin-biotin complex
AKT	AKT serine/threonine kinase 1
AOM	Azoxymethane
APC	Adenomatous polyposis coli
APS	Ammonium peroxodisulfate
BRAF	B-Raf proto-oncogene, serine/threonine kinase
BrdU	Bromodeoxyuridine
CAC	Colitis-associated cancer
COAD	Colon adenocarcinoma
CpG	Cytosine phosphate guanidine
CRC	Colorectal cancer
Cy3	Cyanine 3
DAB	3,3-diaminobenzidine
DAPI	4',6-diamidino-2-phenylindole
DC	Dendritic cell
DEPC	Diethyl pyrocarbonate
DMEM	Dulbecco's modified eagle medium
DMSO	Dimethyl sulfoxide
DNA	Deoxyribonucleic acid
dNTP	Deoxynucleotide triphosphate
DSS	Dextran sulphate sodium
E.coli	*Escherichia coli*
ECL	Electrochemiluminescence
ECM	Extracellular matrix
EDTA	Ethylenediaminetetraacetic acid
EMT	Epithelial–mesenchymal transition
FBS	Fetal bovine serum
FISH	Fluorescence *in situ* hybridization
FITC	Fluorescein
FL	Floxed
GSEA	Gene Set Enrichment Analysis
H&E	Haematoxylin & eosin
i.p.	Intra-peritoneal
IBD	Inflammatory bowel disease
IEC	Intestinal epithelial cell
IHC	Immunohistochemistry
IL-	Interleukin
IVC	Individually ventilated cages
KRAS	KRAS proto-oncogene and GTPase
LOH	Loss of heterozygosity

Abbreviation	Description
miRNA	Micro RNA
MMP	Matrix metalloprotease
mRNA	Messenger RNA
NGS	Next-generation sequencing
NF-κB	Nuclear factor kappa B
ORF	Open reading frame
PAI-1	Serpin family E member 1
PBS	Phosphate buffered saline
PCR	Polymerase chain reaction
PFA	Paraformaldehyde
PIK3CA	Phosphatidylinositol-4,5-bisphosphate 3-kinase catalytic subunit alpha
READ	Rectal adenocarcinoma
RNA	Ribonucleic acid
SDS	Sodium dodecyl sulfate
SEM	Standard error of the mean
SMAD4	SMAD family member 4
STAT	Signal transducer and activator of transcription
TAM	Tumor associated macrophages
TBST	Tris-buffered saline with 0.1% Tween 20
TCGA	The Cancer Genome Atlas
TEMED	Tetramethylethylenediamine
TF	Transcription factor
TGFβ	Transforming growth factor beta
Th	T helper
TLR	Toll-like receptor
TP53	Tumor protein p53
Treg	T regulatory cells
UTR	Untranslated region
WB	Western blotting
Wnt	Mouse homolog of wingless

1 Introduction

1.1 Cancer

Cancer is a major health problem worldwide. It is the second leading cause of death globally and 8.8 million people died from cancer in 2015 (http://www.who.int/features/factfiles/cancer/en/). Ten leading cancer types for the estimated deaths in the United States are shown in Figure 1 (Siegel et al., 2018), notably in both genders lung cancer is most common cancer type, which leads to death.

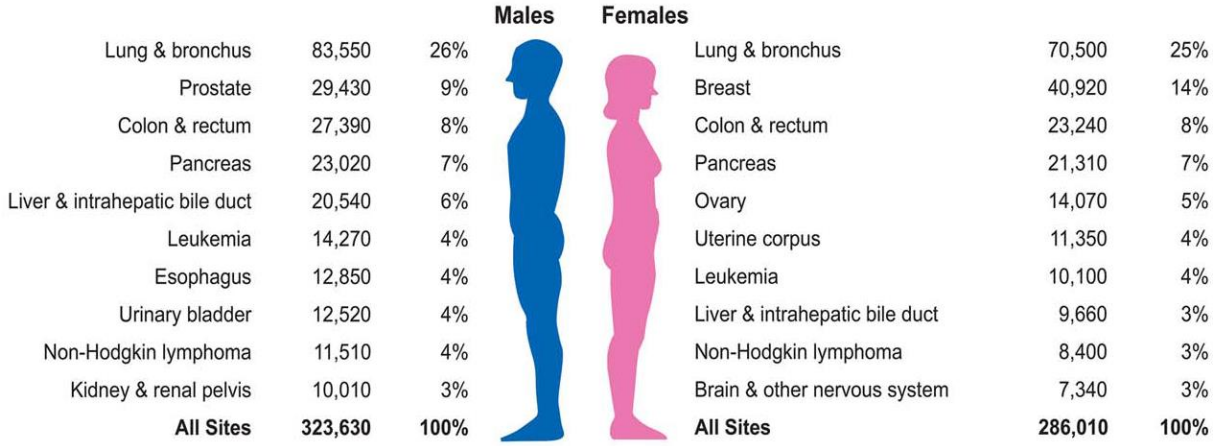

Figure 1. Estimated deaths caused by ten leading cancer types in the United States. Estimates are rounded to the nearest 10 and cases exclude basal cell and squamous cell skin cancers and *in situ* carcinoma except urinary bladder. Figure and legend are taken from (Siegel et al., 2018).

Cancer is a complex disease that involves dynamic changes in the genome. There are more than 200 different tumor entities that reflect differences in cell of origin, acquired somatic mutations, wide range of altered transcriptional networks and influences of local tissue microenvironments (Lambert et al., 2017). Hanahan and Weinberg grouped different biological capabilities that are acquired during multistep development of human tumors into ten “hallmarks of cancer” as shown in Figure 2 (Hanahan and Weinberg, 2011). These hallmarks include sustaining proliferative signaling, evading growth suppressors, resisting cell death, enabling replicative immortality, inducing angiogenesis, activating invasion and metastasis, reprogramming of energy metabolism, avoiding immune destruction, genomic instability and tumor microenvironment.

Figure 2. The hallmarks of cancer.
Ten fundamental features acquired during tumor development. The figure is taken from (Hanahan and Weinberg, 2011).

1.2 Colorectal cancer

Colorectal cancer (CRC) is one of the major health concerns and the 4TH leading cause of cancer-related deaths worldwide (McGuire, 2016). Also in United States it is the 3rd leading cause of cancer-related deaths (Siegel et al., 2018). It is estimated that 140,250 patients will be diagnosed with CRC and that 50,630 patients will die from the disease by 2018 in the US (Siegel et al., 2018).

CRC is a multistep process (Figure 3) and histologically it begins with early changes from normal to hyperproliferative epithelium followed by the development of adenomas, which are thought to be precursors of carcinomas (Cherry, 2011). These histological changes are driven by the genetic or epigenetic inactivation of tumor suppressor genes and activation of oncogenes (Fearon and Vogelstein, 1990). In most cases, colorectal tumorigenesis begins with stabilization of the key transcription factor β-catenin by loss of *APC* or more rarely, by activating mutations in the *CTNNB* gene (Morin et al., 1997). This results in constitutive activation of the Wnt-pathway (Ashton-Rickardt et al., 1989), the major signaling pathway in self-renewal of the intestinal stem-cell compartment. Additional mutations, such as *KRAS,* lead to early

adenomas, whereas *TP53* inactivation in late stages has been associated with invasive carcinomas and metastasis formation (Fearon and Vogelstein, 1990; Jones et al., 2008).

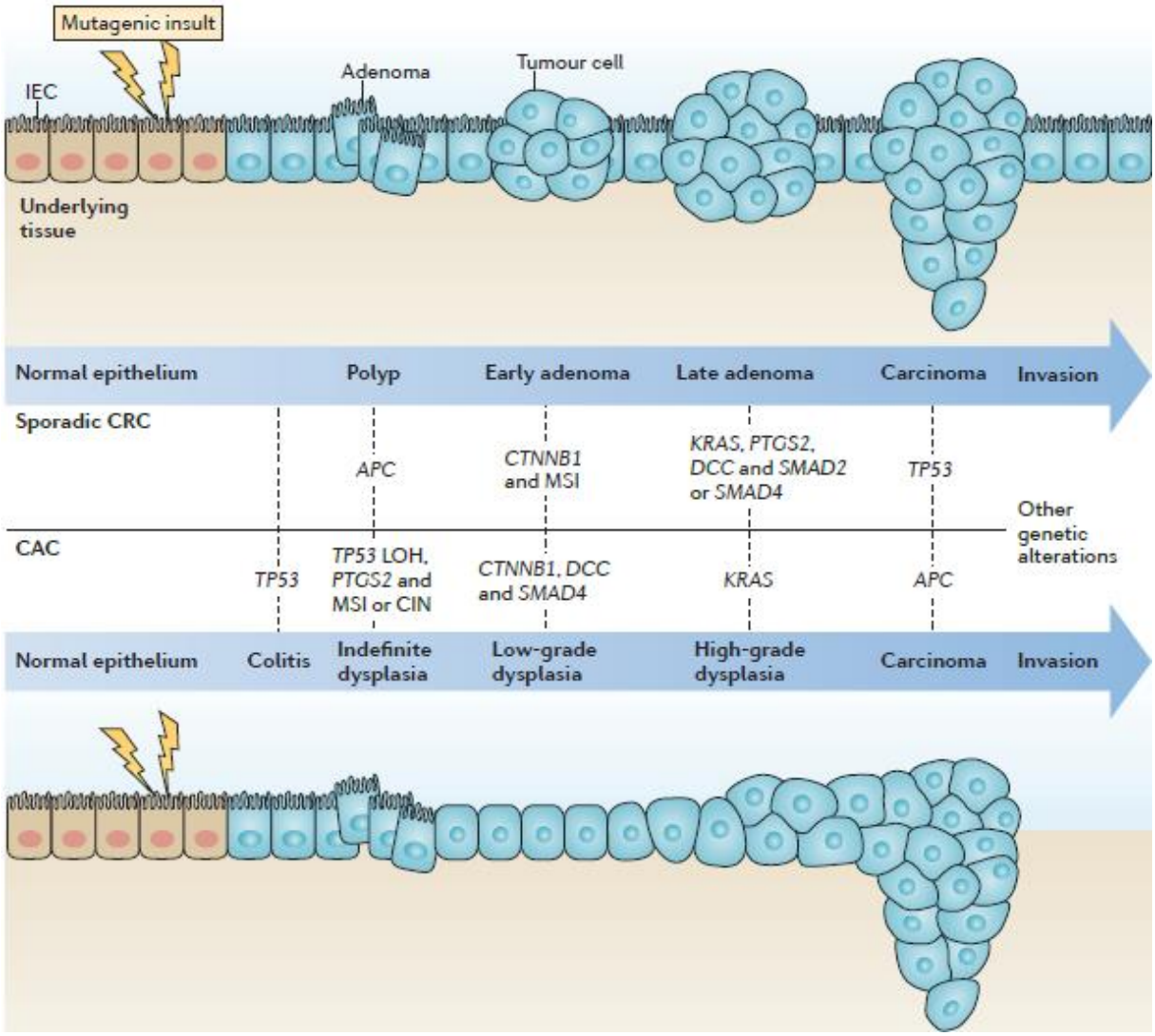

Figure 3. Canonical mechanisms of sporadic colorectal cancer (CRC) and colitis-associated cancer (CAC) development.
Upper panel represents molecular and morphological changes during sporadic CRC progression; lower panel represents molecular and morphological changes during CAC progression. Sequence and frequency of these changes show differences between CRC and CAC. The figure is taken from (West et al., 2015).

1.3 Colitis-associated cancer

Inflammatory bowel disease (IBD) is a chronic relapsing condition characterized by intestinal damage which is caused by a barrier defect and microbiota influx resulting in high levels of inflammation (Francescone et al., 2015). The two major

forms of IBD are ulcerative colitis (UC) and Crohn´s Disease (CD), which both may progress to colitis-associated colon-cancer (CAC) (Grivennikov, 2013). CD increases the cumulative risk of CAC by up to 8% and UC up to 20 % after 30 years of active disease (Canavan et al., 2006; Eaden et al., 2001; Rubin et al., 2012).

CAC and CRC display similarities, such as microsatellite instability (MSI), activation of the oncogene *KRAS*, activation of *COX2*, mutation and eventual loss of heterozygosity (LOH) of *TP53* and mutation of *APC*. However, the sequence and frequency of these events differ between CAC and CRC. For example, mutations in *APC* occur early in CRC, whereas they occur in later stages of CAC. In addition, *TP53* mutations occur early in CAC and in a late stage of CRC ((West et al., 2015) Figure 3).

To understand the molecular changes leading to the colorectal cancer development, different mouse models have been developed that mimic colitis-associated colon cancer and sporadic colon cancer. There are animal models, which spontaneously develop CAC, such as *IL10* and *Gαi2* knockout mice and chemically induced CAC models, like those receiving dextran sulphate sodium (DSS) or a combination of DSS with azoxymethane (AOM), 1,2-dimethylhydrazine (DHM) or iron (Kanneganti et al., 2011).

DSS treatment induces apoptosis within the intestinal epithelium, and therefore disrupting the epithelial barrier, allowing penetration of commensal microbiota into the lamina propria. This triggers an inflammatory response resulting in an upregulation of proinflammatory cytokines such as IL2, IL4 and IL6 (Clapper et al., 2007). Repetitive administration of DSS induces chronic colitis. In combination with a preceding treatment of pro-carcinogen AOM it triggers adenoma development in the distal colon resembling the CAC frequently observed in UC patients (Clapper et al., 2007). These adenomas show signs of Wnt pathway activation as it is observed in human CACs frequently (Aust et al., 2001).

Mouse models of CAC are excellent tools to decipher the underlying mechanisms which connect inflammation and cancer (Grivennikov, 2013). In mouse models, like those used in this study, single injection of the carcinogen AOM is not sufficient to induce colonic tumor formation unless coupled with the induction of chronic colitis. However, multiple injections of the carcinogen (AOM) induce colonic tumorigenesis within a time period of 4 months. In the present study, this treatment

scheme is used as a model of sporadic carcinogenesis in combination with *Tp53* deficiency.

1.4 The P53 tumor suppressor protein

The P53 protein, which is encoded by *TP53* gene, was also named as the “guardian of genome” since it is a key player in the DNA damage response (Lane, 1992). Since its discovery in 1979, P53 has been studied extensively. After its discovery, it was thought to be an oncogene. However, studies in 1989 demonstrated that wild-type P53 suppresses growth and oncogenic transformation (Finlay et al., 1989). Moreover, inactivating *TP53* mutations are common in human tumors (Baker et al., 1989). These and many subsequent studies confirmed its role as a major tumor suppressor.

P53 protein is a transcription factor, which is activated in response to cellular stresses, such as oncogenic signals, DNA damage and hypoxia (Bieging et al., 2014). It promotes the expression of a large number of target genes that mediate senescence, cell cycle arrest and apoptosis. The wide range of regulators that control P53 activity in many distinct biological processes were summarized in a recent review ((Kastenhuber and Lowe, 2017) Figure 4.). The responses to P53 activation highly depend on cell type, epigenetic state, tissue microenvironment and the kind of cellular stress (Kastenhuber and Lowe, 2017). In unstressed cells, P53 is subjected to proteosomal degradation by binding to its negative regulator Mdm2. Various cellular stresses lead to disruption of the P53-Mdm2 interaction by inducing posttranslational modifications of both P53 and Mdm2. This results in P53 stabilization and activation (Kenzelmann Broz and Attardi, 2010).

In addition, numerous studies showed the role of P53 in autophagy (Crighton et al., 2006), mitochondrial respiration (Bensaad et al., 2006; Matoba et al., 2006) and protection of the genome from oxidative stress (Sablina et al., 2005). P53 was reported to support anti-oxidant activity, increase glutamine catabolism, downregulate lipid synthesis, stimulate gluconeogenesis and increase fatty acid oxidation (Kruiswijk et al., 2015). Furthermore, loss of *Tp53* in IECs induces epithelial-mesenchymal transition (EMT), which promotes formation of an inflammatory microenvironment by increasing intestinal permeability in a carcinogen-induced CRC model (Schwitalla et al., 2013).

TP53 is inactivated by mutations in cancer and the frequencies of *TP53* mutations varies between different cancer entities ranging from ~10% in hematopoietic malignancies (Peller and Rotter, 2003) to ~50-70% in colorectal cancer (Iacopetta, 2003). The majority of *TP53* mutations are missense mutations in the DNA binding domain (Kastenhuber and Lowe, 2017) that block the recognition of genomic aberrations.

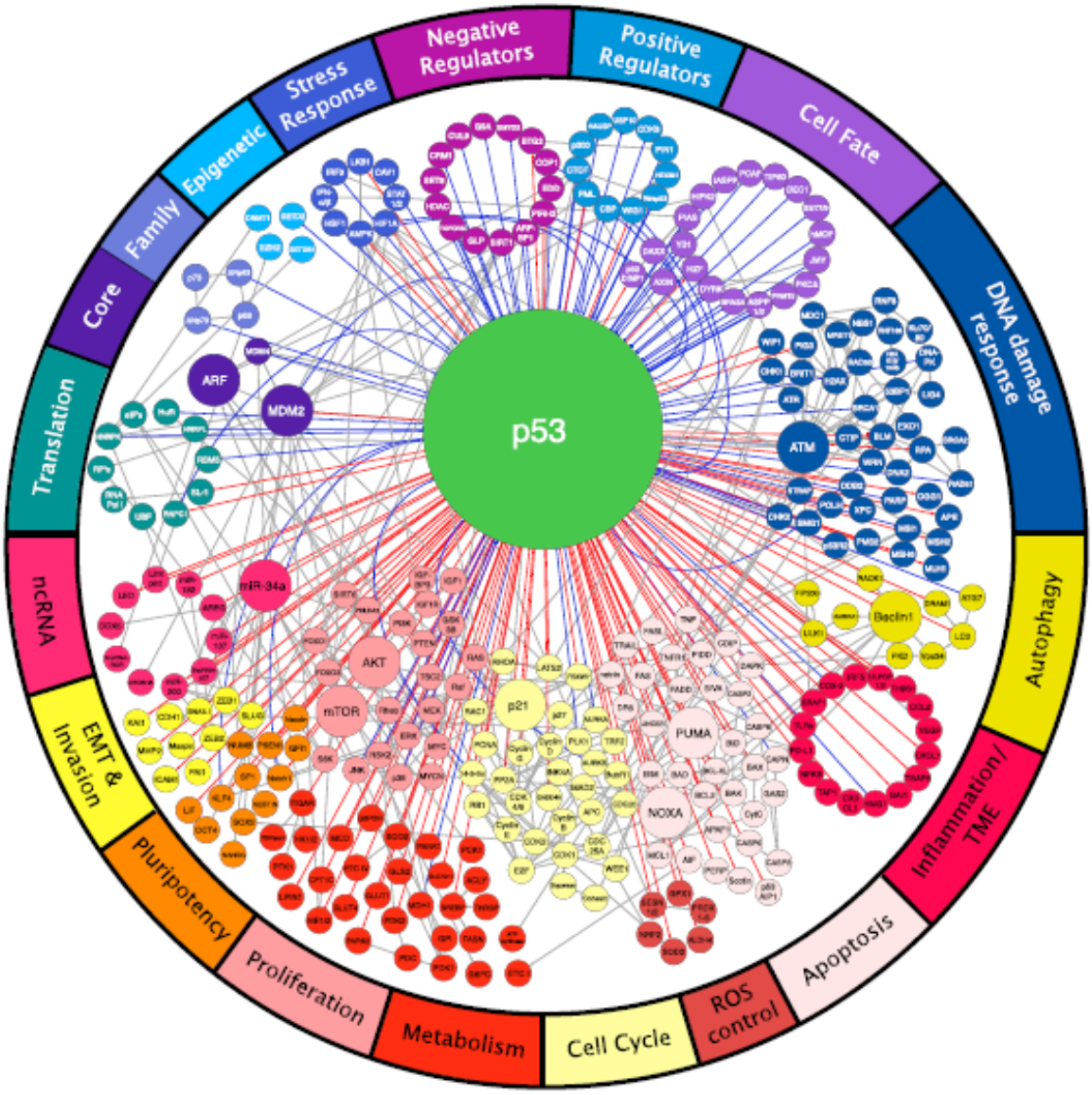

Figure 4. The P53 network.
A wide variety of regulators govern the activity of P53 (top), which, in turn, controls many distinct biological processes (bottom). Each node represents a gene and each line represents an interaction. Direct P53 inputs are indicated as blue lines and direct P53 outputs are indicated as red lines. Noticeably, P53 controls effector processes by activating multiple target genes. Downstream pathways are highly interconnected (gray lines). Figure and legend are taken from (Kastenhuber and Lowe, 2017).

TP53 inactivation occurs at the late stages of colorectal tumorigenesis and mutations in *TP53* are associated with invasion, metastasis and poor patient survival (Jones et al., 2008; Levine and Oren, 2009). Furthermore, the majority (92.1%) of all *TP53* missense mutations also occurs in the DNA binding domain in CRC (Bouaoun et al., 2016). During tumor progression, both somatic and germ-line mutations of *TP53* are followed by loss of heterozygosity (LOH) within chromosome17p (Rivlin et al., 2011).

1.5 microRNAs and the miR-34 family

MicroRNAs (miRNAs) are a subset of small non-coding RNAs that are ~22 nucleotides in length. miRNAs were initially discovered in *Caenorhabditis elegans* (Lee et al., 1993). The canonical miRNA biogenesis begins with the transcription of pri-miRNAs by RNA polymerase II from miRNA genes (Lee et al., 2004). In the next step, a microprocessor complex, that is composed of the ribonuclease enzyme Drosha and the RNA-binding protein DGCR8, cleaves the pri-miRNA to pre-miRNA (70 nucleotide-long precursor hairpin structures) (Gregory et al., 2004). The pre-miRNA is then exported from the nucleus into cytoplasm by Exportin 5 (XPO5)/RanGTP complex (Brownawell and Macara, 2002; O'Brien et al., 2018). In cytoplasm, the pre-miRNA is processed by RNase III protein Dicer, and transforms into 22 nucleotides long mature miRNA (Hutvagner et al., 2001; Ketting et al., 2001). Following this step, strands are incorporated into the RNA-induced silencing complex (RISC), which target specific mRNA molecules by RNA interference (Sontheimer, 2005). The RISC complex consist of Dicer, the trans-activating response RNA-binding protein (TRBP) and Argonaute 2 and it is sufficient for target recognition and cleavage of RNA molecules (Chendrimada et al., 2005; Pratt and MacRae, 2009). The target recognition is carried by the binding of an approximately seven nucleotides long stretch that is in the 5´end of the miRNA, with a complementary sequence that is found in the 3'-UTR of the target mRNA. This binding facilitates the recruitment of the RISC/Ago2 complex to the targeted mRNA, resulting in either inhibition of translation initiation and/or enhancement of mRNA degradation (Bartel, 2009; Ha and Kim, 2014; Huntzinger and Izaurralde, 2011).

Up to date more than 2000 miRNAs have been identified in humans and each individual miRNA can target hundreds of mRNAs (Hammond, 2015). Therefore, miRNAs regulate diverse cellular processes, such as cell cycle control, proliferation,

apoptosis, angiogenesis, migration, metabolism, autophagy, differentiation of stem cells, somatic cell reprogramming and cardiac aging (Rokavec et al., 2014a).

Several miRNA encoding genes have been characterized as oncogenic (for example: *miR-17-5p*, *miR-155*, *miR-221/222, miR-21*,) or tumor suppressive (for example: *let-7, miR-16-1*, *miR-15a*, *miR-34*) (Peng and Croce, 2016). Tumor suppressive miRNAs are frequently down-regulated in many types of cancer and have been shown to play important roles during initiation and progression of cancer (Kohlhapp et al., 2015). miRNAs are frequently found in fragile and other cancer-associated regions of chromosomes as shown by mapping of 186 human miRNA genes (Calin et al., 2004).

In the recent years, the miR-34 family was shown to represent a central mediator of tumor suppression that inhibits several cancer related biological processes, such as proliferation, invasion and metastasis (Rokavec et al., 2014a). In Figure 5, regulation of the miR-34a family is summarized. Seed sequences of miR-34a and miR-34c are identical, whereas seed sequence of the miR-34b is slightly different. Therefore miR-34a and miR-34c share common mRNA targets. *miR-34a* is ubiquitously expressed in mice and showed the highest expression in the brain (Bommer et al., 2007). *miR-34b/c* is predominantly expressed in the lung and almost not detected in other tissues (Bommer et al., 2007). In intestinal epithelia expression levels of *miR-34a* is approximately 1000-fold higher than *miR-34b* and *miR-34c* (Rokavec et al., 2014b). Several studies reported that *miR-34a* and *miR-34b/c* are direct p53 target genes (reviewed in (Hermeking, 2007)). Among the p53-induced microRNAs miR-34a stands out in numerous comprehensive expression studies as the miRNA with the most pronounced induction (Hermeking, 2012). miR-34a is thought to have a central role for p53-mediated tumor suppression conferred by miRNAs which is presumably comparable to the pivotal role of p21 among the protein coding genes induced by p53. Meanwhile, numerous studies have documented the common inactivation of *miR-34a/b/c* by genetic and epigenetic mechanisms in diverse types of tumors (see review by (Rokavec et al., 2014a)). *MIR34A* is silenced by CpG methylation in late stage colorectal tumors (Wang et al., 2016).

miR-34 inactivation alone was not found to be tumorigenic by itself or in combination with an activated *c-Myc* gene in B-cells (Concepcion et al., 2012). However, when additional pro-tumorigenic challenges or other genetic changes were introduced, miR-34 loss promoted tumor formation and/or progression in mice. For

example, we have shown cooperation between *Tp53* and *miR-34a/b/c* loss in a mouse model of prostate cancer (Cheng et al., 2014).

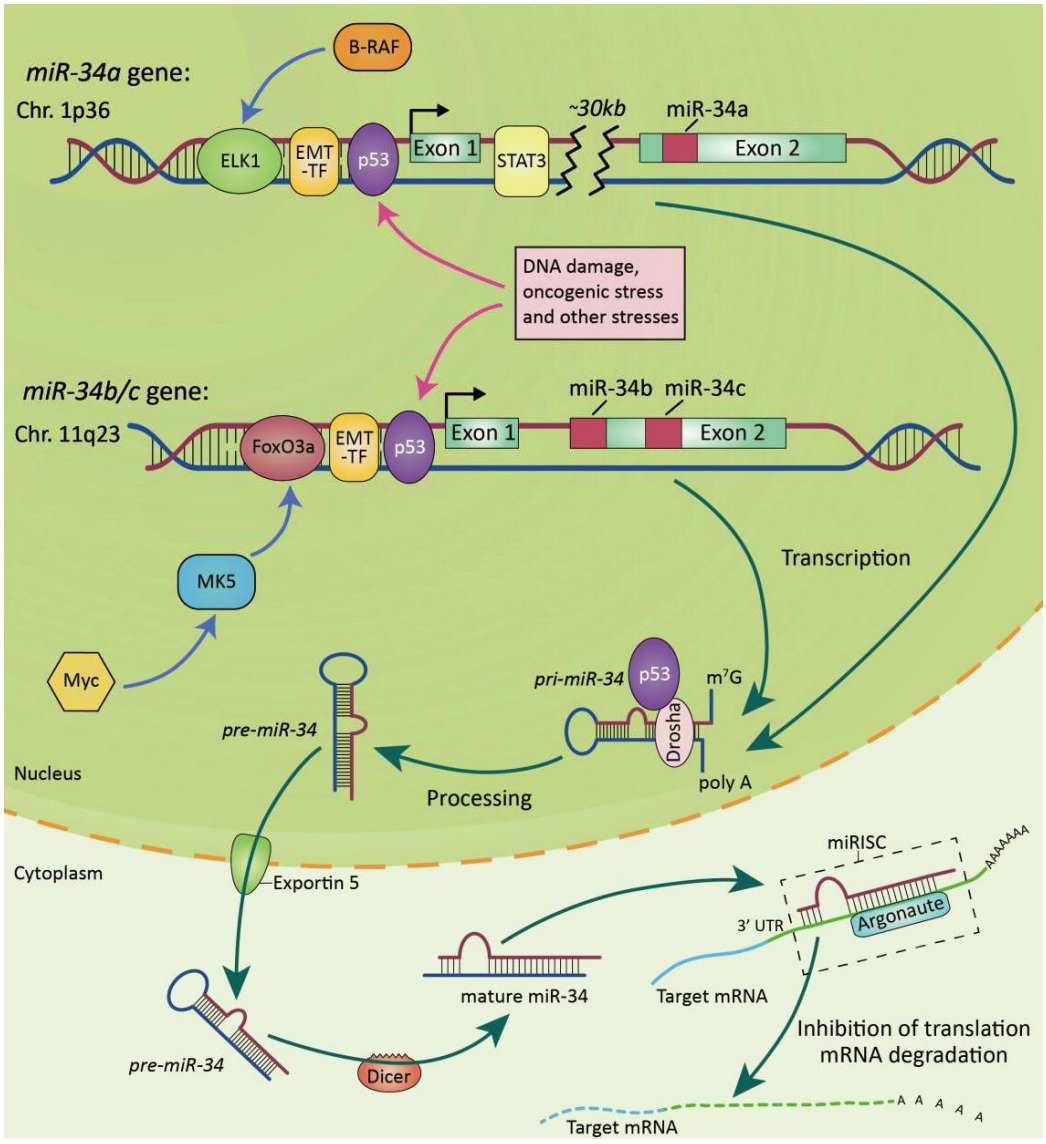

Figure 5. Genomic structure and regulation of the miR-34 family members.
Structure of the miR-34a and miR-34b/c genes. Green and red boxes represent exons and miRNA hairpins, respectively. Horizontal arrows mark transcription start sites. The transcription factors p53, ELK1, and FoxO3a induce, whereas STAT3 and EMT-TF repress the transcription of *miR-34* genes. EMT-TFs represent EMT-inducing transcription factors, such as SNAIL and ZEB1/2. Figure and legend are taken from (Rokavec et al., 2014a).

In addition, deletion of one allele of *miR-34a* in combination with Mdm4 activation was shown to cause adenocarcinomas of the lung (Okada et al., 2014). Recently, our group reported that *Mir34a* and *MiR34b/c* cooperatively suppress adenoma formation in *APC*^{min} mice, which represent a model for hereditary colon cancer, i.e. *familial adenomatous polyposis* (FAP) (Jiang and Hermeking, 2017).

1.6 IL6/IL6R/STAT3 Pathway

IL6 is a growth factor in cancer and an inflammatory, anti-apoptotic cytokine that is linked to NF-κB and STAT3 signaling (Chalaris et al., 2012). It has various physiological functions such as, regulation of immune cell proliferation and differentiation (Garbers et al., 2018). IL6 binds to IL6R and the complex of IL6/IL6R binds to the trans-membrane glycoprotein 130 (gp130) to initiate intracellular signaling as shown in Figure 6 (Schaper and Rose-John, 2015). Protective immunity in host defense and tissue regeneration requires IL6-classic signaling whereas IL6-trans-signaling promotes chronic inflammation and inflammatory tissue damage (Scheller et al., 2011). IL6R is expressed on a few cell types such as leukocytes, hepatocytes, and epithelial cells, whereas gp130 is expressed on all cells (Scheller et al., 2011).

Blockage of IL6 receptor (IL6R) signaling with IL6R neutralizing antibody or sgp130Fc, a fusion protein that blocks IL6 trans-signaling, reduced cancer formation in a mouse model of colitis-associated carcinogenesis (Becker et al., 2004a). This study demonstrated the importance of IL6 trans-signaling, which is mediated by the soluble IL6R (s-IL6R) and that also induces IL6 signaling in cells that do not express IL6R but gp130. The soluble IL6R can either be generated from the membrane bound IL6R by proteolytic cleavage or produced as a spliced IL6R isoform. Together with IL6, the s-IL6R binds to gp130 expressing cells to promote STAT3 signaling (Becker et al., 2004a). Global IL6 deficiency and overexpression of sgp130Fc in transgenic mice further underlined the major role of IL6 signaling and s-IL6R during inflammation *in vivo* (Chalaris et al., 2012; Kopf et al., 1994; Rabe et al., 2008). Lesina et al. described the involvement of IL6 trans-signaling/Stat3/Socs3 in pancreatic intraepithelial neoplasia (PanIN) progression and pancreatic ductal adenocarcinoma (PDAC) development (Lesina et al., 2011). Recently, IL6 trans-presentation has been described as a third mode of IL6 signaling in which dendritic cells (DCs) trans-present IL6 via their own IL6R to T cells (Heink et al., 2017).Trans-presentation of IL6 leads to activation of the Jak/STAT pathway in the T cells and subsequently to the development of pathogenic Th17 cells (Heink et al., 2017). This third mode of IL6 signaling may allow new types of treatments for Th17 cell-driven diseases.

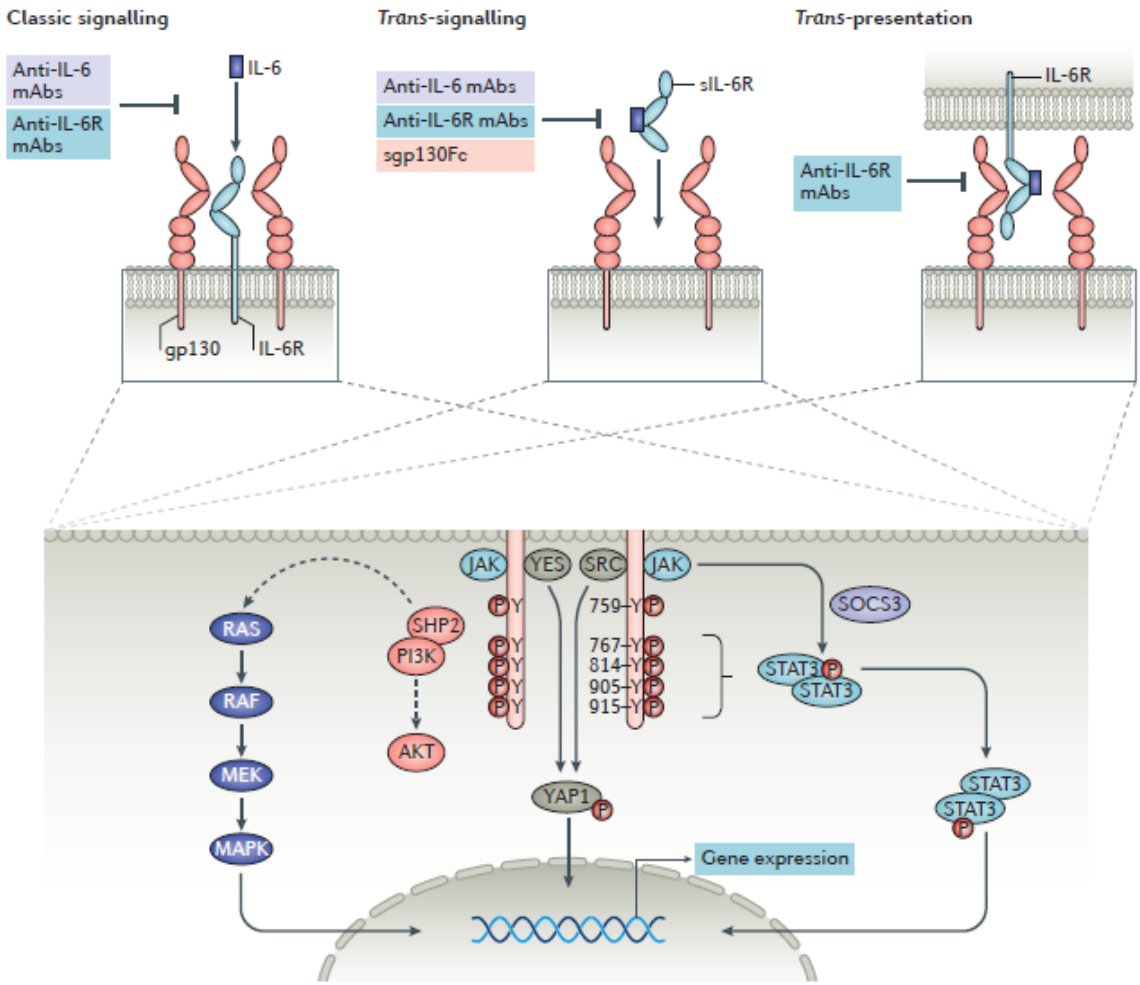

Figure 6. Three different modes of IL6 signaling.
IL6 can either bind to the membrane-bound IL6 receptor (IL6R) (classic signaling), to soluble forms of the IL6R (*trans*-signaling), or it is presented from dendritic cells via their membrane-bound IL6R to T cells (*trans*-presentation). Classic signaling is blocked by antibodies against IL6 and IL6R. *Trans*-signaling is blocked by antibodies against IL6 and IL6R and by the soluble form of glycoprotein 130 (sgp130Fc, Olamkicept). *Trans*-presentation is blocked only by antibodies against IL6R. All three modes of signaling converge on the plasma membrane in homodimerization of the signal-transducing receptor subunit gp130, activating the intracellular signaling cascades Janus kinase (JAK)–signal transducer and activator of transcription (STAT), mitogen-activated protein kinase (MAPK), phosphoinositide 3-kinase (PI3K) and YES-associated protein 1 (YAP). Figure and legend are taken from (Garbers et al., 2018).

Moreover, in *APC*^{min} mice as well as in colitis-associated cancer and colon cancer mouse models, IL6 was shown to stimulate the proliferation of premalignant enterocytes (Fenton et al., 2006). Another report showed that myeloid cells derived IL6 acts as a tumor promoter during intestinal carcinogenesis by protecting intestinal epithelial cells from apoptosis and promoting the proliferation of premalignant cells (Bollrath et al., 2009; Grivennikov et al., 2009). Moreover, Naugler et al. reported that

IL6-deficient mice develop less N-nitrosodiethylamine (DEN)-induced hepatocellular carcinoma. Furthermore, they observed a gender-biased production of IL6, which was higher in male mice. Accordingly, the female mice were partially protected from hepatocellular carcinoma due to the inhibitory effect of estrogen on IL6 production, whereas male mice were highly susceptible (Naugler et al., 2007). In addition, IL11, whose effects on cancer cells are also mediated thorough the gp130/STAT3 pathway has been shown to have a predominant effect on tumor formation compared with IL6 in mouse models of sporadic and inflammation associated colon cancer as well as gastric cancer (Putoczki et al., 2013).

Therapeutic strategies have been developed to target the components of the IL6/IL6R/STAT3 pathway which are summarized in a recent review (Garbers et al., 2018). Olamkicept (scgp130Fc), which selectively inhibits IL6 trans-signaling by sequestering IL6-sIL6R, is currently being evaluated in phase II clinical trials in IBD and ulcerative colitis patients. Anti-IL6R antibodies block classic, trans-signaling and trans-presentation, whereas scgp130Fc only inhibits trans-signaling. Notably, trans-IL6 signaling promotes chronic inflammation and inflammatory tissue damage (Scheller et al., 2011).

The transcription factor STAT3 is required for tissue repair and immune homeostasis and represents one of the main mediators of inflammation-induced carcinogenesis. Originally the STAT3 signaling pathway was described in hepatocytes as a component of the acute phase response in inflammation and later it has been recognized as a major driving factor in tumorigenesis and its activation has been shown in a variety of tumors including CRC (Bollrath and Greten, 2009).

STAT3 is activated by various cytokines including the IL6 family of cytokines, comprised of IL6, IL11, ciliary neurotrophic factor (CNTF), oncostatin M (OSM), leukemia inhibitory factor (LIF), cardiotrophin 1 (CT-1), cardiotrophin-like cytokine (CLC), and IL-27 (Rose-John, 2018), the IL10 family members (Hutchins et al., 2013) and various growth factors, including epidermal growth factor (EGF), hepatocyte growth factor (HGF), and platelet derived growth factor (PDGF). Furthermore, non-receptor tyrosine kinases, such as Abl or Src also activate STAT3 (Chakraborty et al., 2017). STAT3 increases cell survival by upregulating the expression of the anti-apoptotic proteins, such as Bcl-2 and Bcl-XL, whereas it promotes cell proliferation by upregulating the expression of the proto-oncogene *MYC,* cyclin D1, cyclin D2 and cyclin B (Elinav et al., 2013). The formation of adenomas were prevented by

intestinal epithelial cell specific deletion of *STAT3* by regulation of cyclin D1, D2 and B expression, whereas hyperactivation of STAT3 in gp130Y757F mice promoted intestinal tumor growth (Bollrath et al., 2009). Additional evidence for the importance of STAT3 in tumor promotion was provided by the intestinal deletion of the STAT3 inhibitor SOCS3, which increased tumor development, whereas ectopic SOCS3 expression reduced tumor cell proliferation (Rigby et al., 2007).

Recently, we found that miR-34a regulates IL6R/STAT3 signaling in colorectal carcinogenesis (Rokavec et al., 2014b). miR-34a functions in the context of a feedback-loop consisting of IL6R, STAT3 and miR-34a. In this loop, IL6 activates STAT3 via IL6R. STAT3 then directly represses the expression of *miR-34a*. Repressed miR-34a cannot target IL6R to down-regulate its expression; as a result the IL6R/STAT3 pathway is activated further (Figure 7). The repression of miR-34a also induces SNAIL expression which contributes to EMT (Rokavec et al., 2014b).

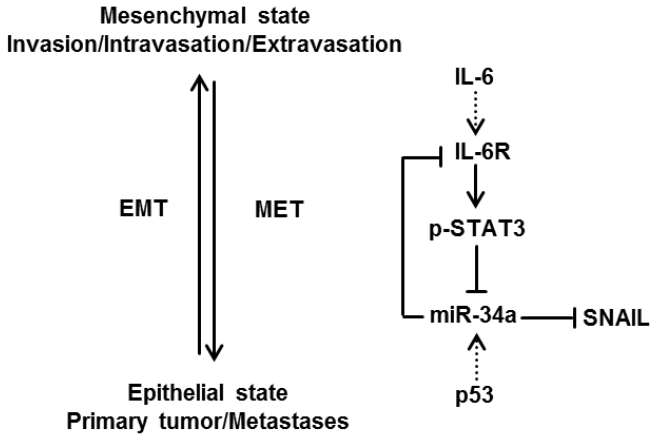

Figure 7. Schematic representation of the IL-6R/STAT3/miR-34a feedback loop and its potential involvement in cancer progression. The activation of the loop by IL-6 induces EMT and shifts the cellular phenotype towards a mesenchymal state that facilitates invasion, intravasation, and extravasation steps during metastasis. Figure and legend are taken from (Rokavec et al., 2014b).

1.7 Cancer metastasis

Cancer metastasis is responsible for 90% of cancer mortality (Elinav et al., 2013). During tumor progression cancer cells acquire the ability to invade into the surrounding tissue, enter into blood vessels and travel to distant organs via the blood stream. There the cells penetrate through the vascular wall and form metastatic colonies. These subsequently proliferate into clinically detectable metastasis (Lambert et al., 2017). This multi-step process of metastasis is summarized in Figure 8. A large variety of molecular pathways contribute to these complex cellular events within tumor cells. In addition, each step of the invasion-metastasis cascade is

supported by non-neoplastic stromal cells of the TME (Valastyan and Weinberg, 2011).

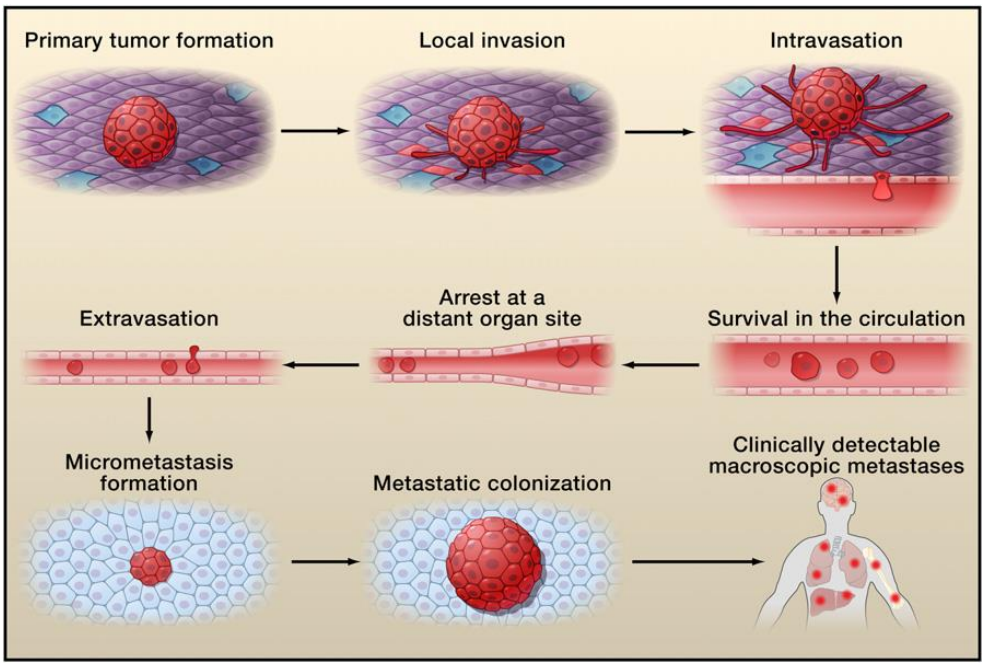

Figure 8. The invasion and metastasis cascade.
Tumor cell metastasis requires distinct features including intravasation, survival in circulation, extravasation and colonization at distant organs. Tumor cells are shown in red. The figure is taken from (Valastyan and Weinberg, 2011).

The first step of the metastatic process is the epithelial mesenchymal transition (EMT) in which cancer cells develop mesenchymal characteristics, such as invasion through basal membranes and increased migration. Loss of E-cadherin expression is a key step in EMT and *E-cadherin* expression is regulated by transcription factors, such as SNAIL, TWIST, KISS, ZEB1 and ZEB2. These factors are activated by pro-inflammatory cytokines TNF, IL1 and IL6 which induce NFκB and STAT3 signaling (Sullivan et al., 2009; Yu et al., 2007). For example, it was shown that TNF-α signaling stabilizes Snail, which represses E-cadherin and thereby promotes metastasis of colon cancer cells (Wu et al., 2009).

Our results demonstrated STAT3 activation by IL6 directly represses the expression of the *MIR34A* gene via a conserved STAT3-binding site in its first intron in human colorectal cancer cells (Rokavec et al., 2014b). Notably, miR-34a directly targets and suppresses SNAIL (Kim et al., 2011; Siemens et al., 2011), whereas miR-34 family members are directly repressed by SNAIL via direct promoter binding in CRC cell lines (Siemens et al., 2011). Another study in breast cancer

demonstrated that miR-34a/c suppresses metastasis by inhibiting migration and invasion by targeting the *Fra-1* oncogene (Yang et al., 2013).

One of the important suppressors of metastasis is the P53 tumor suppressor, which controls the transcription of genes that are involved in canonical metastasis pathways, including cell adhesion, invasion, motility, EMT, stemness, anoikis, and ECM interactions (Powell et al., 2014). *TP53* is mutated or lost in over 50% of all human cancers and in some tumors that retain wild-type *TP53*, defects in the up- or downstream of the P53 pathway are detected (Kim and Lozano, 2018). P53 suppresses metastasis, at least in part, by negatively regulating SNAIL, SLUG and TWIST levels via inducing microRNAs of miR-34a and miR-200 family (Powell et al., 2014). Accordingly, *P53*-deficient tumors show a poor prognosis (Brosh and Rotter, 2009). Also, in a mouse model of sporadic colorectal cancer, intestinal epithelial specific deletion of *Tp53* was shown to promote invasive carcinomas and results in lymph node metastases (Schwitalla et al., 2013). In *Tp53*-deficient mice colon tumors expression of Vimentin and Twist was elevated, whereas expression of E-cadherin was decreased, indicating that these has undergone EMT (Schwitalla et al., 2013). However, many of the mechanisms of p53-mediated suppression of metastasis and the role of its downstream targets, such as miR-34a, still remain to be determined.

2 Aim of Study

Present study had following aims:

1. Characterization of the role of germ-line *Mir34a*-deficiency in a mouse model of colitis-associated cancer

- Evaluation of the tumor suppressor function of *Mir34a* in colitis associated carcinogenesis
- Validation of altered IL6r/Stat3 pathway and its effects in *Mir34a*-deficient colon tumors

2. Characterization of the role of IEC-specific *Mir34a*-and *Tp53*-deficiency in a mouse model of sporadic colorectal cancer

- Identification of differentially regulated pathways in *Mir34a/Tp53*-deficient colon tumors
- Establishment of alternative therapy approaches by inhibition of up-regulated Mir34a-targets in *Mir34a/Tp53*-deficient tumors
- Validation of the expression of chosen Mir34a-target genes in human primary colorectal tumor samples

3 Materials and methods

3.1 Materials

3.1.1 Chemicals and reagents

Application	Chemical Compound	Supplier
In Vivo	Azoxymethane (AOM)	Sigma-Aldrich, St. Louis, MD, USA
	Dextran sulfate sodium salt	MP-Biomedicals, California, USA
	MR-16-1	Chugai-Pharmaceuticals, Shizuoka, Japan
	Tiplaxtinin	Angene-Chemicals, Nanjing, China
	Isotype-control IgG1	Biolegend, California, USA
Cell Culture	Dimethyl-sulfoxide (DMSO)	Carl Roth, Karlsruhe, Germany
	Dulbecco's modified eagle's medium (DMEM)	Invitrogen, Karlsruhe, Germany
	Fetal bovine serum (FBS)	Gibco®, Life Technologies, Darmstadt, Germany
	Hank´s balanced salt solution (HBSS)	Gibco®, Life Technologies, Darmstadt, Germany
	Penicillin-Streptomycin (10,000 U/ml)	Gibco®, Life Technologies, Darmstadt, Germany
Genotyping	dNTPs (deoxynucleotides triphosphate)	Thermo Fisher Scientific, Waltham, MA, USA
	Ethidium bromide	Carl Roth, Karlsruhe, Germany
	Gene Ruler 100bp plus DNA ladder	Thermo Fisher Scientific, Waltham, MA, USA
	O'Gene Ruler 1kb DNA ladder	Thermo Fisher Scientific, Waltham, MA, USA
	Sea plaque® agarose	Lonza, Basel, Switzerland
	Tween® 20	Sigma-Aldrich, St. Louis, MD, USA
Western-Blotting	Ammonium peroxodisulfate (APS)	Carl Roth, Karlsruhe, Germany
	β-mercaptoethanol	Sigma-Aldrich, St. Louis, MD, USA
	Bromophenol blue	Carl Roth, Karlsruhe, Germany
	Complete mini protease inhibitor cocktail	Roche Diagnostics, Mannheim, Germany
	ECL/HRP substrate	Merck Millipore, Billerica, MA, USA
	Immobilon-P PVDF, 0.45µm Membrane	Merck Millipore, Billerica, MA, USA
	Methanol	Carl Roth, Karlsruhe, Germany
	Nonidet®P40 substitute	Sigma-Aldrich, St. Louis, MD, USA
	PageRuler™ Prestained Protein Ladder	Fermentas, Waltham, Massachusetts, USA
	PhosSTOP Phosphatase Inhibitor Cocktail	Roche Diagnostics, Mannheim, Germany
	Rotiphorese gel 30 (37,5:1)	Carl Roth, Karlsruhe, Germany
	Skim milk powder	Fluka, Sigma-Aldrich, St.Louis, MD, USA
	Sodium dodecyl sulfate (SDS)	Carl Roth, Karlsruhe, Germany
	temed (tetramethylethylendiamin,1,2-bis (dimethylamino) –ethan)	Carl Roth, Karlsruhe, Germany
	Tris-base	Carl Roth, Karlsruhe, Germany

Application	Chemical Compound	Supplier
qPCR	Fast SYBR® Green Master Mix	Applied Biosystems, Foster City, CA, USA
	Fast SYBR Green Master Mix Universal RT	Exiqon A/S, Vedbaek, Denmark
Histology	Bovine serum albumin	Sigma-Aldrich, St. Louis, MD, USA
	2-(4-Amidinophenyl)-6-indolecarbamidine-dihydrochloride (DAPI)	Carl Roth, Karlsruhe, Germany
	Hematoxylin	Vector Labs, Burlingame, USA
	Hydrogen peroxide	Carl Roth, Karlsruhe, Germany
	Paraformaldehyde	Santa Cruz, Dallas, Texas, USA
	ProLong Gold antifade	Invitrogen, Karlsruhe, Germany
	Target Retrieval Solution, Citrate pH 6	Dako, Agilent Technologies, USA
	Triton X 100	Carl Roth, Karlsruhe, Germany
	Xylol	Carl Roth, Karlsruhe, Germany
Luciferase Reporter Assay	Ampicillin	Sigma-Aldrich, St. Louis, MD, USA
	Ethidium bromide	Carl Roth, Karlsruhe, Germany
	Formamide	Sigma-Aldrich, St. Louis, MD, USA
	Gene Ruler 100bp plus DNA ladder	Thermo Fisher Scientific, Waltham, MA, USA
	Hi-Di™ Formamide	Applied Biosystems, Foster City, CA, USA
	HiPerFect Transfection Reagent	Qiagen, Hilden, Germany
	LB-Agar (Lennox)	Carl Roth, Karlsruhe, Germany
	LB-Medium (Luria/Miller)	Carl Roth, Karlsruhe, Germany
	OPTI-MEM®Reduced Serum Medium	Life Technologies, Darmstadt, Germany
	Sea plaque® agarose	Lonza, Basel, Switzerland

3.1.2 Enzymes

Application	Enyzme	Supplier
Genotyping	HOT FIREPol® DNA Polymerase	Solis BioDyne, Estonia
	Proteinase K	Sigma-Aldrich, St. Louis, MD, USA
Cloning	Pfu DNA Polymerase	Thermo Fisher Scientific, USA
	Restriction Endonucleases (AgeI, PstI)	New England BioLabs, Germany
	T4 DNA Ligase	Thermo Fisher Scientific, USA
Cell Culture	Trypsin (10x, phenol-red free)	Invitrogen, Karlsruhe, Germany

3.1.3 Kits

Application	Kit	Supplier
qPCR	miRCURY LNATM Universal RT microRNA PCR – Universal cDNA Synthesis Kit II	Exiqon A/S, Vedbaek, Denmark
	QIAshredder	Qiagen, Hilden, Germany
	RNeasy Plus Total RNA Isolation Kit	Qiagen, Hilden, Germany

Application	Kit	Supplier
qPCR	Verso cDNA Synthesis Kit	Thermo Fisher Scientific, Waltham, MA, USA
Western-Blotting	BCA Protein Assay Kit	Thermo Fisher Scientific, Waltham, MA, USA
Histology	DAB Substrate Kit	Vector Labs, Burlingame, USA
	Streptavidin/Biotin Blocking Kit	Vector Labs, Burlingame, USA
	VECTASTAIN Elite ABC HRP Kit	Vector Labs, Burlingame, USA
Cloning	BigDye® Terminator v3.1 Cycle Sequencing Kit	Life Technologies, Darmstadt, Germany
	DyeEx® 2.0 Spin Kit	Qiagen, Hilden, Germany
	QIAquick Gel Extraction Kit	Qiagen, Hilden, Germany
	QIAquick PCR Purification Kit	Qiagen, Hilden, Germany
	Pure Yield™ Plasmid Midiprep System	Promega, Mannheim, Germany
Luciferase Reporter Assay	Dual-Luciferase® Reporter Assay System	Promega, Mannheim, Germany

3.1.4 Primary Antibodies

Antibody	Species	Catalog No.	Supplier	Application	Dilution	Source
BrdU	Human Mouse	MCA2060	AbD Serotec; Bio-Rad, California, USA	IHC	1:400	Rat
β-catenin	Human Mouse	D10A8	Cell Signaling, Massachusetts, USA	IHC	1:500	Rabbit
p-Stat3	Human Mouse	9145 XP	Cell Signaling, Massachusetts, USA	IHC WB	1:300 1:1000	Rabbit
Cleaved-Caspase-3	Mouse	9664	Cell Signaling, Massachusetts, USA	IHC	1:500	Rabbit
p-H2AX	Human Mouse	9718	Cell Signaling, Massachusetts, USA	IHC	1:480	Rabbit
F4/80	Mouse	MF48000	Invitrogen, Karlsruhe, Germany	IHC	1:200	Rat
CD3	Human Mouse	A0452	Dako, Agilent Technologies, USA	IHC	1:200	Rabbit
Pai-1	Human Mouse	SC-8979	Santa Cruz, Dallas, Texas, USA	WB	1:200	Rabbit
Pai-1	Human	MAB10390	Abnova, Taiwan	IHC	1:500	Mouse
β-actin	Mouse	A2066	Sigma-Aldrich, St. Louis, MD, USA	WB	1:1000	Rabbit
α-tubulin	Human Mouse	T-9026	Sigma-Aldrich, St. Louis, MD, USA	WB	1:1000	Mouse
Ki67	Mouse	12202	Cell Signaling, Massachusetts, USA	IHC	1:500	Rabbit
IL-6R	Human Mouse	SC-661	Santa Cruz, Dallas, Texas, USA	IHC WB	1:500 1:1000	Rabbit

Antibody	Species	Catalog No.	Supplier	Application	Dilution	Source
Snail	Mouse	NBP1-19529	Novus Biologicals, Colarado, USA	WB	1:500	Rabbit
Snail	Mouse	AP20370PU-N	Acris, Rockville, MD, USA	IHC	1:150	Rabbit

3.1.5 Secondary Antibodies

Antibody	Catalog No.	Supplier	Application	Dilution	Source
anti-mouse HRP	W4021	Promega, Mannheim, Germany	WB	1:10000	Goat
anti-rabbit HRP	A0545	Sigma-Aldrich, St.Louis, MD, USA	WB	1:10000	Goat
Biotinylated Rabbit Anti-Rat	E0468	Dako, Agilent Technologies, USA	IHC	1:500	Rabbit
Biotinylated Goat Anti-Rabbit	E0432	Dako, Agilent Technologies, USA	IHC	1:500	Goat

3.1.6 Vectors

Name	Insert	Source
PGL3-Control-MCS	Firefly luciferase	Promega, Mannheim, Germany
PGL3-*Pai-1*	Mouse *Pai-1* 3´UTR	This study
PGL3-*Pai-1*-mutated-SM	Mouse *Pai-1* 3´UTR Mir34a SM mutated	This study
pRL	*Renilla* luciferase	Promega, Mannheim, Germany

3.1.7 Oligonucleotides

3.1.7.1 Oligonucleotides used for genotyping

Name	Sequence (5’ - 3’)	Product
miR-34a-Fwd	ACCTTGCAGGTGCTCAGAAT	Floxed 368 bp
miR-34a-Rev-2	TGGAGCTAACGGAGTGTGTG	Wildtype 510 bp
miR-34a-Rev-4	CTACCCAAGCTCGACGAAGT	Knockout 623 bp
miR-34a-Rev-8	TGCAGCACTTCTAGGGCAGT	
Tp53-Forward	CACAAAAACAGGTTAAACCCAG	Floxed 380 bp
Tp53-Reverse	AGCACATAGGAGGCAGAGAC	Wildtype 300bp
Cre-Forward	ACCTGAAGATGTTCGCGATTATCT	Transgene 370 bp
Cre-Reverse	ACCGTCAGTACGTGAGATATCTT	

3.1.7.2 Oligonucleotides used for cloning

Name	Sequence (5’ - 3’)	Application
Mmu-AgeI-Pai1-Forward	ATATACCGGTCAAACCTGCCCCTC	Cloning 3’-UTR
Mmu-PstI-Pai1-Reverse	TATACTGCAGGGGGAGGGAGGG	
Pai1-clone-seq-Forward1	CCAGTGCAAGTGCAGGTGC	Sequencing Insert
Pai1-clone-seq-Reverse1	TATACTGCAGGGGGAGGGAGGG	

3.1.7.3 Oligonucleotides used for qPCR

Name	Sequence (5' - 3')
Mmu-cMyc-Forward	CCTAGTGCTGCATGAGGAGA
Mmu-cMyc-Reverse	TCTTCCTCATCTTCTTGCTCTTC
Mmu-IL-6-Forward	CTCTGGGAAATCGTGGAAAT
Mmu-IL-6-Reverse	CCAGTTTGGTAGCATCCATC
Mmu-IL-6Rα-Forward	GCAAGAATCCTCGTCCATGT
Mmu-IL-6Rα-Reverse	GTGGAGGAGAGGTCGTCTTG
Mmu-Pai1-Forward	GACACCCTCAGCATGTTCATC
Mmu-Pai1-Reverse	AGGGTTGCACTAAACATGTCAG
Mmu-Cyclophilin-Forward	ATGGTCAACCCCACCGTGT
Mmu-Cyclophilin-Reverse	TTCTGCTGTCTTTGGAACTTTGTC
Mmu-IL-11-Forward	GTGGCTGTGGAGAAGCTGTG
Mmu-IL-11-Reverse	GAAGGTCCACGGGAAAGACAC
Mmu-Snail-Forward	CACACGCTGCCTTGTGTCT
Mmu-Snail-Forward	GGTCAGCAAAAGCACGGTT
Mmu-Vimentin-Forward	ATCGACAAGGTGCGCTTCC
Mmu-Vimentin-Reverse	TTGCCCTGGCCCTTGA
Mmu-Zeb1-Forward	GCTGGCAAGACAACGTGAAAG
Mmu-Zeb1-Reverse	GCCTCAGGATAAATGACGGC
Mmu-Cldn15-Forward	GGCTTCCTGGGCCTCTTTC
Mmu-Cldn15-Reverse	AGCAGCTTGGCCTTCTTGG
Mmu-Cldn6-Forward	ACTATGCTGCGCCTGCTCTTCTGG
Mmu-Cldn6-Reverse	GATATTCGGAGGGTCCCCGAGA
Mmu-Muc1-Forward	GAGCCAGGACTTCTGGTAGGCT
Mmu-Muc1-Reverse	GGCTTCACCAGGCTTACGTAGT
Mmu-Muc5-Forward	GATCCATCCATCCCATTTCTACC
Mmu-Muc5-Reverse	TTGCTTATCTGACTACCACTTGTTGA

3.1.8 Buffers and Solutions

Tail lysis buffer:

- 1.5M Tris/HCL
- 200 mM NaCl
- 0.2% SDS
- 5 mM EDTA

Proteinase K buffer:

- 0.1 M Tris (pH 8.5)
- 0.2 M NaCl
- 5 mM EDTA (pH 8.0)
- 0.2% SDS

„Vogelstein“ PCR buffer (10X) (Vogelstein and Kinzler, 1999):

- 166 mM NH_4SO_4
- 670 mM Tris (pH 8.8)
- 67 mM $MgCl_2$
- 100 mM β-mercapto-ethanol

RIPA buffer (for protein lysis):

- 1% NP40
- 0.5% Sodium deoxycholate
- 0.1% SDS
- 150 mM NaCl
- 50 mM TrisHCl (pH 8.0)

Laemmli buffer (2X):

- 125 mM TrisHCl (pH 6.8)
- 4% SDS
- 20% glycerol
- 0.05% bromophenol blue
- 10% β-mercaptoethanol

SDS buffer:

- 50 mM Tris (pH 8.1)
- 100 mM NaCl
- 0.5% SDS
- 5 mM EDTA

10x Running buffer (5L, for SDS-PAGE):

- 720 g Glycin
- 150 g Tris base
- 50 g SDS
- pH 8.3-8.7
- 5 L ddH_2O

Transfer buffer:

- 200 mM glycine
- 20% methanol
- 25 mM Tris base (pH 8.6)

10x TBS-T (5L):

- 500 ml 1M Tris (pH 8.0)
- 438.3 g NaCl
- 50 ml Tween20
- 5 L ddH2O

PBS (10X):

- 1.37 M NaCl
- 27 mM KCl
- 100 mM Na2HPO4
- 18 mM KH2PO4
- Adjust pH to 7.2 wih HCl

In situ hybridization buffer (Schwitalla et al., 2013):

- 0.9 M NaCl
- 20 mM Tris/HCl pH7.3
- 0.01% SDS

3.1.9 Laboratory Equipment

Device	Supplier
5417C table-top centrifuge	Eppendorf, Hamburg, Germany
ABI 3130 genetic analyzer capillary sequencer	Applied Biosystems, Foster City, USA
AxioPlan 2 Microscope System	Carl Zeiss, Oberkochen, Germany
CF40 Imager	Kodak, Rochester, New York, USA
Cell culture flasks, Multiwell plates and Conical Tubes	Corning, New York, USA
Fisherbrand FT-20E/365 transilluminator	Fisher Scientific, Schwerte, Germany
Forma scientific CO2 water jacketed incubator	Thermo Fisher Scientific, Waltham, MA, USA
GeneAmp® PCR System 9700	Applied Biosystems, Foster City, USA
Heraeus Megafuge 1.0R	Thermo Fisher Scientific, Waltham, MA, USA
KAPPA ImageBase software	KAPPA opto-electronics, Gleichen, Germany
LSM 700 Laser Scanning Confocal Microscope	Carl Zeiss, Oberkochen, Germany
Mini-PROTEAN®-electrophoresis system	Bio-Rad, Munich, Germany
MultiImage Light Cabinet	Alpha Innotech, Johannesburg, South Africa
ND 1000 NanoDrop Spectrophotometer	NanoDrop products, Wilmington, DE, USA
Neubauer counting chamber	Carl Roth, Karlsruhe, Germany
Polytron PT 1200E tissue homogenizer	Kinematica, Luzern, Switzerland
Orion II luminometer	Berthold Technologies, Bad Wildbad, Germany
Varioskan Flash Multimode Reader	Thermo Fisher Scientific, Waltham, MA, USA
Waterbath	Memmert GmbH, Schwabach, Germany

3.2 Methods

3.2.1 Mouse models

Mir34a$^{FL/FL}$ and *Mir34a*$^{-/-}$ mice

The generation of *Mir34a*$^{-/-}$ mice with a C57BL6/SV129 back-ground was performed by Dr. Lodygin and has been described in our publication (Rokavec et al. 2014). Gene specific deletions were generated by using homologous recombination with a vector containing *Mir34a* or *Mir34b/c* sequences flanked by *loxP* sites and an intronic Neomycin resistance (*Neo*) cassette flanked *frt* sites individually. The *Neo* cassette was removed by crossing with *flp*-mice and germ-line *Mir34a* knock-out mice were generated by crossing with *CMVCre* mice. When *Mir34a*$^{FL/FL}$ mice were crossed to a mice line expressing a Cre recombinase under the control of a promoter of interest, *Mir34a* expression was stopped. In order to get *Mir34a*$^{FL/FL}$ mice in FvB background, we performed 5 backcrosses to FvB mice (5 crosses to FvB mice theoretically correspond to at least 96% of FvB background).

Tp53$^{FL/FL}$ mice

In *Tp53*$^{FL/FL}$ mice exons 2-10 of the *Tp53* gene are flanked by loxP sites (Jonkers, Meuwissen et al. 2001). Cre mediated recombination under the control of a promoter of interest generates a *Tp53 null*-allele in targeted tissue.

Villin-Cre mice

This mouse line harbors the Cre recombinase under control of the mouse *Villin* promoter (Madison, Dunbar et al. 2002). Cre recombinase recombines genes flanked by loxP sequences. Crossing of mice of the *Villin-Cre* line with a mouse containing a loxP-flanked gene of interest “floxed”, leads to tissue-specific deletion of the targeted sequence.

Genotype	Background	Source
Mir34a$^{FL/FL}$	C57BL/6J and FvB	This work
Mir34a$^{-/-}$	C57BL/6J	This work
Tp53$^{FL/FL}$	FvB	The Jackson Laboratory
Mir34a$^{FL/FL}$/*Tp53*$^{FL/FL}$	FvB	This work
Villin-Cre	C57BL/6J and FvB	The Jackson Laboratory

3.2.2 Genotyping

Mice tails were lysed overnight at 60°C in 95 µl tail lysis buffer supplemented with 5 µl Proteinase K (Qiagen). The enzymatic digestion was stopped by heat inactivation at 95°C for 10 min. Samples were diluted 1:10 with distilled water and centrifuged for 5 min at 13200 rpm. Supernatants were used for polymerase chain reaction (PCR).

Genotyping PCR conditions for each gene are indicated in below:

Mir34a genotyping:

Master mix and thermocycler conditions:

Component	Volume (µl)
Vogelstein PCR Buffer (10X)	2.5
10 mM dNTPs	1
10 µM 34a-Fwd-Primer	2
10 µM 34a-Rev.2-Primer	1
10 µM 34a-Rev.4-Primer	1.5
10 µM 34a-Rev.8-Primer	0.5
Hot Firepol Taq Polymerase	0.5
dH_2O	16.5
Genomic DNA	1
Total	25

PCR-conditions		
Step	**Temperature**	**Time**
Initiation	95°C	15 min.
37 Cycles	95°C	30 sec.
	59°C	30 sec.
	72°C	40 sec.
Final elongation	72°C	3 min.

P53 genotyping:

Master mix and thermocycler conditions:

Component	Volume (µl)
Invitrogen PCR Buffer (10X)	2
50 mM $MgCl_2$	1
10 mM dNTPs	0.4
10uM p53-Fwd.-Primer	0.5
10uM p53-Rev.-Primer	0.5
Hot Firepol Taq Polymerase	0.15
dH_2O	13.95
Genomic DNA	1.5
Total	20

PCR-conditions		
Step	**Temperature**	**Time**
Initiation	94°C	10 min.
35 Cycles	94°C	30 sec.
	58°C	30 sec.
	72°C	30 sec.
Final elongation	72°C	7 min.

Villin-Cre genotyping:

Master mix and thermocycler conditions:

Component	Volume (µl)
Vogelstein PCR Buffer (10X)	2.5
10 mM dNTPs	2
10 µM 370-Fwd-Primer	1.2
10 µM 370-Rev.-Primer	1.2
Hot Firepol Taq Polymerase	0.2
dH_2O	15.9
Genomic DNA	2
Total	25

PCR-conditions		
Step	**Temperature**	**Time**
Initiation	94°C	10 min.
35 Cycles	94°C	30 sec.
	58°C	30 sec.
	72°C	30 sec.
Final elongation	72°C	7 min.

All genotyping primers are listed under section 3.1.7.1.

3.2.3 AOM/DSS and 6XAOM administration

To induce colitis-associated carcinogenesis mice at the age of 6 to 10 weeks were intraperitoneally (i.p.) injected with 10 mg/kg Azoxymethane (AOM, Sigma) once at day 0 and once at day 21 of the model. Five days after first AOM injection, mice received 2% dextran sulfate sodium salt (DSS, MP-Biomedicals) in the drinking water for 5 days, followed by 16 days of regular water (first and second cycles). During the third cycle, no AOM and only 2% DSS were administered. At day 110, mice were sacrificed.

For sporadic colorectal carcinogenesis model, mice were injected i.p. with 10 mg/kg AOM, six times in weekly intervals and on week 16 all mice were sacrificed.

3.2.4 Treatment with MR16-1 and Tiplaxtinin

For blocking IL6R activity mice were i.p. injected weekly with 1 mg antibody against mouse IL6R (MR16-1, kindly provided by Chugai Pharmaceuticals) or, as isotype control, 1 mg Rat IgG1 (GoInVivo-Biolegend). The Pai-1 inhibitor Tiplaxtinin was purchased from Angene chemicals (Nanjing, Jiangsu Province China). Tiplaxtinin supplemented food (1 g tiplaxtinin/kg chow) was given from week 9 to 16 to mice and prepared by Ssniff-Special Diets (Soest, Germany).

All animal protocols were approved by the local authorities (Regierung von Oberbayern, AZ: 55.2-1-54-2532-201-2014).

3.2.5 Intestinal epithelial cell (IEC) isolation

For IEC isolation, intestine were opened longitudinally and chopped into small pieces and incubated in 1xHBSS supplemented with 30 mM EDTA for 10 min on a rocking-platform at 37°C. The tube was vortexed for 30 seconds and placed, incubated on ice. The supernatant including detached epithelial cells was transferred into a new falcon tube and centrifuged at 1500 rpm for 10 min at 4 °C. The pelleted epithelial cell were washed with PBS, transferred to Eppendorf tubes and centrifuged at 5000 rpm for 5 min at 4°C. The supernatants were discarded and the cell pellets were snap frozen in liquid nitrogen and stored at -80°C.

3.2.6 Bromodeoxyuridine (BrdU) injection and sacrifice of the mice

BrdU is incorporated in the DNA instead of thymidine during cell proliferation. The incorporation of BrdU by proliferating cells was detected by immunohistochemistry. 90 minutes before sacrifice, mice were injected i.p. with 75 mg/kg BrdU (Sigma) that was dissolved in PBS.

3.3 Human samples

Formalin-fixed, paraffin-embedded (FFPE) colon cancer samples of 61 patients who underwent surgical tumor resection at the Ludwig-Maximilians University of Munich (LMU) between 1994 and 2005 were used for PAI-1 IHC. All tumors were located on the right side of the colon. Tissue microarrays (TMAs) were generated with 6 representative 1 mm cores of each case. 5 µm TMA sections were prepared, deparaffinized and stained with anti-PAI-1 (Abnova) mouse monoclonal antibody on a Ventana Benchmark XT Autostainer with UltraView Universal DAB and alkaline phosphatase detection kits (Ventana Medical Systems). All procedures involving human tumor biopsies were performed with the approval of the ethics committee of the Ludwig-Maximilians University Munich.

3.4 Histology

3.4.1 Haematoxylin & Eosin (H&E) staining

For H&E staining, FFPE tissues were cut in to 2 µm thick slides. H&E staining were performed by an automated slide staining system according to standard protocols.

3.4.2 Fluorescence *in situ* hybridization (FISH)

For FISH, the universal eubacteria probe (EUB338) and negative control probe (NON338) were employed to visualize intestinal bacteria cells as described (Schwitalla et al., 2013). The 5'-FITC-labeled EUB338 DNA probe (5'-GCTGCCTCCCGTAGGAGT-3') and 5'-Cy3-labeled NON338 DNA probe (5'-CGACGGAGGGCATCCTCA-3') were synthesized by Metabion. Freshly prepared 3 µm paraffin sections were deparaffinized in Xylol and incubated for 10 minutes in 100% EtOH. The bacterial probes were diluted to a final concentration of 1 ng/ µL in pre-warmed hybridization buffer (described under section 3.1.8) and the hybridization was performed at 50°C overnight. Afterwards, the hybridized tissue sections were washed 3 times for 15 minutes in pre-warmed hybridization buffer, rinsed in distilled water and mounted with DAPI containing medium.

3.4.3 Immunohistochemical analysis

For each immunohistochemical staining, 2 µm thick FFPE slides were used. Tissue sections were deparaffinized. After dehydration, for antigen retrieval, the tissue sections were boiled for 20 minutes in a microwave in antigen unmasking solution (Dako, citrate, pH 6). After cooling down, to quench endogenous tissue peroxidases, slides were treated for 10 minutes with 3% H2O2/PBS solution. Next, tissue sections were washed with PBS and blocked for 30 minutes using 3% BSA/PBS supplemented with avidin-block (2 drops per ml, Vector) to block unspecific binding sites for antibodies at room temperature. Then, tissue sections were incubated with the primary antibody against the epitope of interest diluted in 3% BSA/PBS plus biotin-block (2 drops per ml, Vector Laboratories) over night at 4 °C (respective dilutions are indicated under section 3.1.4). The next day, tissue sections were washed twice for 5 minutes with PBS. The secondary antibody conjugated with Biotin (Vector Laboratories) was diluted 1:500 in 3% BSA/PBS for incubation with the

tissue sections for 30 min. An ABC complex solution consisting of avidin dehydrogenase and biotinylated horseradish peroxidase (Vector Laboratories) was prepared by adding 2 drops of each solution A & B to 5 mL PBS and incubated for 30 min at 4°C prior to use. After washing with PBS the tissue slides were incubated for 30 min with ABC complex solution. For the DAB (3,3'-diaminobenzidine) color reaction, 2 drops of buffer were mixed with 4 drops of DAB and 2 drops of peroxidase (DAB Kit, Vector Laboratories) in 5 ml of distilled water. The staining solution was applied to the tissue slides until the staining for the target of interest was appropriate. The reaction was stopped in distilled water. Nuclei were counterstained with hematoxylin for 1 minute, washed with distilled water and dehydrated.

3.5 RNA/DNA analysis

3.5.1 RNA Isolation

Total RNA from animal tissues was isolated with RNeasy Plus Total RNA Isolation Kit (Qiagen). Tissues were lysed in 600 µl of RTL buffer supplemented with 1% β-mercaptoethanol by using a tissue homogenizer (Polytron PT 1200 E). Next, tissue lysates were passed through QIAshredder columns (Qiagen). The flow-through was then used for RNA isolation according to manufacturer's protocol. RNA was eluted in RNase-free water. The amount and quality of the isolated RNA was measured by NanoDrop spectrophotometer (Thermo Fisher Scientific). RNA samples were stored in -80°C until use.

3.5.2 cDNA synthesis

250 ng-1 µg of total RNA was used to generate cDNA by using Verso cDNA synthesis kit (Thermo Fisher Scientific) according to the manufacturer's protocol. Resulting cDNA samples were stored at -20°C.

3.5.3 Quantitative real time PCR (qPCR) analysis

Analysis of mRNA expression was carried out by using Fast SYBR Green Master Mix (Applied Biosystems) on a LightCycler 480 (Roche). The reaction mix per well contained 7,5 µl of SYBR-Green MasterMix, 5,5 µl of distilled water, 1 µl of cDNA and 1 µl of the respective primer mix (containing 20 mM each: forward and reverse primer). Results are represented as fold induction using the ΔΔCt method

(Pfaffl, 2001) with the control set to 1 as described before (Menssen et al., 2007). The individual mRNA levels were normalized to Cyclophilin expression. Primers used for qPCR are listed under section 3.1.7.3.

3.5.4 RNA sequencing

Total RNA from murine tumors was isolated as described above. RNA profiling was done in triplicates (3 RNA samples per genotype; each tumor RNA sample represented a pool of 3 tumors isolated from the same mouse). Random primed cDNA libraries were generated and sequenced using the HiSeq2500 (Illumina) platform by GATC (Konstanz, Germany). Each sample was covered by at least 30 million single reads of 50 bp length. The raw reads were cleaned by trimming of adaptor sequences and low quality sequences with average quality scores less than 20. Trimmed reads were mapped to the mm10 mouse reference genome and processed using the RNA-seq module of the CLC Genomics Workbench software (Qiagen Bioinformatics) with default settings. Expression (reads) was normalized by using the RUV-method (Risso et al., 2014). Mice displayed increase in the degree of tumor aggressiveness (tumor number/size/invasiveness) from wt over *Mir34a*$^{\Delta IEC}$ and *p53*$^{\Delta IEC}$ to *Mir34a*$^{\Delta IEC}$*p53*$^{\Delta IEC}$ mice. Therefore, differentially expressed genes were determined by a t-test for trend based on Spearman correlation between expression and genotypes ranked in the order: wt, *Mir34a*$^{\Delta IEC}$, *p53*$^{\Delta IEC}$, *Mir34a*$^{\Delta IEC}$*p53*$^{\Delta IEC}$. For principal component analyzes the ClustVis tool was used (Metsalu and Vilo, 2015). Gene Set Enrichment Analyses (GSEA) were performed using the GSEA software (Broad Institute, Boston, USA) and data from the molecular signature database (MSigDB) (Subramanian et al., 2005). The significance of enrichments is presented by normalized enrichment scores in false discovery rate (FDR) adjusted q-values. Expression profiling data was deposited in the Gene Expression Omnibus website (Accession No. GSE99452).

3.5.5 Analysis of expression and methylation data from online patient data sets

mRNA expression, methylation (beta-values determined by 450K BeadChip arrays (Illumina)), and clinical data of Colon adenocarcinoma (COAD) and rectal adenocarcinoma (READ) cohorts were obtained from the TCGA data portal (tcga-data.nci.nih.gov/tcga/tcgaDownload.jsp) (Cancer Genome Atlas, 2012), MD

Anderson standardized data browser (http://bioinformatics.mdanderson.org/TCGA/databrowser/), and the UCSC cancer browser (https://genome-cancer.ucsc.edu). *Tp53* mutation data was obtained from cBIO and OASIS (Cerami et al., 2012; Hafi et al., 2016). For representation of RNA-Seq. results the Expectation-Maximization (RSEM) normalized expression values from the Illumina RNASeqV2 (genes) datasets were used. Methylation of miR-34a was determined by averaging the methylation levels of the 7 CG sites (450k BeadChip probes cg04413644, cg04112567, cg03521358, cg06658816, cg02924110, cg24167422, and cg12385729) located in the CpG island in the miR34a promoter (Lodygin et al., 2008). For binary classification (high/low methylation), the mean methylation was used as a cut-off. The CMS classification of TCGA samples was obtained from Synapse (www.synapse.org). Expression and clinical data of GSE39582, GSE37892, GSE17536, and GSE14333 datasets was down- loaded from NCBI GEO (www.ncbi.nlm.nih.gov/geo). The association of PAI-1 expression with nodal status or metastasis was calculated by Student's t-test. The significance of Kaplan-Meier survival curves was calculated with a log-rank test. For binary classification of cases (high/low expression), receiver operated characteristics (ROC) curve analysis were used to determine optimal cut-off values using the Cut-off Finder tool (http://molpath.charite.de/cutoff/assign.jsp).

3.6 Protein analysis

3.6.1 Preparation of protein lysates

For protein extraction, tissues were lysed by mechanical homogenization with a micro-pistil in 200 µl ice-cold protein lysis buffer Lysates were incubated for 10 minutes on ice, centrifuged at 13200 rpm at 4°C for 10 minutes to pellet cell debris. Protein containing supernatants were stored at -80°C.

3.6.2 Western blot analysis

For western blotting, protein concentration was measured with BCA Protein Assay Kit (Thermo Fisher Scientific) by Varioskan Flash Multimode Reader (Thermo Scientific) using the SkanIt RE for Varioskan 2.4.3 software (Thermo Scientific). 30-40 µg of protein were adjusted to a volume of 24 µl by filling up with protein lysis buffer, and 8 µl of 4x Laemmli buffer was added. The samples were boiled at 95°C

for 5 minutes, cooled down on ice, briefly centrifuged and loaded onto the gel. The gel was run at 100 volt in 1x running buffer. Proteins were transferred on Immobilon PVDF membranes (Millipore) by using Mini-Protean-electrophoresis system (Bio-Rad) in 1x transfer buffer 90 minutes at 350 mA. After the transfer, membrane was washed in TBS-Tween 20 (TBST) and incubated for 30 minutes at room temperature with 3% (w/v) skim milk (Roth)-TBST to block unspecific binding of antibody. Then, the membrane was incubated with a primary antibody (listed under section 3.1.4) at 4°C, overnight. Next day, membrane was washed 3 times, 10 minutes with TBST. HRP-coupled secondary antibody (listed under section 3.1.5) of choice was applied onto the membrane at room temperature for 1 hour. Then, membrane was washed 3 times for 10 minutes with TBST. For detection, ECL solution (Millipore) was applied to the membrane for 5 minutes and signals were recorded with a 440CF imaging system (Kodak).

3.7 Cloning

3.7.1 Cloning of *Pai-1* 3´-UTR sequence into PGL3 plasmid

The predicted wild-type and mutated miR-34a seed match sequence in 3´UTR of mouse *Pai-1* that contains Age1 and Pst1 restriction sites on 5´ and 3´ ends respectively were generated by annealing synthetic oligos and inserted into pGL3-control-MCS vector (downstream of a firefly luciferase ORF), and verified by sequencing.

3.7.2 Digestion

Digestion of the vector and the insert were performed by using manufacturer´s protocol (New England Biolabs) at 37°C for 2 hours. The restriction of the plasmid was confirmed on a 1% agarose gel. The linearized plasmid fragment was eluted from the agarose gel using a Gel Extraction Kit (Qiagen).

3.7.3 Ligation

Ligation of DNA constructs was performed overnight at 4°C by using 1 U of T4 Ligase (Invitrogen) in a total volume of 20 µL using a vector-insert molecular ratio of 1:3.

3.7.4 Transformation

In order to transform Pgl3-Pai-1 vector that harbors ampicillin resistance, competent bacteria *E. coli* XL-1 blue strain was used. A 200 µL aliqot of competent bacteria was thawed on ice for 5 minutes and approximately 100 ng of DNA plasmid was added on and incubated 30 minutes on ice. The heat shock was performed for 90 seconds at 42 °C and then transformed bacteria were placed on ice for additional 2 minutes. 800 µL of antibiotic-free LB medium was added on and then bacteria were incubated for 1h at 37 °C shaking before the bacterial culture was plated on LB-Agar plates including ampicillin. The plates were incubated overnight at 37 °C.

3.7.5 Isolation of plasmid DNA from bacteria

Single colonies from transformed bacteria on LB-agar plates were inoculated either in 2 ml or 150 ml of LB-broth containing 100 µg/ml ampicillin and incubated overnight while at 37 °C (shaking at 225 rpm). In order to isolate a plasmid from the bacterial culture Pure Yield™ Plasmid Midiprep System (Promega) was used according to the manufacturer´s protocol for DNA purification. The DNA concentration was determined by using NanoDrop (Thermo Scientific).

3.7.6 Colony PCR

To identify the orientation of DNA inserts colony PCR was performed. For this purpose, 20 µl of a PCR master mix containing vector and/or insert specific primers, dNTPs, 10x Vogelstein PCR buffer and FIREPol® DNA polymerase (Solis BioDyne) was prepared. Single colonies were picked from the LB-agar plate and transferred into corresponding PCR tube. The PCR cycling conditions were as the following: 95°C for 5 minutes, followed by 25 cycles of 95°C for 20 seconds, 55°C for 30 seconds and 72°C for X minute/s (1 minute per 1 kb length of the expected PCR product), and then another 72°C for 7 minutes. PCR fragment length was assessed by an agarose gel electrophoresis (percentage of the gel was prepared according to the expected product size).

3.7.7 Sequencing

To verify whether desired DNA sequence was introduced into Pgl3-plasmid, DNA sequencing was performed according to the BigDye Terminator v1.1 Cycle Sequencing Kit´s protocol (Life Technologies). Briefly, a master mix was prepared

containing Big Dye Terminator V1.1, 5×Sequencing buffer, primer (10 µM) and plasmid (1 µg/ml). Then PCR program was run by 15 cycles of each 10 seconds at 96°C and 90 seconds at 60°C. Later, the DyeEx 2.0 Spin Kit (Qiagen) was used according to the manufacturer's protocol with a 5417C centrifuge (Eppendorf). After that, purified DNA was mixed with Hi-Di Formamide (Applied Biosystems), and loaded into to ABI3130 genetic analyzer capillary sequencer (Applied Biosystems) for sequencing. Data was analyzed by the 3130 Data Collection Software v3.0 and the sequencing analysis software 5.2 (Applied Biosystems).

3.8 Cell culture

3.8.1 Cultivation

H1299 cancer cell line was cultured in Dulbecco's modified Eagle's medium (DMEM, Invitrogen) with 10% fetal bovine serum (Invitrogen), penicillin (100U/ml), 0.1mg/ml streptomycin (Gibco) at 5% CO_2, 37°C. CT26 cell line was cultured in RPMI 1640 medium (Invitrogen) supplemented with 10% fetal bovine serum (Invitrogen), penicillin (100U/ml), 0.1mg/ml streptomycin (Gibco) at 5% CO_2, 37°C. CT26 cells were transfected with *pre-miR-34a* (Ambion, PM11030) or with a negative control (Ambion, neg. control #1) for 48 hours by using Lipofectamine 2000 transfection reagent (Invitrogen).

3.8.2 Transfection of oligonucleotides and vector constructs

Transfections of oligonucleotides and vector constructs were carried out using freshly trypsinized and seeded cells in the medium and cell-culturing format of choice, preferentially into a six- or twelve-well format, 24 hours before transfection.

For transfection of oligonucleotides or plasmid DNA into the cells, HiPerFect (Qiagen) transfection reagent was used. For six-well format, the transfection reagent mix contained 100 µl Opti-MEM (Invitrogen), 10 µl HiPerFect (Qiagen) and 10 µl of the respective oligonucleotide (10 µM) (Ambion – Applied Biosystems, final concentration (100 nM)) or 4 µg of the plasmid DNA. Transfection reagent added last to the mix and incubated 15 minutes before drop-wise application of the mix on to the cells. 48 hours later, cells were harvested for the luciferase reporter assay.

3.9 Luciferase assay

For luciferase assays, H1299 cells were seeded in 12-well format dishes at $3x10^4$ cells/well, and transfected after 24 hours with 100 ng of the respective firefly luciferase reporter plasmid, 20 ng of *Renilla* reporter plasmid as a normalization control and 25 nM of pre-*miR-34a* (Ambion, PM11030) or a negative control oligonucleotide (Ambion, neg. control #1) by using HiPerfect transfection reagent (Qiagen). After 48 hours a Dual Luciferase Reporter assay (Promega) was performed according to manufacturer's instructions. Fluorescence intensities were measured with an Orion II luminometer (Berthold) in 96-well format and analyzed with the SIMPLICITY software package (DLR). Primers used for cloning and sequencing are given under section 3.1.7.2.

3.10 Statistics

The association between *miR-34a* methylation/*TP53* mutation and distant metastasis was calculated using the Chi-square test for trend. The association between *miR-34a* methylation/*TP53* mutation and survival was calculated using the log-rank test for trend. The association of PAI-1 expression with nodal status or metastasis was calculated by Student's t-test. Survival curve of mice was analyzed by Kaplan-Meier method with a log-rank test. Results were expressed as mean ± SEM. Differences were analysed by a two tailed Student's t-test. Calculations were performed using Prism5 (Graph Pad Software Inc.) and *P*-values ≤ .05 were considered as significant, $P^* \leq .05$; $P^{**} \leq .01$; $P^{***} \leq .001$.

4 Results

4.1 Germ-line *Mir34a*-deficiency increases tumor load and invasion in a colitis associated model of colorectal carcinogenesis

Previously, we have shown that miR-34a plays an important role in intestinal epithelial cells in response to IL6 mediated inflammation (Rokavec et al., 2014b). Accordingly, miR-34a functions in the context of a positive feedback-loop consisting of IL6R, STAT3 and miR-34a where IL6 activates STAT3 via IL6R, STAT3 then directly represses the expression of miR-34a, which targets and down-regulates IL-6R. Furthermore, results by Dr. Rokavec and Dr. Li, indicated that IL6 effectively induces EMT in colorectal cancer (CRC) cell lines, which is mediated by the direct repression of miR-34a by STAT3. Moreover, CRC cell lines with mesenchymal and therefore invasive features consistently showed up-regulation of this feedback loop. Similarly, primary colorectal tumors that develop distant metastasis displayed an association with activation of the IL6R/STAT3/miR-34a feed-back loop.

In order to analyze the relevance of an IL6R/STAT3/miR-34a feedback loop in an autochthonous colorectal tumor model, the well-established azoxymethane/dextran sodium sulfate (AOM/DSS) model was employed (Neufert et al., 2007), which closely recapitulates human colitis-associated cancer (CAC). Since miR-34a was expressed more than approximately 1000-fold higher levels than miR-34b and miR-34c in intestinal epithelia and approximately 180-fold higher in intestinal tumors (data not shown), I focused on the role of miR-34a in CAC. Compared to wt mice, expression of *Mir34a* was markedly elevated in colon tissue of mice with intestinal cell–specific *Stat3* deletion ($Stat3^{\Delta IEC}$) (Figure 9A). DSS treatment of $Mir34a^{F/F}$ mice for 5 days resulted in decreased expression of *Mir34a* in colon epithelial cells accompanied by an induction of IL6 expression in colon tissue (Figure 9B-C). Therefore, Mir34a is also repressed by inflammatory signaling *in vivo*, which is known to involve Stat3 activation (Grivennikov et al., 2010).

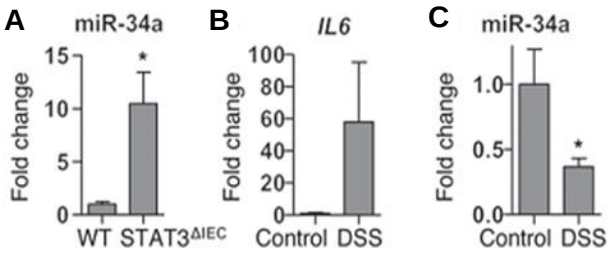

Figure 9. Altered expression of *Mir34a* and *IL6* after short-DSS treatment. **(A)** Expression of *Mir34a* in colon tissue of wt and *Stat3*$^{\Delta IEC}$ mice. cDNAs for this experiment were provided by Prof. Florian Greten and Paul Ziegler. **(B)** Expression of *IL6* mRNA in colon tissue of *Mir34a*$^{F/F}$ mice after 5 days of DSS treatment. **(C)** Expression of *Mir34a* in colon epithelial cells of *Mir34a*$^{F/F}$ mice after 5 days of DSS treatment. Mean values ± SEM are provided. *$P < 0.05$.

In order to investigate the role of Mir34a in AOM/DSS-induced carcinogenesis, *Mir34a*-deficient (*Mir34a*$^{-/-}$) mice were employed which had been generated in the Hermeking lab. previously. *Mir34a*$^{-/-}$ mice did not display an obvious phenotype or any spontaneous tumor formation and showed normal Mendelian inheritance (data not shown). Upon AOM/DSS treatment, the incidence and size of tumors were significantly enhanced in *Mir34a*$^{-/-}$ mice compared to *Mir34a*$^{F/F}$ mice (Figure 10A-C). Moreover, *Mir34a*-deficient colon tumors revealed increased cell proliferation and decreased apoptosis compared to *Mir34a*-proficient tumors (Figure 10D-E). Importantly, approximately 70% of *Mir34a*$^{-/-}$ mice displayed invasive tumors that penetrated through the muscularis mucosa, whereas none of the tumors from *Mir34a*$^{F/F}$ mice showed invasion (Figure 10F-G). Loss of TP53 has been suggested to be essential for colon tumor invasion (Fearon and Vogelstein, 1990) and was recently linked to activation of NF-κB and Stat3 (Schwitalla et al., 2013), which also comprise important signaling nodes in CAC (Bollrath et al., 2009; Grivennikov et al., 2009). Sequencing the entire *Tp53* coding region in tumors from 6 *Mir34a*$^{F/F}$ and 10 *Mir34a*$^{-/-}$ mice did not reveal any mutations in either genotype. Therefore, the deletion of *Mir34a* presumably substituted for the inactivation of *Tp53* as a requirement for invasiveness.

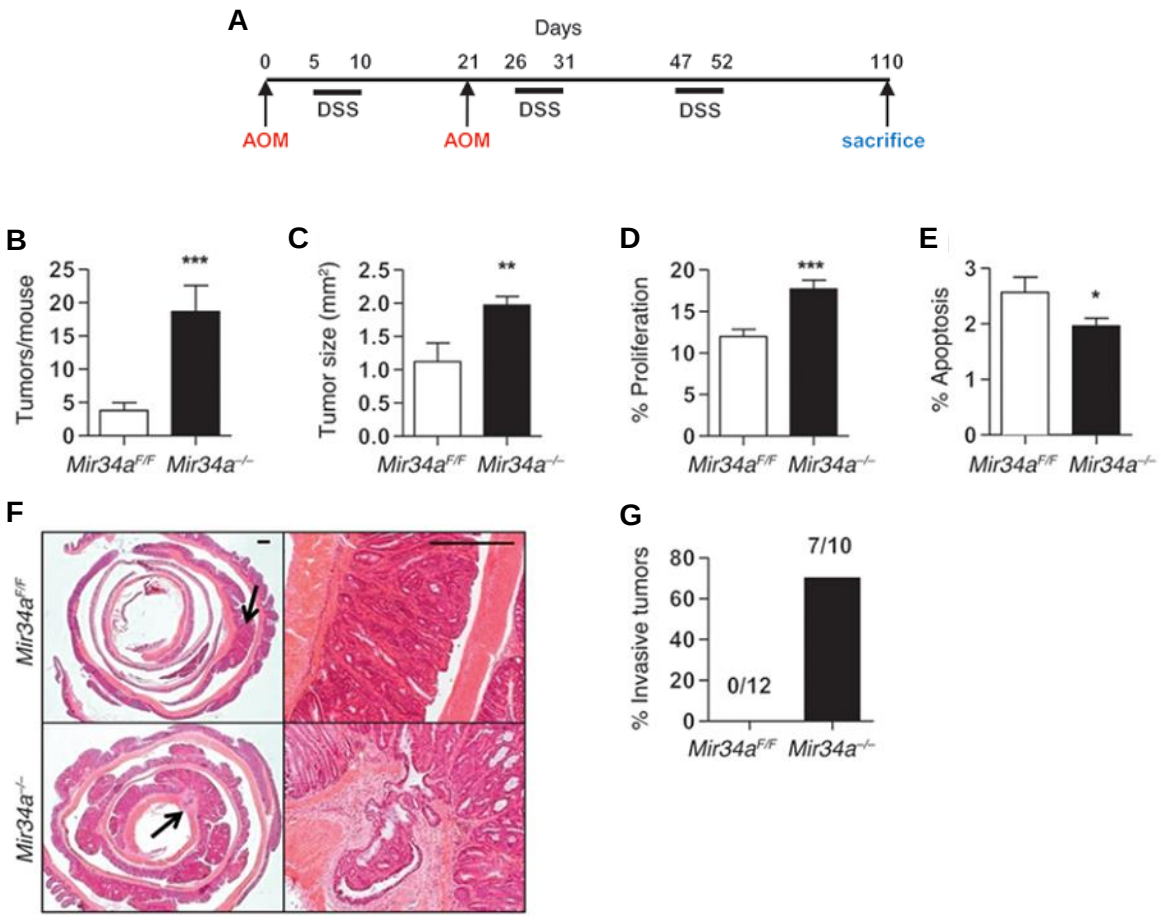

Figure 10. Deletion of *Mir34a* facilitates tumor invasion after AOM/DSS treatment. **(A)** Schematic overview of the AOM/DSS treatment to induce CAC. Injections (i.p.) of 10 mg/kg AOM were performed once at day 0 and once at day 21. Five days after AOM injection, mice received 2% DSS in the drinking water for 5 days, followed by 16 days of regular water. During the third cycle, no AOM and only 2% DSS were administered. At day 110, mice were sacrificed. **(B)** Tumor incidence in indicated mice (n ≥ 10 mice for each genotype). **(C)** Mean tumor size in indicated mice (n ≥ 5 mice for each genotype). **(D)** Tumor cell proliferation was determined by BrdU incorporation. Percentage of proliferation indicates BrdU-positive cells (n ≥ 10 tumors of each genotype). **(E)** Tumor cell apoptosis was determined by detection of cleaved caspase-3. Percentage of positive cells is indicated (n ≥ 10 tumors of each genotype). **(F)** H&E-stained sections of colons from *Mir34a*$^{F/F}$ and *Mir34a*$^{-/-}$ mice with arrows indicating magnified areas showing tumor morphology and representative invasive colon carcinoma in *Mir34a*$^{-/-}$ mice. Scale bars: 500 µm. **(G)** Percentage of mice showing invasive tumors for indicated genotypes. Number of mice with invasive tumors/total number of mice for each genotype is indicated above the bars. Mean values ± SEM are provided. **P* < 0.05; ***P* <0 .01; ****P* <0 .001.

4.2 *Mir34a*-loss activates IL6R/Stat3 signaling in colitis-associated tumors and allows invasion

In order to show *Mir34a*-deficiency regulates IL6R/Stat3 axis, *Mir34a* expression levels were checked after siRNA-mediated knock-down of Stat3 in the murine colorectal cancer cell line CMT93, which is known to expresses constitutively active phospho-Stat3 (pStat3). In line with this hypothesis, *Mir34a* expression was elevated after Stat3 knock-down (Figure 11A). Furthermore, *Mir34a*$^{-/-}$ mice showed increased phosphorylation of Stat3 and elevated expression of IL6R in tumor cells compared to *Mir34a*$^{F/F}$ mice (Figure 11B-C). Also, the levels of the EMT inducer and Mir34a target SNAIL was markedly increased in *Mir34a*$^{-/-}$ mice, suggesting that tumor cells in these mice underwent EMT (Figure 11B-C). Finally, *Mir34a*$^{-/-}$ tumors displayed increased Stat3 phosphorylation and expressed higher levels of IL6R, SNAIL and ZEB1 protein and RNA compared to *Mir34a*$^{F/F}$ tumors (Figure 11D-E).

Taken together, *Mir34a*-loss activates IL6R/Stat3 signaling in colitis-associated tumors and allows EMT, invasion and metastasis.

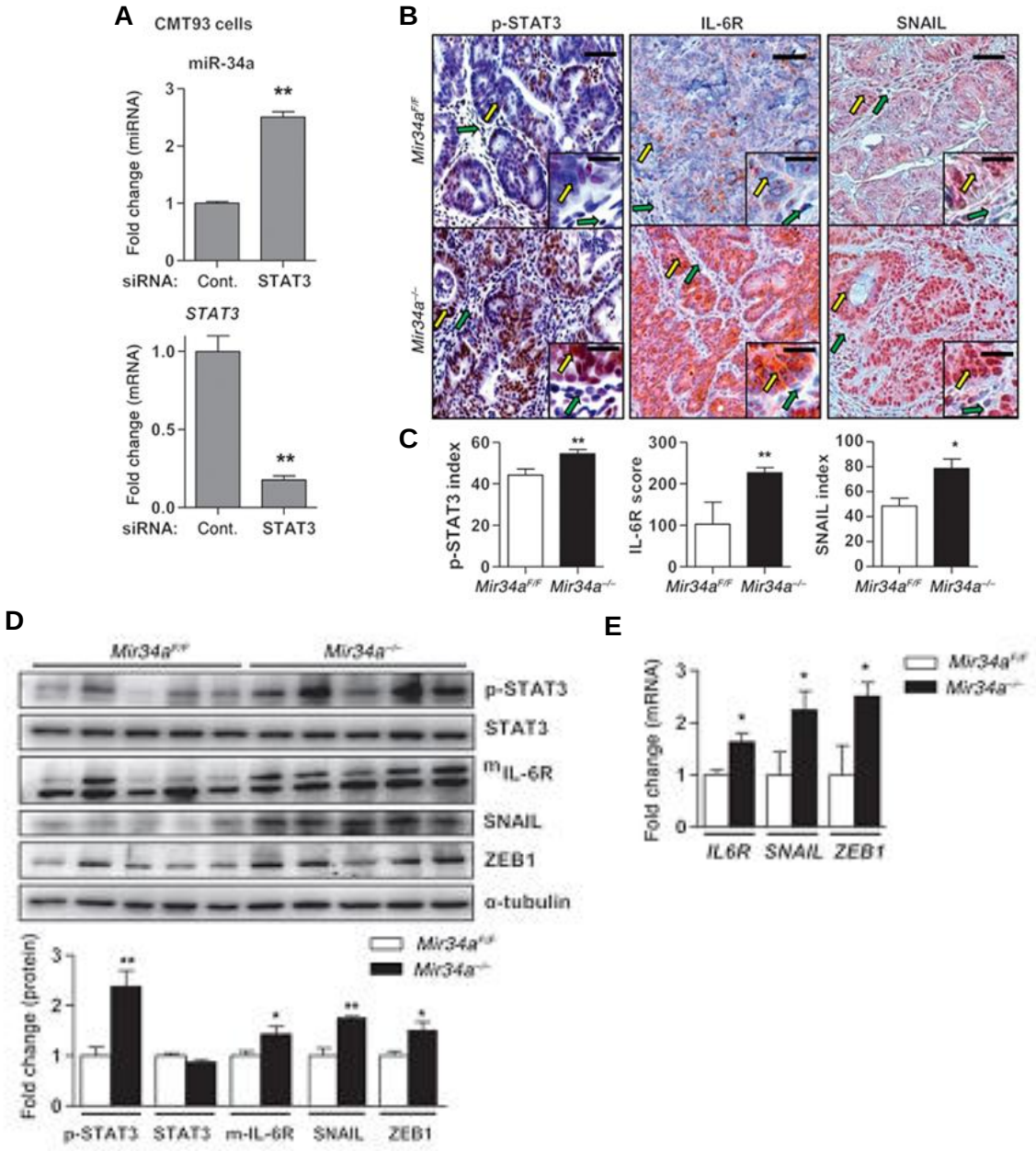

Figure 11. The tumors of *Mir34a*$^{-/-}$ mice show characteristics of EMT and enhanced IL6R/STAT3 signaling. (A) Expression of mature *miR-34a* and *Stat3* in mouse rectal cancer cell line CMT93 transfected with control or Stat3 siRNA. cDNA samples from CMT93 cells were generated by Paul Ziegler and provided us by Prof. Florian Greten.
(B and C) Immunohistochemical analysis of p-STAT3, IL6R, and SNAIL in tumors of *Mir34a*$^{F/F}$ and *Mir34a*$^{-/-}$ mice. Yellow and green arrows indicate tumor and stoma cells, respectively. Scale bars: 50 µm; 20 µm (insets). Bar charts (C) show the percentage of positive tumor cells (index; p-STAT3 and SNAIL) or expression score (IL6R) determined (n ≥10 tumors from each genotype). **(D)** Western blot analysis of indicated proteins in lysates prepared from tumors of *Mir34a*$^{F/F}$ and *Mir34a*$^{-/-}$ mice (n = 5 from each genotype). Relative densitometric quantifications of indicated proteins are shown in lower panel. **(E)** qPCR analysis of indicated mRNAs in tumors of *Mir34a*$^{F/F}$ and *Mir34a*$^{-/-}$ mice (n = 3 from each genotype). A,C,E: Bars represent mean values ± SEM. **P* <0 .05; ***P* < 0.01; ****P* <0 .001.

4.3 *Mir34a* and *Tp53* cooperatively suppress colorectal tumorigenesis

In this second part of the study, cooperative effects of Mir34a and Tp53 were investigated and characterized in a sporadic colon cancer model.

TP53 and *MIR34a* are frequently inactivated by mutation or CpG methylation in CRC (Fearon and Vogelstein, 1990; Siemens et al., 2013). So far it has not been determined whether the combined inactivation of these genes was clinically relevant. Therefore correlation between *TP53* mutation and *MIR34A* CpG methylation was analyzed. In 208 CRC samples represented within the TCGA database, patients with *TP53* mutated and *MIR34A* CpG methylated colorectal tumors had poorest survival (Figure 12A). Moreover, patients with distant metastasis (M1) had significantly higher numbers of primary colorectal tumors with simultaneous MIR34a methylation and TP53 mutation than patients without distant metastasis (M0) (Figure 12B). Therefore, the combined inactivation of *MIR34a* and *TP53* is associated with a poor prognosis and distant metastasis in CRC patients.

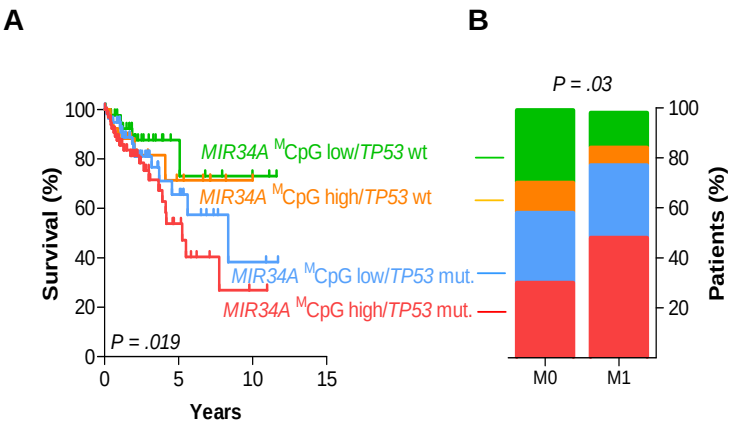

Figure 12. *miR-34a* methylation and *TP53* mutation are associated with poor survival and distant metastasis in CRC patients.
Association of *miR-34a* methylation and *TP53* mutation with **(A)** overall survival in CRC patients (n=177) and **(B)** distant metastasis in CRC patients (n=207). Significance was calculated by the (A) log-rank test for trend and (B) by the Chi-square test for trend. ^{M}CpG: DNA methylation. *P* values are provided as $*P < 0.05$. Figures **(A-B)** were generated by Dr. Matjaz Rokavec.

As expected, *MIR34A methylation* and expression showed a significant, negative correlation in these samples (Figure 13A). Notably, colorectal tumors with mutant *TP53* showed more pronounced correlation between miR-34a promoter methylation and down-regulation of miR-34a expression compared to colorectal tumors with wt *TP53* (Figure 13B-C). In addition, we found that colorectal tumors with

mutant *TP53* display higher levels of CpG methylation within the *MiR-34a* promoter, which was associated with decreased miR-34a expression when compared to colorectal tumors with wt *TP53* (Figure 13D-E). Furthermore, miR-34a expression was the lowest in tumors with both, elevated *MIR34A* methylation and *TP53* mutation (Figure 13F).

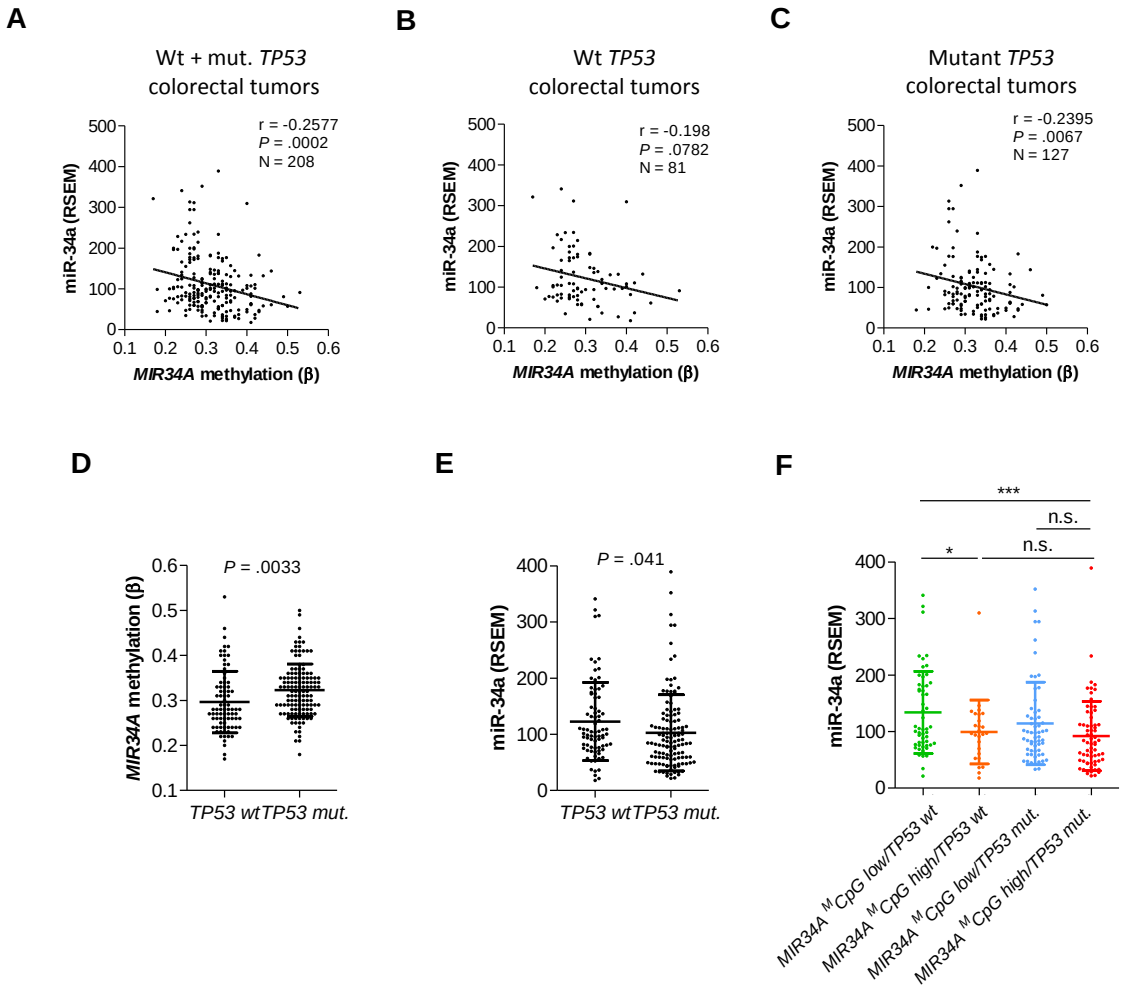

Figure 13. Preferential miR-34a silencing in CRCs with mutant *TP53*.
CRC samples from 208 patients of the TCGA CRC dataset (COAD+READ) that have a confirmed *TP53* wild type (wt; n=81) or *TP53* mutant (n=127) status were analyzed. **(A)** Correlation of miR-34a expression and methylation in 208 CRCs. Correlation of miR-34a expression and methylation in **(B)** *TP53* wt and **(C)** *TP53* mutant CRCs. (A-C) Correlation coefficients (r) and p-values were calculated by Spearman correlation. **(D)** Methylation of MIR34A in *TP53* wt vs. *TP53* mut. CRCs: **(E)** Expression of miR-34a in *TP*53 wt (n=81) vs. mut. (n=127) CRCs. (D+E) Significance was calculated by Student´s t-test **(F)** miR-34a expression in, 208 CRCs. Significance was calculated by one-way ANOVA with Dunnett multiple-comparisons post-test. *P* values are provided as **P* < 0.05 and ****P* <0 .001. Figures **(A-F)** were generated by Dr. Matjaz Rokavec.

These results prompted us to experimentally determine whether the *Mir34a* and *Tp53* genes cooperatively suppress colorectal tumorigenesis and to investigate the underlying molecular mechanisms in a mouse model of sporadic CRC. In addition, this would allow us to test potential therapeutic strategies for the treatment of *Mir34a*/*Tp53*-deficient colorectal carcinomas. For this purpose we generated mice with *Mir34a* and *Tp53* alleles flanked by *loxP* sites, which permit intestinal epithelial cell (IEC) specific deletion by Cre recombinase expressed from a *Villin* promoter (Figure 14A). We did not analyze the effect of *Mir34b/c*-deficiency in this study, since *Mir34b/c* is expressed at least hundred times lower than *Mir34a* in IECs (data not shown). Mice with IEC-specific deletion of *Mir34a* (*Mir34a*$^{\Delta IEC}$) or *Tp53 (Tp53*$^{\Delta IEC}$), as well as their combined deletion (*Mir34a*$^{\Delta IEC}$*Tp53*$^{\Delta IEC}$) did not display any overt phenotype or any signs of spontaneous tumorigenesis in the colon (data not shown). Tp53 expression was decreased in the IECs of *Mir34a*$^{\Delta IEC}$ mice compared to *Mir34a*$^{Fl/Fl}$/*Tp53*$^{Fl/Fl}$ mice and it was absent in *Tp53*$^{\Delta IEC}$ and *Mir34a*$^{\Delta IEC}$*Tp53*$^{\Delta IEC}$ mice (Figure 14B). *Mir34*$^{Fl/Fl}$/*Tp53*$^{Fl/Fl}$ mice were used as controls. To induce sporadic CRC, 6-10 week old mice were treated weekly with the carcinogen Azoxymethane (AOM), which is known to induce activating *β-catenin* mutations (Takahashi et al., 2000), for a period of 6 weeks as described previously (Schwitalla et al., 2013) (Figure 14C).

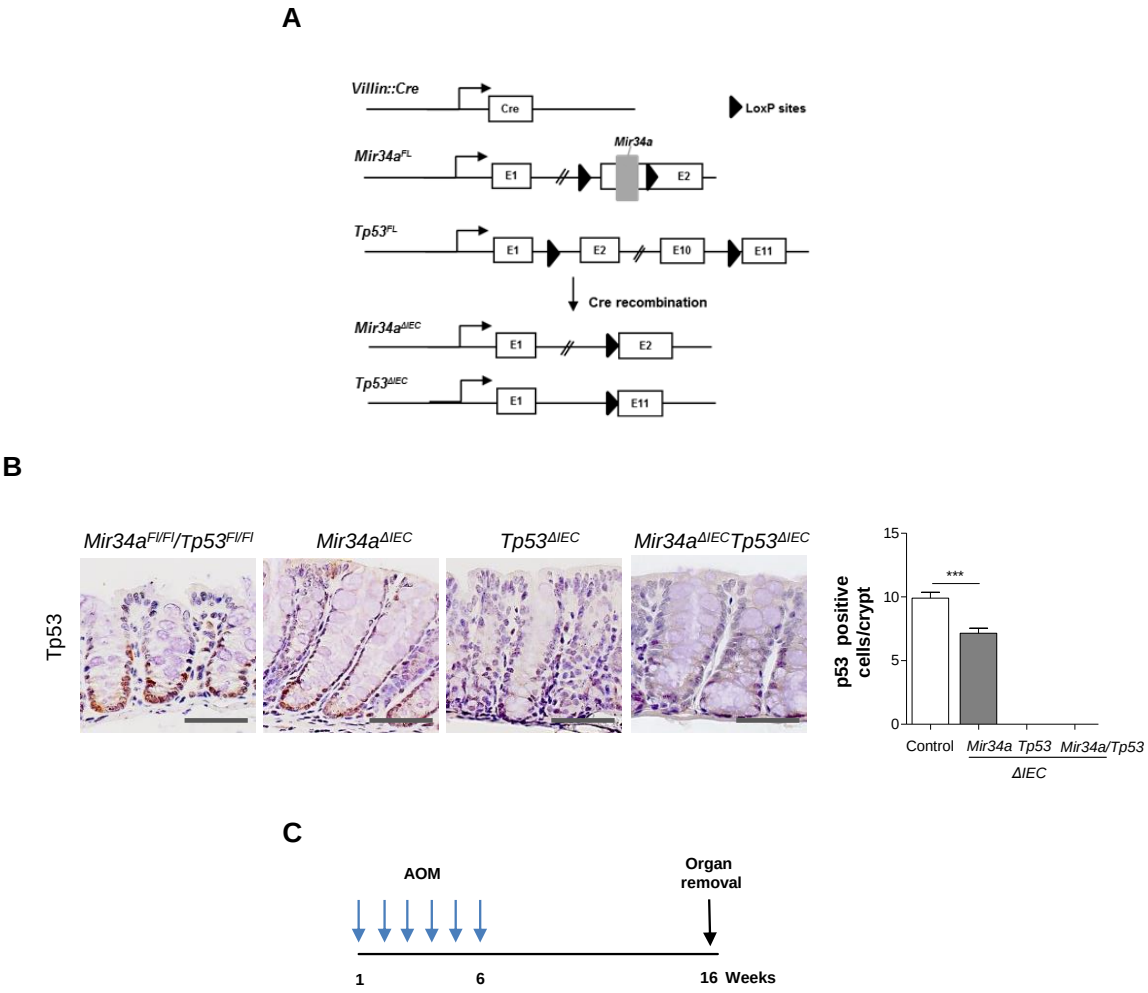

Figure 14. Strategy for IEC-specific deletion of *Mir34a/Tp53* and treatment scheme employed for generating sporadic CRCs in mice.
(A) Schematic illustration of the genetic strategy employed for intestinal epithelial cell (IEC) specific deletion of *Mir34a* and *Tp53*. LoxP sites are indicated by triangles. Open rectangles represent exons. Arrows indicate the transcriptional start sites. **(B)** 8 hours after i.p. AOM injection (10mg/kg) intestinal tissue was isolated from the indicated mice and 2 µM FFPE sections were prepared. Detection of Tp53 in normal colon epithelium by IHC. Number of positive cells was determined in ≥50 crypts per mouse (n=2 mice for each genotype). Mean values ±SEM are provided. Mean values ±SEM are provided, $^{*}P < 0.05$, $^{***}P < 0.001$ by Student´s t-test. **(C)** Scheme for inducing sporadic CRCs by weekly i.p. injection of mice with AOM (10 mg/kg).

16 weeks after the initial treatment all *Mir34a*$^{\Delta IEC}$*Tp53*$^{\Delta IEC}$ mice had already succumbed to advanced CRC formation with ascites, whereas only ~60% of *Tp53*$^{\Delta IEC}$ mice succumbed to CRCs by 24 weeks. At this time-point none of the *Mir34a*$^{Fl/Fl}$/*Tp53*$^{Fl/Fl}$ and *Mir34a*$^{\Delta IEC}$ mice displayed any complications due to CRC formation (Figure 15A).

Deletion of *Mir34a* or *Tp53* increased the number and size of colonic tumors (Figure 15B, C, and D). Combined deletion of *Mir34a* and *Tp53* further increased these effects. Moreover, the size distribution of tumors was skewed towards larger tumors in $Mir34a^{\Delta IEC}Tp53^{\Delta IEC}$ mice (Figure 15E). None of the analyzed mice showed tumors in other organs. Taken together, these results show that *Mir34a* and *Tp53* cooperatively suppress colorectal tumorigenesis.

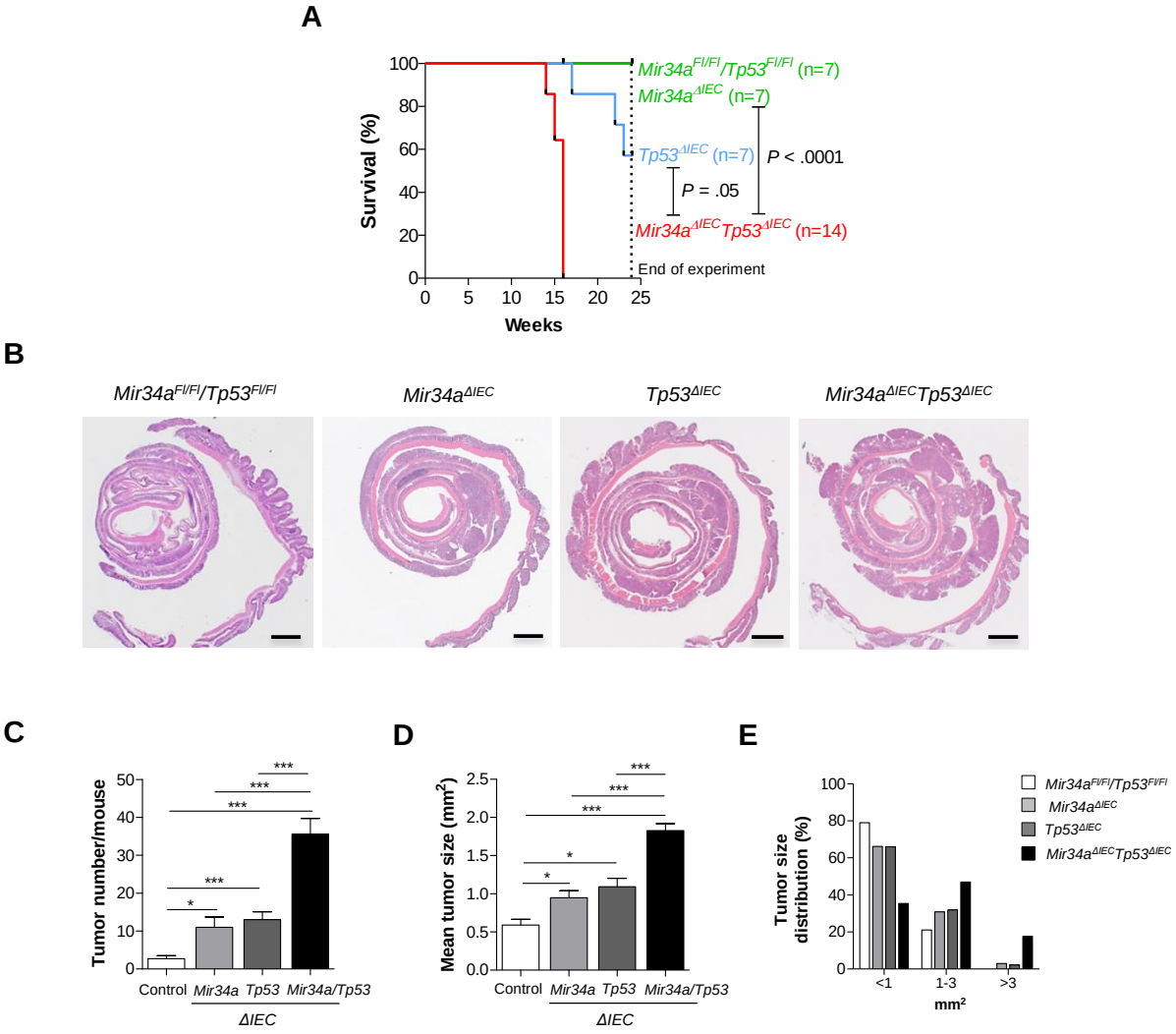

Figure 15. *Mir34a* and *Tp53* cooperatively suppress CRC initiation, growth, invasion and metastasis.

(A) Kaplan-Meier survival analysis of mice with the indicated genotypes. Significance was calculated by a log-rank test. **(B)** Representative morphology of intestinal tumors 16 weeks after initial AOM injection. Scale bars represent 1 mm. **(C)** Tumor incidence and **(D)** mean size in mice with the indicated genotypes (n=7 per genotype) **(E)** Size distribution of tumors. C-E: 7 mice of each genotype were sacrificed at week 16. Mean values ±SEM are provided, $^{*}P < 0.05$, $^{***}P < 0.001$ by Student´s t-test. "Control" corresponds to $Mir34a^{Fl/Fl}/Tp53^{Fl/Fl}$ mice.

Whereas *Mir34a*$^{Fl/Fl}$/*Tp53*$^{Fl/Fl}$ and *Mir34a*$^{\Delta IEC}$ mice did not display invasive tumors, colonic tumors invaded into the submucosa in *Tp53*$^{\Delta IEC}$ and *Mir34a*$^{\Delta IEC}$*Tp53*$^{\Delta IEC}$ mice (Figure 16A). Invasion was more pronounced in the *Mir34a*$^{\Delta IEC}$*Tp53*$^{\Delta IEC}$ mice than in *Tp53*$^{\Delta IEC}$ mice (Figure 16B). In addition, only CRCs in *Mir34a*$^{\Delta IEC}$*Tp53*$^{\Delta IEC}$ mice showed peritoneal invasion (Figure 16C). Therefore, advanced tumors with obstructive growth and aggressive invasion into the peritoneal cavity in *Mir34a*$^{\Delta IEC}$*Tp53*$^{\Delta IEC}$ mice might explain their shortened survival when compared to mice with other genotypes. Notably, only *Mir34a*$^{\Delta IEC}$*Tp53*$^{\Delta IEC}$ mice showed lymph node metastasis by week 16 (Figure 16A-C). In a previous report, lymph node metastases in *Tp53*$^{\Delta IEC}$ mice could only be detected by week 24, whereas after 16 and 20 weeks primary tumor were only associated with local invasion (Schwitalla et al., 2013). Therefore, the combined inactivation of *Mir34a* and *Tp53* enhances invasion and accelerates lymph-node metastasis of colonic tumors.

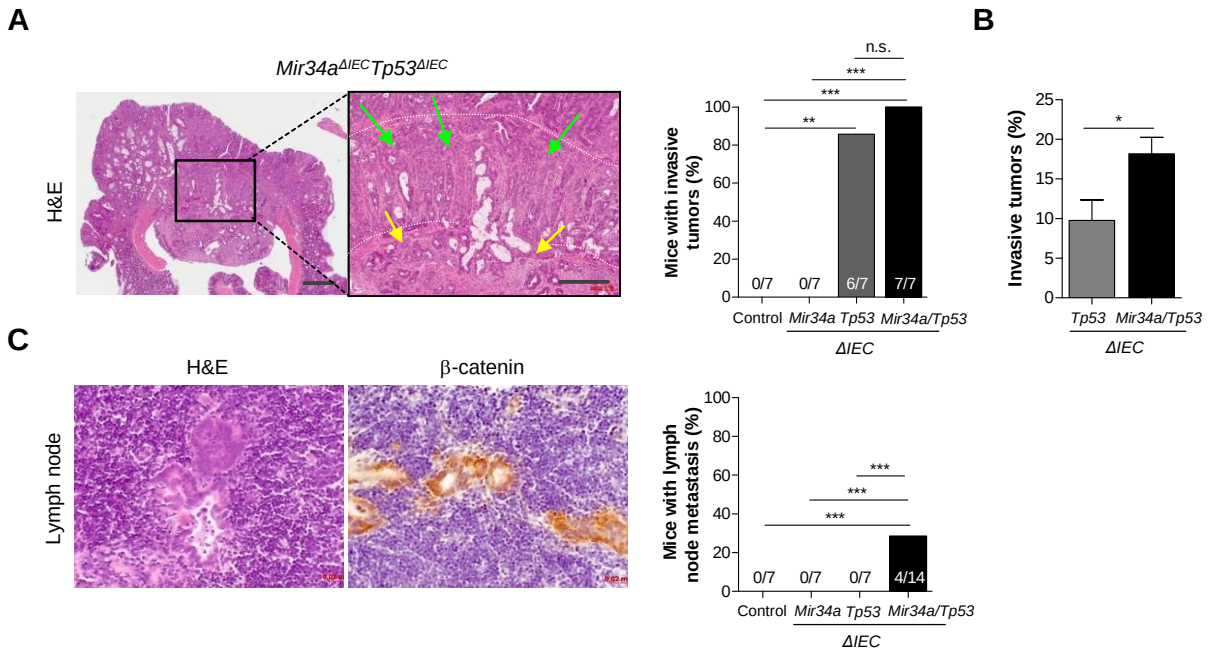

Figure 16. Combined *Mir34a* and *Tp53* deletion enhances invasion and metastasis.

(A) (left) H&E stained sections. Detection of tumor cell invasion. White dashed line: lamina muscularis mucosae as the border of primary tumor and invasive area green arrows: invasion to submucosa; yellow arrows invasion to muscularis externa. Scale bars: 50 µm and 100 µm (insert). (right) Quantification of tumor invasion (n=7 mice per genotype). **(B)** Quantification of invasive tumors (91 tumors from *p53*$^{\Delta IEC}$ mice and 249 tumors from *Mir34a*$^{\Delta IEC}$*p53*$^{\Delta IEC}$ mice were evaluated, n=7 mice per genotype). **(C)** (left) Detection of metastasized cells in lymph nodes of *Mir34a*$^{\Delta IEC}$*Tp53*$^{\Delta IEC}$ mice. (right) Frequency of lymph-node metastasis. Mean values ±SEM are provided, $^{*}P$ <0.05, $^{**}P$ <0.01, $^{***}P$ <0.001 by Student´s t-test. (A) Significance was calculated by Fisher´s exact test, p values are provided as $^{**}P$ < 0.01, $^{***}P$ <0 .001. “Control” corresponds to *Mir34a*$^{Fl/Fl}$/*Tp53*$^{Fl/Fl}$ mice.

4.4 Enhanced proliferation in the presence of DNA damage in *Mir34a/Tp53*-deficient IECs

The genotoxic agent AOM induces DNA damage in the colonic epithelium of rodents and Tp53-dependent apoptosis in IECs (Toft et al., 1999). Previously, the increased tumor formation observed in AOM-treated *Tp53*$^{\Delta IEC}$ mice was linked to a decrease in apoptosis (Schwitalla et al., 2013). Here, the combined loss of *Tp53* and *Mir34a* further reduced the frequency of IECs undergoing apoptosis 8 hours after treatment with AOM (Figure 17A). Moreover, the frequency of epithelial cells positive for the DNA damage marker phosphorylated γ-H2AX and cellular proliferation was increased in colonic crypts of *Mir34a*$^{\Delta IEC}$*p53*$^{\Delta IEC}$ mice when compared to crypts lacking only *Tp53* or *Mir34a* (Figure 17B-C). Taken together, these results suggest that the combined deficiency of *Mir34a* and *Tp53* allows IECs to escape DNA damage-induced apoptosis and cell cycle arrest. The continuing proliferation of *Mir34a*/*Tp53*-deficient cells that have acquired DNA damage may not allow adequate repair and ultimately lead to an increased number of mutations in oncogenes and tumor-suppressor genes which may cause the increased rate of colonic tumor initiation of *Mir34a*$^{\Delta IEC}$*Tp53*$^{\Delta IEC}$ mice.

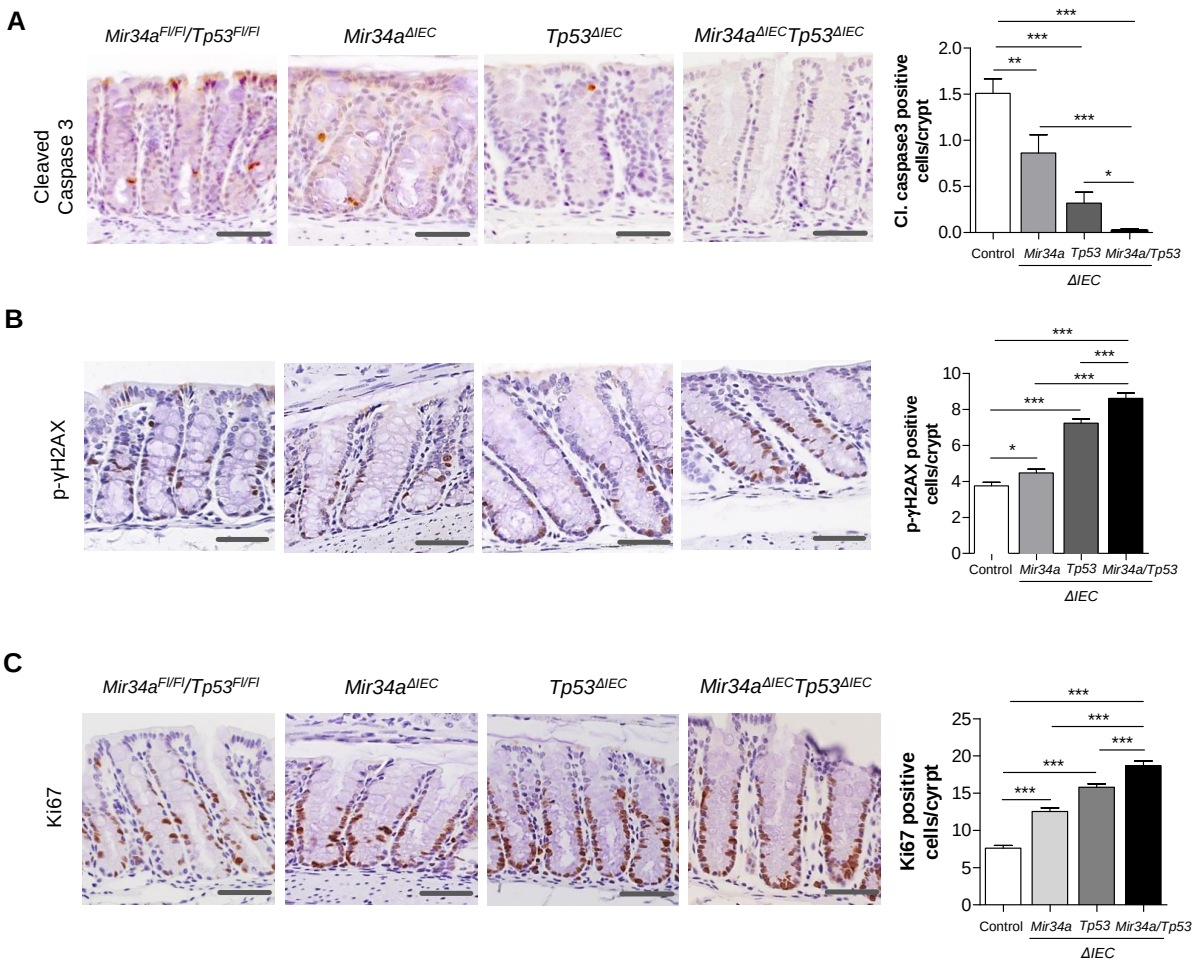

Figure 17. Enhanced proliferation in the presence of DNA damage in *Mir34a/Tp53*-deficient IECs.
8 hours after i.p. AOM injection (10mg/kg) intestinal tissue was isolated from the indicated mice and 2 µM FFPE sections were prepared.
(A) Detection of apoptosis in normal intestinal epithelium by cleaved caspase 3 IHC. Number of positive cells was determined in ≥50 crypts per mouse (n=2 mice for each genotype). **(B)** Detection of phosphorylated γH2AX (p-γH2AX) as in A. **(C)** Detection of Ki67-positive cells as in A. (A-C) Mean values ±SEM are provided, **P* < 0.05, ***P* <0.01, ****P* < 0.001 by Student´s t-test. Scale bars: 50 µm. "Control" corresponds to *Mir34a*$^{Fl/Fl}$/*Tp53*$^{Fl/Fl}$ mice.

4.5 Enhanced survival, proliferation and stromal infiltration in *Mir34a/Tp53*-deficient CRCs

Since the combined deletion of *Mir34a* and *Tp53* in IECs enhanced the size of colonic tumors, we hypothesized that this may be due to increased tumor cell proliferation and decreased apoptosis. Indeed, colonic tumors from *Mir34a*$^{\Delta IEC}$*Tp53*$^{\Delta IEC}$ mice displayed the highest proliferation and lowest apoptosis rates when compared to tumors from mice with the other genotypes (Figure 18A, B).

Since enhanced infiltration of tumors with bacteria and macrophages has previously been implicated in CRC progression (Schwitalla et al., 2013), we determined whether these parameters are affected by combined deletion of *Tp53* and *Mir34a*. Indeed, infiltration of F4/80-positive macrophages was highest at the invasion front of tumors from *Mir34a*$^{\Delta IEC}$*Tp53*$^{\Delta IEC}$ mice and showed an intermediate increase in *Tp53*$^{\Delta IEC}$ tumors when compared to tumors from *Mir34a*$^{Fl/Fl}$/*Tp53*$^{Fl/Fl}$ and *Mir34a*$^{\Delta IEC}$ mice (Figure 18C). Furthermore, infiltration by CD3^{+}T-cells was increased in tumors of *Mir34a*$^{\Delta IEC}$, *Tp53*$^{\Delta IEC}$ and *Mir34a*$^{\Delta IEC}$*Tp53*$^{\Delta IEC}$ mice when compared to *Mir34a*$^{Fl/Fl}$/*Tp53*$^{Fl/Fl}$ mice (Figure 18D).

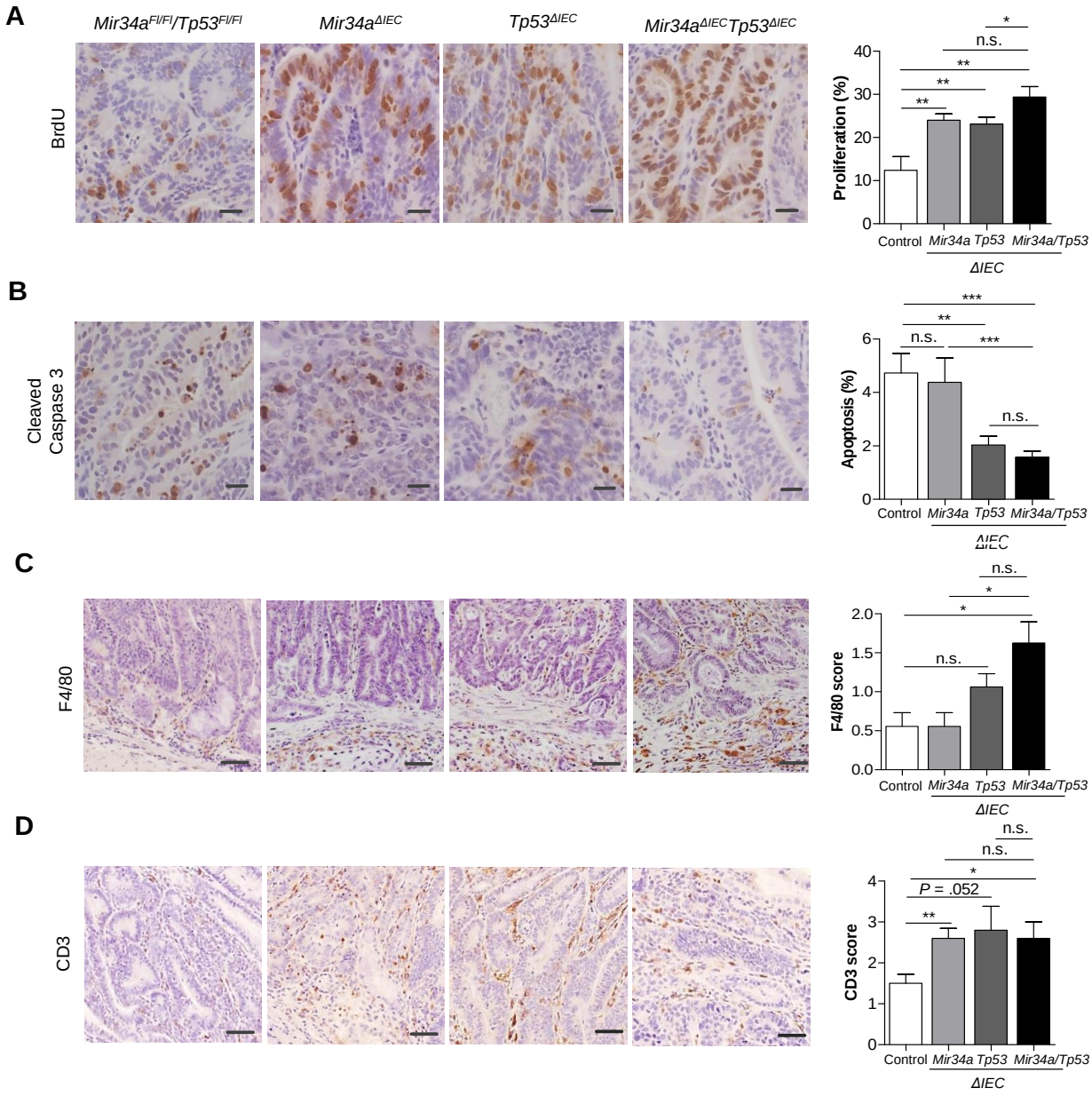

Figure 18. Enhanced survival, proliferation and infiltration in *Mir34a/Tp53*–deficient tumors.

(A) Proliferation of tumor cells was determined by BrdU incorporation. (left panels) Representative IHC detection of BrdU incorporation. (right) Quantification of proliferation (n=5 mice for each genotype). **(B)** Determination of apoptosis of tumor cells by IHC for cleaved caspase 3. (left) Representative IHC detection of cleaved caspase 3. (right) Quantification of apoptosis (n≥5 mice for each genotype). **(C)** (left) Representative IHC detection of F4/80^{+}macrophages at the invasion front of tumors. (right) Quantification of F4/80-positive cells in CRCs (n≥3 mice per genotype). **(D)** (left) Representative IHC staining of CD3^{+}T-cells in tumors. (right) Quantification of CD3^{+}T-cells in tumors (n≥3 mice per genotype). (A-D) Mean values ±SEM are provided. n.s. not significant, **P* <0 .05, ***P* < 0.01, ****P* <0.001 by Student´s t-test. Scale bars: 50 µm. "Control" corresponds to *Mir34a*$^{Fl/Fl}$/*Tp53*$^{Fl/Fl}$ mice.

Notably, tumors from *Mir34a*$^{\Delta IEC}$*Tp53*$^{\Delta IEC}$ mice showed increased bacterial infiltration when compared to tumors from *Mir34a*$^{Fl/Fl}$/*Tp53*$^{Fl/Fl}$, as well as *Tp53*- and *Mir34a*-deficient mice, which displayed an intermediate degree of infiltration (Figure 19A). Therefore, combined *Mir34a* and *Tp53* inactivation presumably enhances a barrier-defect. In line with the most pronounced bacterial infiltration, the mRNA levels of tight junction components *Claudin15*, *Claudin6* and *Mucin5* were down-regulated in *Mir34a*$^{\Delta IEC}$*Tp53*$^{\Delta IEC}$ CRCs to a larger extent than in the single knock-out tumors (Figure 19B-D). On the other hand, expression of *Mucin1*, whose elevated expression has been associated with a higher tumor stage in CRC (Lugli et al., 2007), was up-regulated in *Mir34a*$^{\Delta IEC}$*Tp53*$^{\Delta IEC}$ CRCs (Figure 19E).

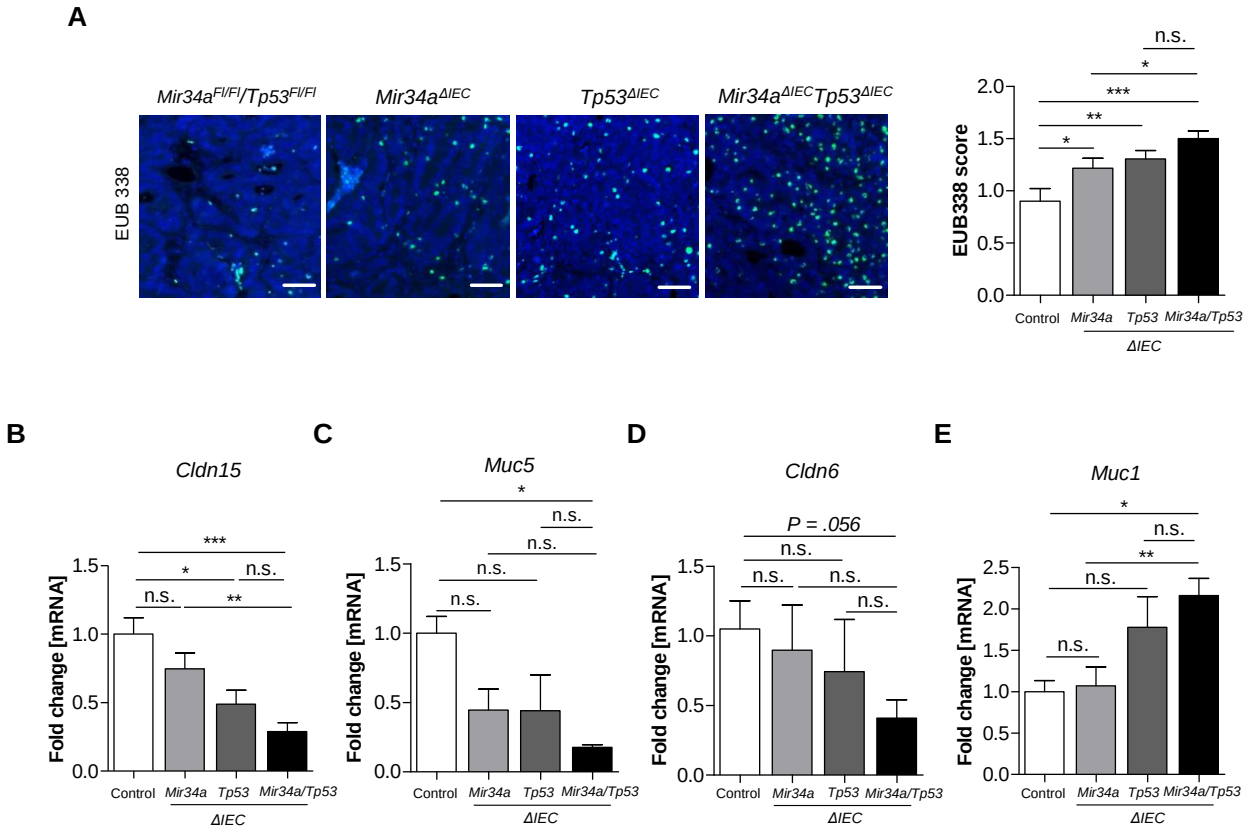

Figure 19. Effect of *Mir34a/Tp53* inactivation in tumors on bacterial infiltration and expression of tight junction components.
(A) (left) Detection of microbes using FISH with a FITC-labeled universal eubacteria probe EUB 338. (right) Quantification of EUB338 scoring (n≥3 mice per genotype). **(B-E)** qPCR analysis of *Cldn15*, *Muc5*, *Cldn6* and *Muc1* mRNAs in tumors of indicated genotypes (n≥5 tumors per genotype). Mean values ±SEM are provided, n.s. not significant, **P* < 0.05, ****P* <0 .001 by Student´s t-test. "Control" corresponds to *Mir34a*$^{Fl/Fl}$/*Tp53*$^{Fl/Fl}$ mice.

Interestingly, down-regulation of *Claudin15*, *Claudin6* and *Mucin5* mRNA expression was also observed in normal IECs of *Mir34a*$^{\Delta IEC}$, *Tp53*$^{\Delta IEC}$, *Mir34a*$^{\Delta IEC}$*Tp53*$^{\Delta IEC}$ mice not treated with AOM (Figure 20A-C). However, colonic epithelia of these mice did not display bacterial infiltration (Figure 20D). Therefore, the down-regulation of these genes is not sufficient to cause a barrier defect in normal colon epithelium. Further changes that occur during tumor progression (e.g. EMT) may cooperate with the down-regulation of the barrier components and thereby contribute to the bacterial infiltration. In addition, the enhanced bacterial infiltration in *Mir34a*$^{\Delta IEC}$*Tp53*$^{\Delta IEC}$ mice might alter the recruitment of myeloid cells. The resulting inflammatory tumor microenvironment may further promote tumor progression.

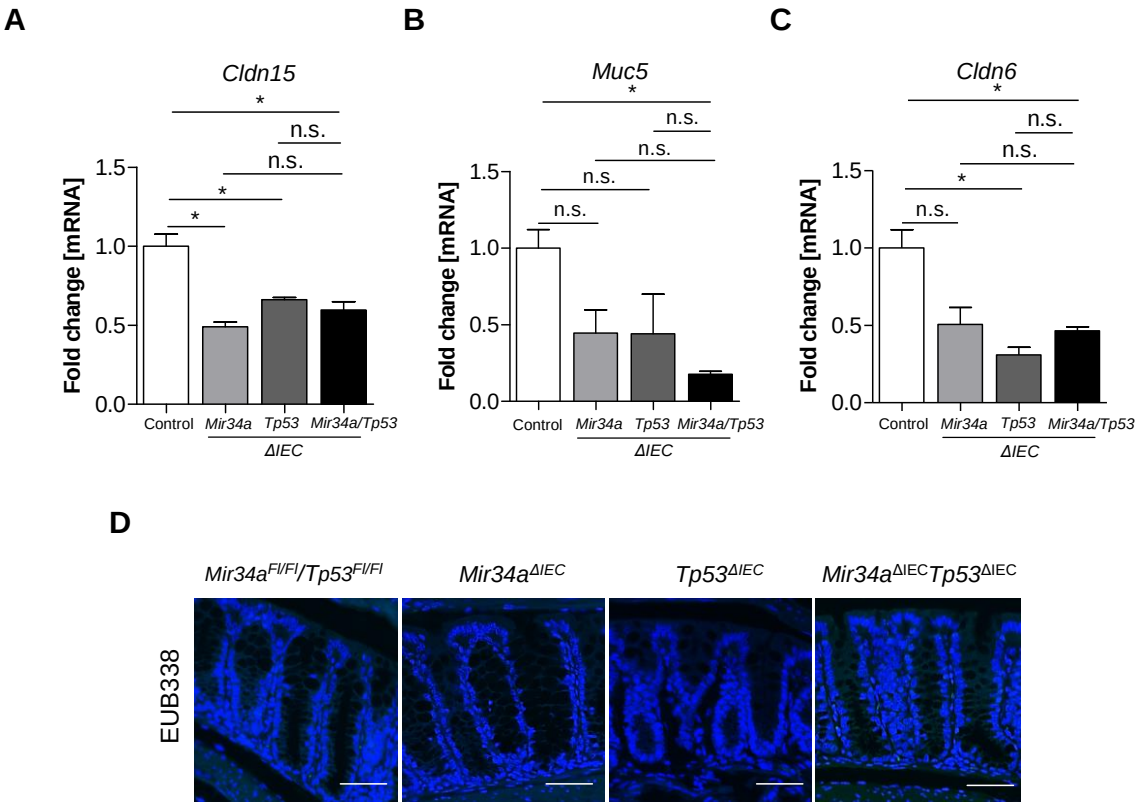

Figure 20. Effect of *Mir34a/Tp53* inactivation in normal colon epithelium on bacterial infiltration and expression of tight junction components.
(A-C) qPCR analysis of *Cldn15*, *Muc5*, *Cldn6* and *Muc1* mRNAs in normal colon epithelium of indicated genotypes (n≥5 tumors per genotype). **(D)** (left) Detection of microbes using FISH with a FITC-labeled universal eubacteria probe EUB 338. (right) Quantification of EUB338 scoring (n=2 mice per genotype). Mean values ±SEM are provided, n.s. not significant, **P* < 0.05 by Student´s t-test. "Control" corresponds to *Mir34a*$^{Fl/Fl}$/*Tp53*$^{Fl/Fl}$ mice.

4.6 RNA expression profiles of *Mir34a*$^{\Delta IEC}$*Tp53*$^{\Delta IEC}$-deficient tumors

In order to identify mediators of the enhanced CRC progression resulting from combined inactivation of *Mir34a and Tp53,* we compared the mRNA expression profiles of AOM-induced colonic tumors derived from *Mir34a*$^{Fl/Fl}$/*Tp53*$^{Fl/Fl}$, *Mir34a*$^{\Delta IEC}$, *Tp53*$^{\Delta IEC}$ and *Mir34a*$^{\Delta IEC}$*Tp53*$^{\Delta IEC}$ mice. For each genotype RNAs obtained from 9 tumors derived from three mice were subjected to RNA-Seq. Since we had observed an increase in the degree of tumor aggressiveness from *Mir34a*$^{Fl/Fl}$/*Tp53*$^{Fl/Fl}$ over *Mir34a*$^{\Delta IEC}$ *and Tp53*$^{\Delta IEC}$ to *Mir34a*$^{\Delta IEC}$*Tp53*$^{\Delta IEC}$ mice, we aimed to identify mRNAs that were increasingly expressed in this order and would therefore be potentially associated with increased aggressiveness by performing a t-test for trend. Thereby, 1284 up- and 1372 down-regulated mRNAs matching to this pattern were identified (P <0.05; Figure 21A). In addition, principle component analysis of mRNA expression profiles showed a good concordance between the three samples sequenced for each genotype (Figure 21B). Gene Set Enrichment Analyses (GSEA) revealed that up-regulated mRNAs were enriched in Hallmark MSigDB signatures associated with tumor initiation and progression, such as c-Myc targets, hypoxia, epithelial mesenchymal transition (EMT), inflammatory response and Kras signaling (Figure 21C). As expected, down-regulated mRNAs displayed the most significant enrichment within the Tp53 pathway hallmark MSigDB signature (Figure 21D). Comparison of the signature of RNAs significantly up-regulated in *Mir34a*$^{\Delta IEC}$*Tp53*$^{\Delta IEC}$ tumors (t-test for trend; P <0.05) with the consensus molecular subtypes (CMS) of human CRC (Dienstmann et al., 2017; Guinney et al., 2015) represented in the TCGA database showed highest concordance with the CMS4 subtype, which displays mesenchymal characteristics associated with a high metastatic potential and the poorest prognosis of all CRC subtypes (Figure 21E). In accordance with an enrichment of c-Myc targets among up-regulated mRNAs, *c-Myc* mRNA expression was most significantly up-regulated in tumors from *Mir34a*$^{\Delta IEC}$*Tp53*$^{\Delta IEC}$ mice and to a lower degree in *Tp53*-deficient tumors (Figure 21F).

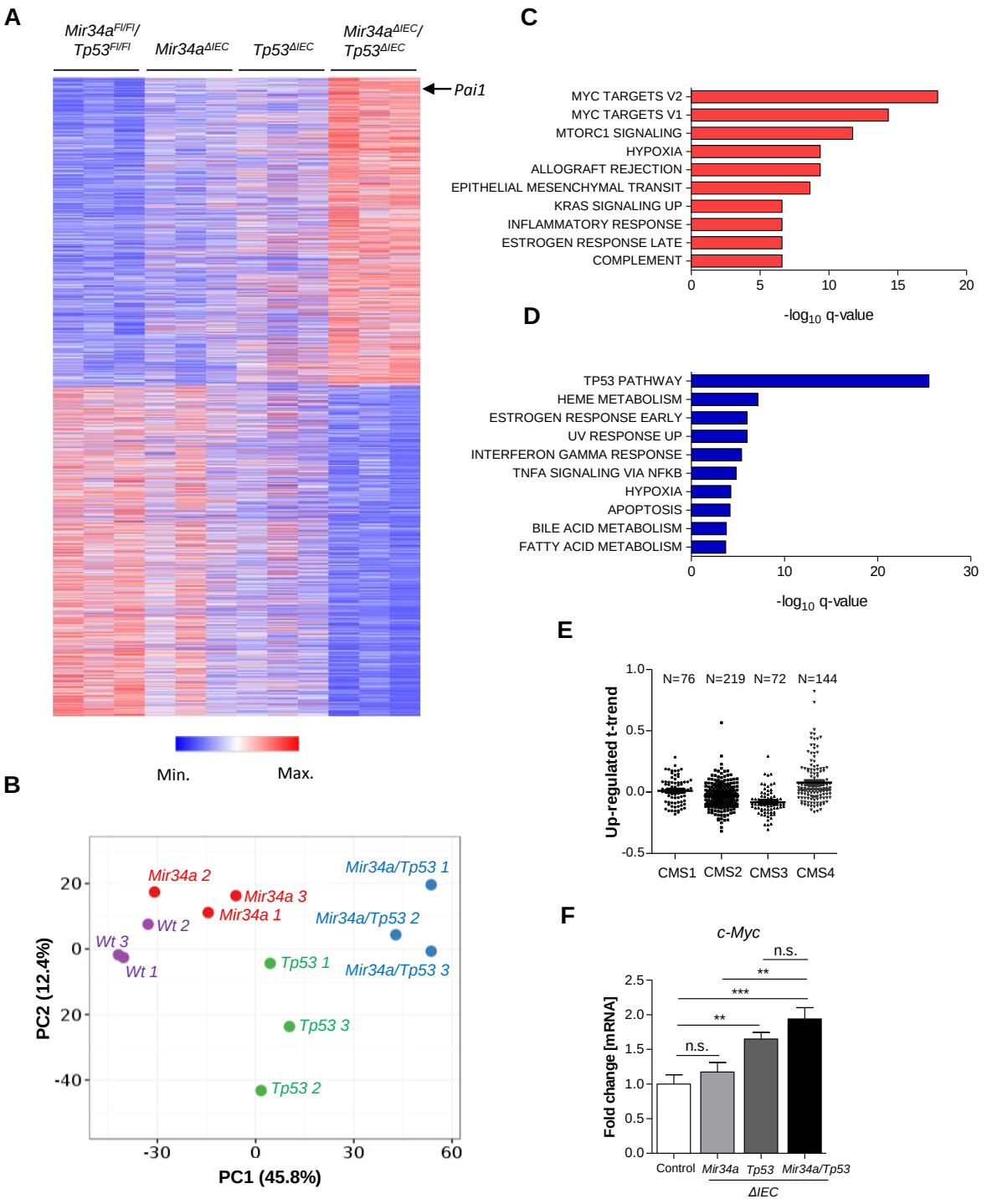

Figure 21. RNA expression profiles of *Mir34a*$^{\Delta IEC}$ and/or *Tp53*$^{\Delta IEC}$–deficient tumors.
(A) Heat-map of mRNA expression in colon tumors with the indicated genotypes. RNAs that displayed a significant (t-test for trend; **P* <0.05) up- or down-regulation from *Mir34a*$^{FI/FI}$/*Tp53*$^{FI/FI}$ to *Mir34a*$^{\Delta IEC}$*Tp53*$^{\Delta IEC}$ mice are shown. **(B)** Principal component analysis of RNA expression in tumors from mice with the indicated genotypes. **(C-D)** GSEA analyzes of the RNAs that displayed a significant (t-test for trend; **P* < 0.05) up- (C) or down-regulation (D) in tumors from *Mir34a*$^{FI/FI}$/*Tp53*$^{FI/FI}$ to *Mir34a*$^{\Delta IEC}$*Tp53*$^{\Delta IEC}$ mice. The ten MSigDB Hallmark gene sets with the most significant association are shown. **(E)** Association of signature of mRNAs up-regulated in colon tumors of *Mir34a*$^{\Delta IEC}$*Tp53*$^{\Delta IEC}$ mice with the consensus molecular subtypes (CMS) of CRC in TCGA CRC datasets. N is number patients

in each CMS group. Expression of the mRNA signature was calculated as average of z-score normalized expression of all mRNAs from the signature in the TCGA CRC dataset. **(F)** qPCR analysis of c-*Myc* mRNA in tumors of mice with the indicated genotypes (n≥7 tumors per genotype). Mean values ±SEM are provided, n.s. is not-significant, ***P* < 0.01, ****P* < 0.001 by Student´s t-test. "Control" corresponds to *Mir34a*$^{Fl/Fl}$/*Tp53*$^{Fl/Fl}$ mice. Figures **(A-E)** were generated by Dr. Matjaz Rokavec.

4.7 IL6/Stat3 pathway activation in CRCs of *Mir34a*$^{\Delta IEC}$*Tp53*$^{\Delta IEC}$ mice

The comparison of expression profiles of *Mir34a*$^{Fl/Fl}$/*Tp53*$^{Fl/Fl}$ and *Mir34a*$^{\Delta IEC}$*Tp53*$^{\Delta IEC}$ CRCs showed a significant enrichment of the MSigDB IL6/IL6R/Stat3 pathway signature in *Mir34a*$^{\Delta IEC}$*Tp53*$^{\Delta IEC}$ tumors (Figure 22A). Since we have previously shown that Mir34a suppresses colitis-associated colon-cancer (CAC) progression via directly targeting the IL6 receptor (IL6R) and thereby inhibiting Stat3 activity (Rokavec et al., 2014b), we further analyzed the effects of *Mir34a* and/or *Tp53* deletion on the IL6R/Stat3 pathway in sporadic CRCs. By qPCR analysis we confirmed that mRNA levels of *IL6*, *IL11* and *IL6Rα* were significantly increased in *Mir34a*$^{\Delta IEC}$*Tp53*$^{\Delta IEC}$ mice tumors when compared to tumors from *Mir34a*$^{Fl/Fl}$/*Tp53*$^{Fl/Fl}$, *Mir34a*$^{\Delta IEC}$ and *Tp53*$^{\Delta IEC}$ mice (Figure 22B). Moreover, the levels of phosphorylated and therefore activated Stat3 protein were increased in *Tp53*-deficient tumors and further increased in *Mir34a/Tp53*-deficient tumors (Figure 22C). In addition, key mediators of EMT, such as *Snail* and *Zeb1*, as well as EMT effectors, as *Vimentin*, were up-regulated in *Mir34a/Tp53*-deficient tumors (Figure 22D). SNAIL expression was presumably caused by STAT3 activation, since SNAIL represents a known target of STAT3 (Saitoh et al., 2016). Since SNAIL is also a target of miR-34a (Siemens et al., 2011), the loss of *Mir34a* may also directly contribute to the elevated levels of SNAIL. Taken together, the combined inactivation of *Mir34a* and *Tp53* synergistically activates the IL6R/Stat3 pathway to a larger degree than *Tp53* or *Mir34a* inactivation alone.

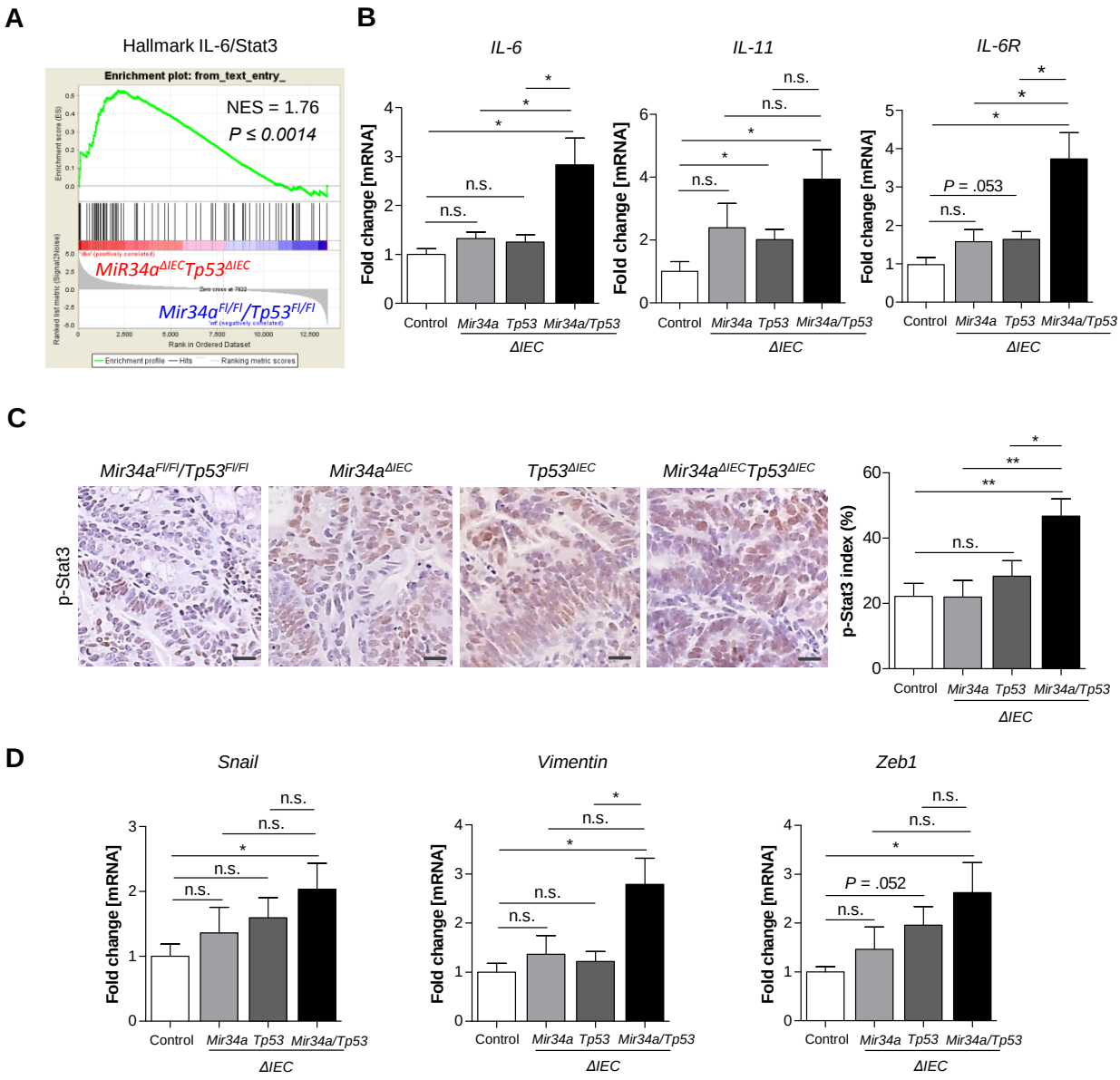

Figure 22. IL6/Stat3 pathway activation in CRCs of *Mir34a$^{\Delta IEC}$Tp53$^{\Delta IEC}$* mice.
(A) GSEA analyzes of the MSigDB Hallmark IL6/Stat3 mRNA signature in the colon tumors from *Mir34a$^{\Delta IEC}$Tp53$^{\Delta IEC}$* versus *Mir34a$^{Fl/Fl}$/Tp53$^{Fl/Fl}$* mice. Figure is generated by Dr. Matjaz Rokavec. **(B)** qPCR analysis of indicated mRNAs in colonic tumors (n≥5 mice per genotype). **(C)** (left) IHC detection of p-Stat3 in tumors of indicated genotypes. Scale bars represent 20 µm. (right) Quantification of p-Stat3-positive cells in CRCs. **(D)** PCR analysis of indicated mRNAs in colonic tumors (n≥5 mice per genotype). (B-D) Mean values ±SEM are provided, n.s. not-significant, **P* <0.05, ***P* < 0.01 by Student´s t-test. "Control" corresponds to *Mir34a$^{Fl/Fl}$/Tp53$^{Fl/Fl}$* mice.

4.8 IL6/Stat3 pathway blockade reduces tumor progression in *Mir34a*$^{\Delta IEC}$*Tp53*$^{\Delta IEC}$ mice

To determine the relevance of IL6R/Stat3 pathway up-regulation for the enhanced tumor progression in *Mir34a*$^{\Delta IEC}$*Tp53*$^{\Delta IEC}$ mice we employed the IL6R-neutralizing antibody MR16-1, which competitively inhibits binding of IL6 to both soluble and membrane-associated IL6R (Becker et al., 2004b). Three weeks after 6xAOM treatment mice received either weekly i.p. injections of 1 mg of MR16-1 antibody or, as a control, 1 mg of isotype-matched IgG1 for a period of 7 weeks (Figure 23A). Detection of reduced Stat3 phosphorylation in colonic tumors of MR16-1 treated animals confirmed the efficacy of IL6R inhibition (Figure 23B). Treatment with MR16-1 did not significantly affect the number of colonic tumors in *Mir34a*$^{\Delta IEC}$*Tp53*$^{\Delta IEC}$ mice (Figure 23C). However, MR16-1 treatment significantly reduced the average tumor size and cell proliferation in *Mir34a*$^{\Delta IEC}$*Tp53*$^{\Delta IEC}$ mice (Figure 23D, E). Importantly, treatment with MR16-1 decreased the size of invasive areas and the incidence of invasive tumors (Figure 23F). In addition, MR16-1 prevented the formation of lymph node metastases (Figure 23G). In summary, blockade of the IL6/IL6R/Stat3 pathway inhibited tumor cell proliferation, invasion and lymph-node metastasis of colonic tumors in *Mir34a*$^{\Delta IEC}$*p53*$^{\Delta IEC}$ mice. Therefore, activation of the IL6R/Stat3 pathway is required for tumor progression in CRC with combined inactivation of *Mir34a* and *Tp53.*

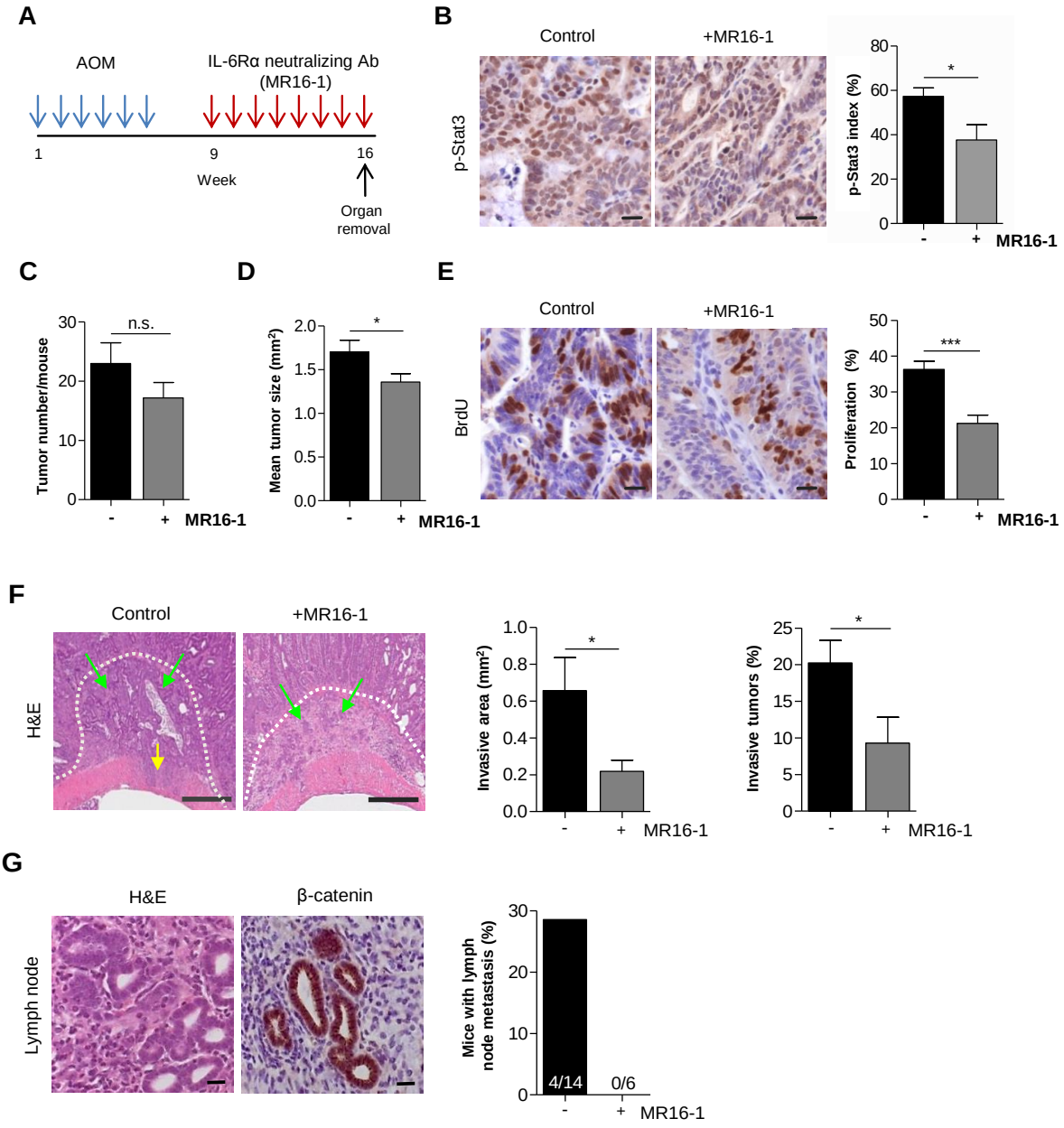

Figure 23. Blocking IL6/Stat3 pathway reduces CRC progression in *Mir34a/Tp53*-deficient mice.

(A) Scheme of therapeutic intervention with the IL6Rα-blocking antibody MR16-1 in the sporadic CRC mouse model. Mice received weekly i.p. injections of MR16-1 (1 mg) or, an IgG1 isotope control antibody (1 mg) 9 to 16 weeks after the initial AOM treatment. **(B)** (left) IHC detection of p-Stat3 in colonic tumors of *Mir34a*$^{\Delta IEC}$*Tp53*$^{\Delta IEC}$ mice with the indicated treatments. Scale bars represent 20 µm. (right) Quantification of p-Stat3-positive cells in tumors. **(C-D)** Tumor incidence and **(D)** mean tumor size (138 tumors from *Mir34a*$^{\Delta IEC}$*Tp53*$^{\Delta IEC}$ mice treated with IgG and 103 tumors from *Mir34a*$^{\Delta IEC}$*Tp53*$^{\Delta IEC}$ mice treated with MR16-1 were evaluated, n=6 mice for each group). **(E)** (left) IHC detection of BrdU incorporation in tumors of *Mir34a*$^{\Delta IEC}$*Tp53*$^{\Delta IEC}$ mice treated as indicated. Scale bars represent 20 µm. (right) Percentage of proliferation in tumors. **(F)** (left) Representative micrographs of tumor invasion in *Mir34a*$^{\Delta IEC}$*Tp53*$^{\Delta IEC}$ mice treated as indicated. White dashed line: *lamina muscularis mucosae* as the border between primary tumor and invasive area; green arrows: invasion to submucosa; yellow arrows invasion to *muscularis externa*. Scale

bars represent 500 µm. Quantification of mean invasive area (middle) and (right) invasion in tumors (11 tumors *Mir34a*$^{\Delta IEC}$*Tp53*$^{\Delta IEC}$ mice treated with IgG and 9 tumors from *Mir34a*$^{\Delta IEC}$*Tp53*$^{\Delta IEC}$ mice treated with MR16-1 were evaluated, n=6 mice for each treatment group). **(G)** (left) Detection of metastatic tumor cells in the lymph nodes of mice of indicated treatments. (right) Quantification of lymph node metastases in *Mir34a*$^{\Delta IEC}$*Tp53*$^{\Delta IEC}$ mice treated as indicated. Scale bars represent 20 µm. (B-F) Mean values ±SEM are provided, **P* <0 .05, ****P* < 0.001 by Student´s t-test, n.s. not-significant.

4.9 Association of elevated PAI-1 with CRC metastasis and poor survival

Among the genes up-regulated in colonic tumors after combined *Mir34a/Tp53*-deletion (Table 9.1) *Pai-1 (Serpine1)* showed the most pronounced correlation with the Hallmark gene sets of EMT and inflammatory response (Tables 9.6 and 9.7) and was also highly associated with the hypoxia related gene set (Table 9.5). *Pai-1* mRNA showed one of the most pronounced up-regulations in IECs *and* colonic tumors of *Mir34a*$^{\Delta IEC}$*Tp53*$^{\Delta IEC}$ mice (Figure 24A) as determined by mRNA-Seq and qPCR analysis (Figure 21A, 24A). Also Pai-1 protein levels were increasingly up-regulated in tumors from *Mir34a-, Tp53-* and *Mir34/Tp53*-deficient mice (Figure 24B). Notably, the *Pai-1* 3'-UTR contains a conserved Mir34a seed-matching sequence, suggesting that it represents a direct Mir34a target (Figure 24C). Indeed, transfection of murine CT26 CRC cells with *pre-miR-34a* oligonucleotides resulted in repression of *Pai-1* mRNA expression (Figure 24D). In addition, a reporter plasmid harboring the *Pai-1* 3'-UTR was repressed by ectopic *pre-miR-34a*, whereas a reporter with a mutant seed-match sequence was refractory to *pre-miR-34a* (Figure 24C, E). Taken together, these results show that *Pai-1* is a direct Mir34a target.

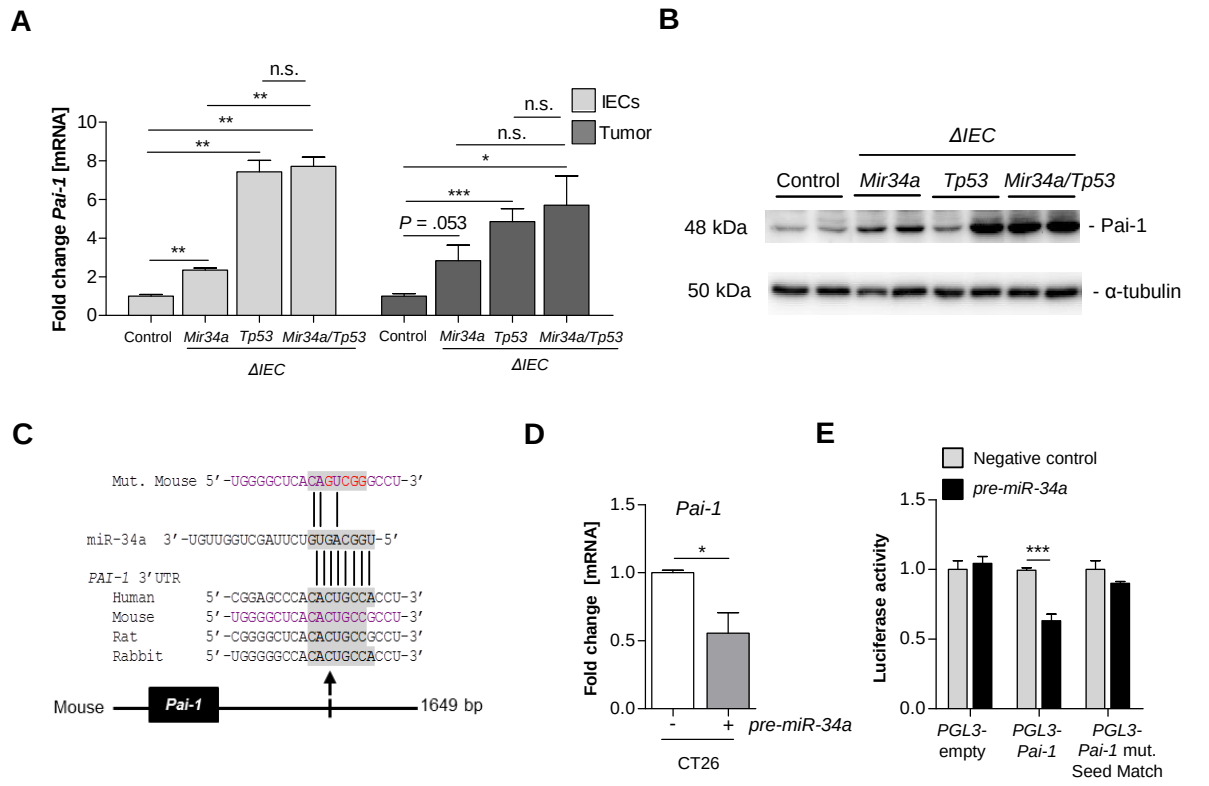

Figure 24. *Pai-1* is a direct miR-34a target.
(A) qPCR analysis of *Pai-1* mRNA expression (left) in intestinal epithelial cells (IECs) and (right) in CRCs (n≥5 tumors per genotype). Mean values ±SEM are provided, **P* < 0.05, ***P* < 0.01, ****P* < 0.001 by Student´s t-test. **(B)** Western blot analysis of Pai-1 protein from CRC lysates (n=2 tumors per genotype). **(C)** Schematic representation of the *Pai-1 (Serpine1)* 3'-UTR indicating the Mir34a seed-matching sequence and its phylogenetic conservation as determined by miRwalk target prediction algorithm. Above the mutations in the seed-matching sequence used in Figure 24E are indicated in red. **(D)** qPCR analysis of *Pai-1* mRNA expression in CT26 cells transfected with pre-miR-34a (n=3 per group). cDNA was provided by Dr. Nassim Bouznad. **(E)** Dual-reporter luciferase assay was performed in H1299 cells transfected with the indicated oligonucleotides and reporter constructs (n=3). "Control" corresponds to *Mir34a*$^{Fl/Fl}$/*Tp53*$^{Fl/Fl}$ mice.

To assess the association between PAI-1 expression and *MIR34A* methylation/*TP53* mutation in human tumors, we employed primary colon cancer samples of 61 patients in which *MIR34A* methylation and *TP53* mutational status had been previously determined (Siemens et al., 2013). In these samples *MIR34A* methylation and expression showed a significant, negative correlation (Siemens et al., 2013). Expression of PAI-1 was increased from *MIR34A* ^{M}CpG low/*TP53* wt over *MIR34A* ^{M}CpG high/*TP53* wt and *MIR34A* ^{M}CpG low/*TP53* mutant to *MIR34A* ^{M}CpG high/*TP53* mutant tumors (Figure 25A). In addition, PAI-1 expression was highest in the invasion front of *MIR34A* ^{M}CpG high/*TP53* mutant tumors. Therefore, the up-

regulation of PAI-1 is conserved between murine and human colorectal tumors that display combined *TP53* and *MIR34A* inactivation.

In order to determine whether elevated PAI-1 expression in colonic tumors is associated with clinical parameters in patients we analyzed the TCGA COAD (colon adenocarcinomas) and READ (rectal adenocarcinomas) database: *PAI-1* expression was significantly elevated in primary tumors from 48 CRC patients when compared to matched normal tissues (Figure 25B). Furthermore, PAI1 expression was significantly elevated in primary colorectal tumors from patients with local (nodal status pN2) or distant metastasis when compared to colorectal tumors without metastasis (Figure 26A, Figure 25C). *PAI-1* mRNA expression was highest in CRC tumors belonging to the mesenchymal subtype CMS4 within the TCGA CRC dataset (Figure 25D). In line with these results, *PAI-1* expression was also elevated in liver metastasis compared to matched primary, colonic tumors of 17 patients (Figure 25E). Furthermore, increased *PAI-1* expression in the primary colorectal tumors was associated with poor overall and relapse-free survival of 628 patients with colorectal adenocarcinomas represented in TCGA database and also in 4 additional, independent cohorts of CRC patients (Figure 25F, Figure 26B-F).

Taken together, these results show that elevated expression of *PAI-1* is associated with a mesenchymal-like cancer cell state, metastasis, and poor survival in human CRC. Therefore, PAI-1 may represent a clinically relevant prognostic marker for CRC.

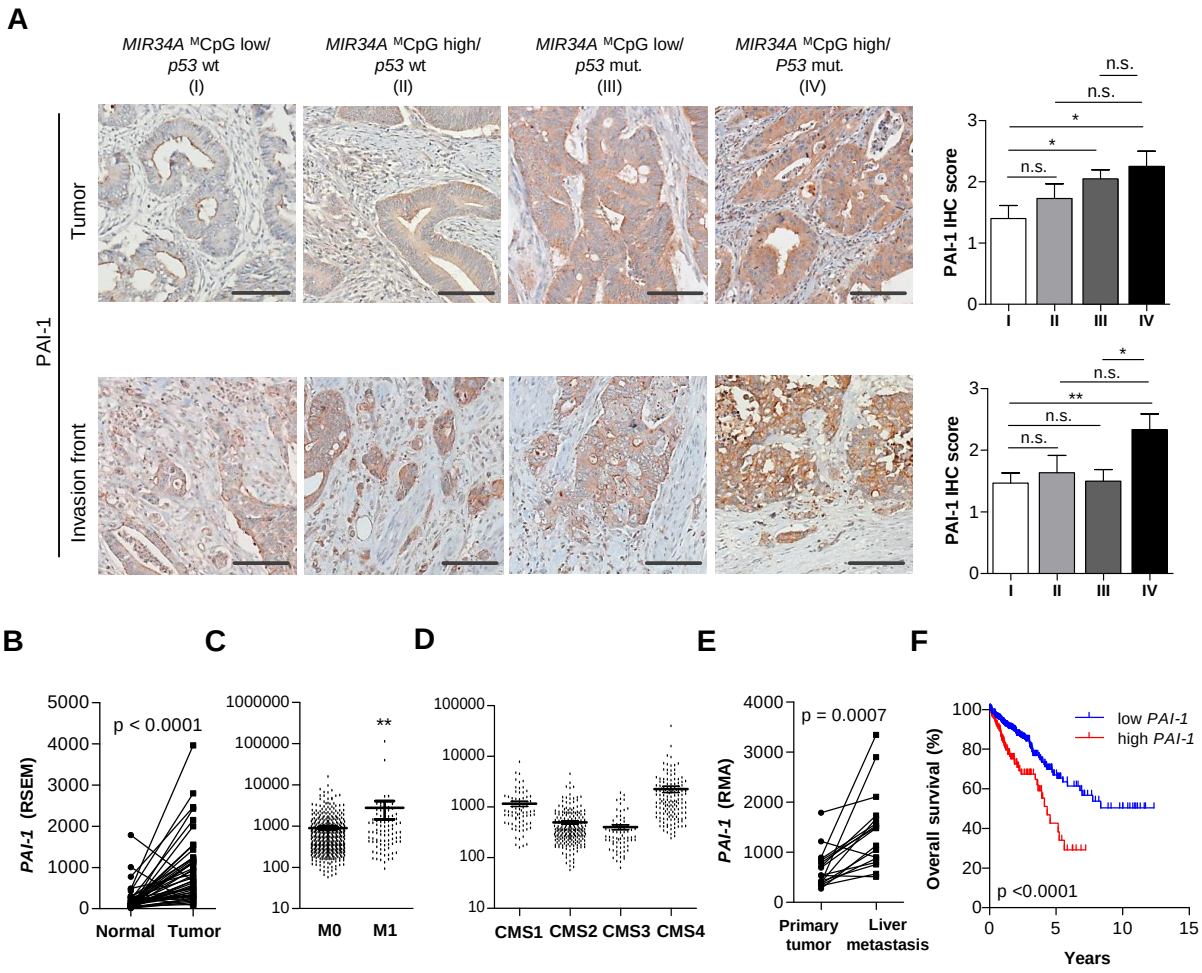

Figure 25. Altered PAI-1 expression in human primary colon carcinomas and association of *PAI-1* expression with different entities from TCGA COAD+READ CRC dataset.

(A) Determination of PAI-1 expression in human primary colon carcinomas by IHC in indicated groups of patients. Number of patients analyzed per each group is: Group I n=15, group II n=12, group III n=22 and group IV n=12. (Upper-panel) (left) Representative micrographs and (right) quantification of PAI-1 expression in tumors, (bottom-panel) similar analysis of the invasive front of the respective CRCs. Scale bars represent 100 µm. Mean values ±SEM are provided, **P*<0.05, ***P*<0.01 by Student´s t-test, n.s. not significant. **(B)** Expression of PAI-1 mRNA in paired samples from normal colonic tissue and CRC tumors from the TCGA CRC dataset (n=48). Significance calculated by paired-t-test. **(C)** Association of PAI-1 mRNA expression with distant metastasis (H) in the TCGA CRC dataset (n=628) comprising colon adenocarcinoma (COAD) and rectal adenocarcinoma (READ). **(D)** Association of PAI-1 mRNA expression with the consensus molecular subtypes (CMS) of colorectal cancer in TCGA COAD+READ CRC dataset (n=628). **(E)** PAI-1 expression in 17 pairs of primary colon cancer tumors and matched liver metastases (data from GSE14297). Significance calculated by paired-t-test. **(F)** Association of PAI-1 mRNA expression with overall survival in the TCGA CRC dataset (n=628). **(A)** Human primary colon carcinoma samples were provided by Prof. Thomas Kirchner and Prof. David Horst. Samples were stained by the diagnostics laboratory, Pathology Institute, LMU, Munich. Meryem Gülfem Öner-Ziegler evaluated the staining, made the pictures, and generated the figure with Prof. David Horst´s approval. (C, D) Values on y-axis are shown in log10 scale. Figures (B-F) were generated by Dr. Matjaz Rokavec.

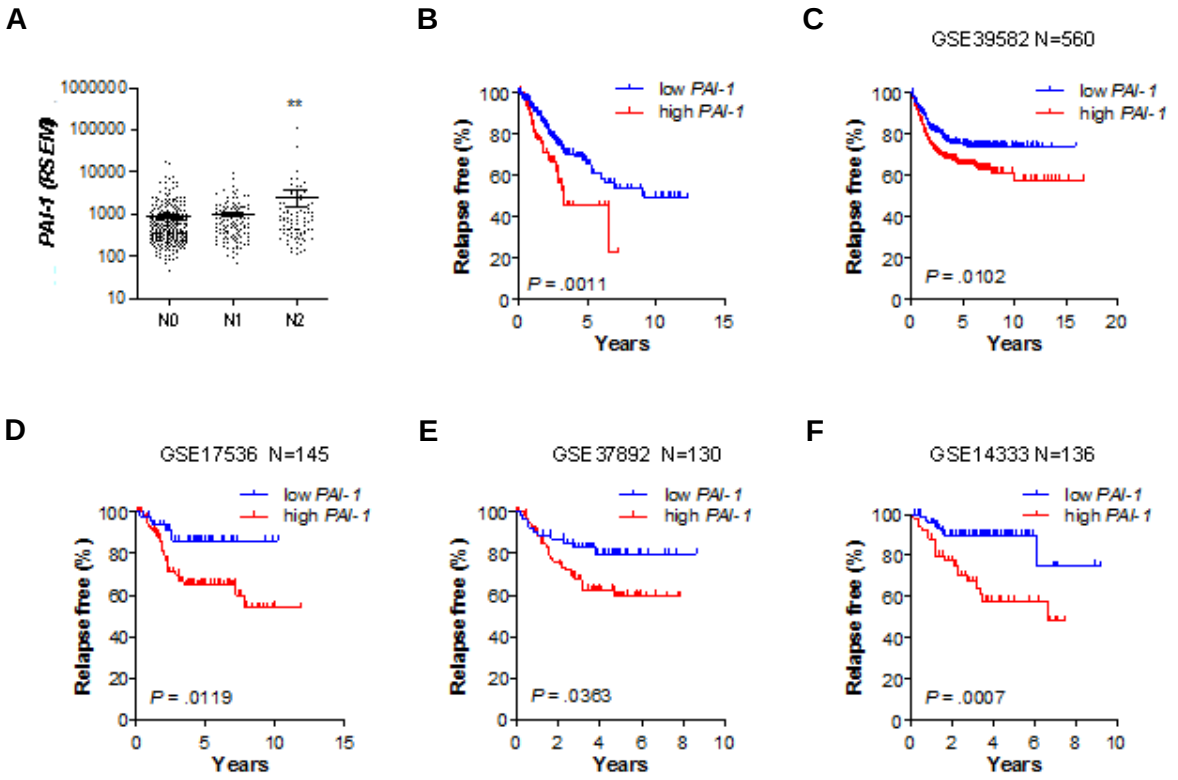

Figure 26. Elevated *PAI-1* mRNA expression is associated with local metastasis and poor survival in additional patient cohorts.
(A) Association of *PAI-1* mRNA expression with nodal status/local metastasis in the TCGA CRC dataset (N=628) comprising colon adenocarcinoma (COAD) and rectal adenocarcinoma (READ). Values on y-axis are shown in log10 scale. **(B)** Association of *PAI-1* mRNA expression with relapse free survival in the TCGA CRC dataset (N = 628). **(C-F)** Association of *PAI-1* mRNA expression with relapse free survival in four different CRC cohorts. Kaplan-Meier survival analysis was used in combination with a log-rank test. Expression and clinical data of GSE39582, GSE37892, GSE17536, and GSE14333 datasets was down- loaded from NCBI GEO (www.ncbi.nlm.nih.gov/geo). Figures (A-F) were generated by Dr. Matjaz Rokavec.

4.10 Targeting of Pai-1 inhibits initiation and progression of *Mir34a/Tp53*-deficient CRCs

To determine the relevance of Pai-1 up-regulation in colonic tumors of *Mir34a*$^{\Delta IEC}$*Tp53*$^{\Delta IEC}$ mice and its therapeutic value we employed Tiplaxtinin, a small drug inhibitor of Pai-1, which was described before (Elokdah, 2004). After treatment with AOM for 6 weeks *Mir34a*$^{\Delta IEC}$*Tp53*$^{\Delta IEC}$ mice were fed with Tiplaxtinin supplemented chow or with normal chow (as controls) starting from week 9 until week 16 (Figure 27A). Treatment with Tiplaxtinin reduced the incidence and size of colonic tumors in *Mir34a*$^{\Delta IEC}$*Tp53*$^{\Delta IEC}$ mice (Figure 27B-D), whereas it did not affect

the rate of apoptosis within these (Figure 27E). In addition, Tiplaxtinin treatment led to decreased cellular proliferation (Figure 27F), which may explain the reduced size of colonic tumors detected in treated *Mir34a*$^{\Delta IEC}$*Tp53*$^{\Delta IEC}$ mice. Moreover, Tiplaxtinin treatment decreased the invasive area of colonic tumors and prevented the formation of lymph node metastases in *Mir34a*$^{\Delta IEC}$*Tp53*$^{\Delta IEC}$ mice (Figure 27G-I).

In summary, inhibition of Pai-1 suppressed the enhanced tumor growth, invasion and lymph node metastasis of colonic tumors in *Mir34a*$^{\Delta IEC}$*Tp53*$^{\Delta IEC}$ mice. These results indicate that elevated expression of Pai-1 critically contributes to the CRC promoting effects of *Mir34a/Tp53*-deficiency.

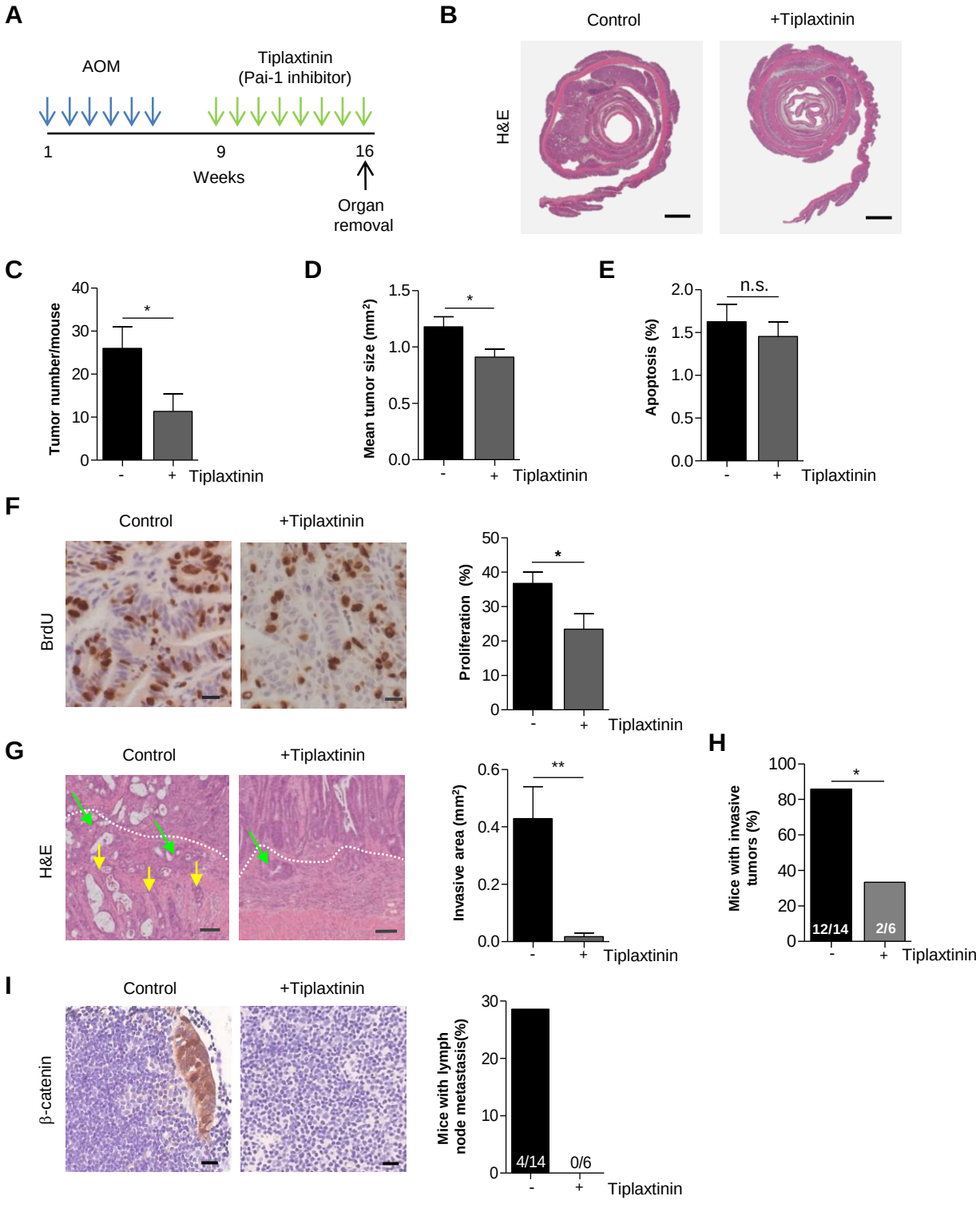

Figure 27. Targeting of Pai-1 inhibits initiation, invasion and lymph node metastasis of *Mir34a/p53*-deficient CRCs.

(A) Therapeutic application of Tiplaxtinin within the 6xAOM protocol. Starting from week 9 mice were fed with Tiplaxtinin supplemented chow (1g Tiplaxtinin/kg chow) or normal chow until week 16 (Control group). **(B)** Representative micrographs of colon morphology from *Mir34a*$^{\Delta IEC}$*Tp53*$^{\Delta IEC}$ fed with normal or Tiplaxtinin supplemented chow. Scale bars represent 1 mm. **(C)** Tumor incidence and **(D)** mean tumor size (n=6 mice for each treatment group; 156 tumors from *Mir34a*$^{\Delta IEC}$*Tp53*$^{\Delta IEC}$ mice treated with normal chow and 68 tumors from

Mir34a$^{\Delta IEC}$*Tp53*$^{\Delta IEC}$ mice treated with Tiplaxtinin supplemented chow were evaluated). **(E)** Quantification of apoptosis in tumor cells as determined by cleaved caspase 3 IHC. **(F)** (left) IHC detection of BrdU incorporation from colonic tumors. Scale bars represent 20 µm. (right) Quantification of proliferation. **(G)** (left) Representative micrographs of tumor invasion in *Mir34a*$^{\Delta IEC}$*Tp53*$^{\Delta IEC}$ mice treated as indicated. White dashed line: lamina muscularis mucosae as the border of primary tumor and invasive area green arrows: invasion to submucosa; yellow arrows invasion to muscularis externa. Scale bars represent 100 µm. **(H)** Quantification of tumor invasion. Significance is calculated by Fisher´s exact test, *P* value is *, *P* <0.05. **(I)** (left) Detection of metastatic cancer cells in the lymph node of mice with indicated treatments. (right) Evaluation of lymph node metastases in *Mir34a*$^{\Delta IEC}$*Tp53*$^{\Delta IEC}$ mice treated as indicated. Scale bars represent 20 µm. **(C-H)** Mean values ±SEM are provided, **P* < 0.05 by Student´s t-test.

Next we determined whether inhibition of the Pai-1 has any effects on the IL6/Stat3 pathway and vice versa. Upon treatment with MR16-1 Pai-1 levels did not change in colonic tumors of *Mir34a*$^{\Delta IEC}$*Tp53*$^{\Delta IEC}$ mice (Figure 28A). Furthermore, Tiplaxtinin treatment did not affect *IL6R* mRNA expression or Stat3 phosphorylation in colonic tumors of *Mir34a*$^{\Delta IEC}$*Tp53*$^{\Delta IEC}$ mice (Figure 28B-C). Therefore, the two pathways are presumably not connected in colon tumors.

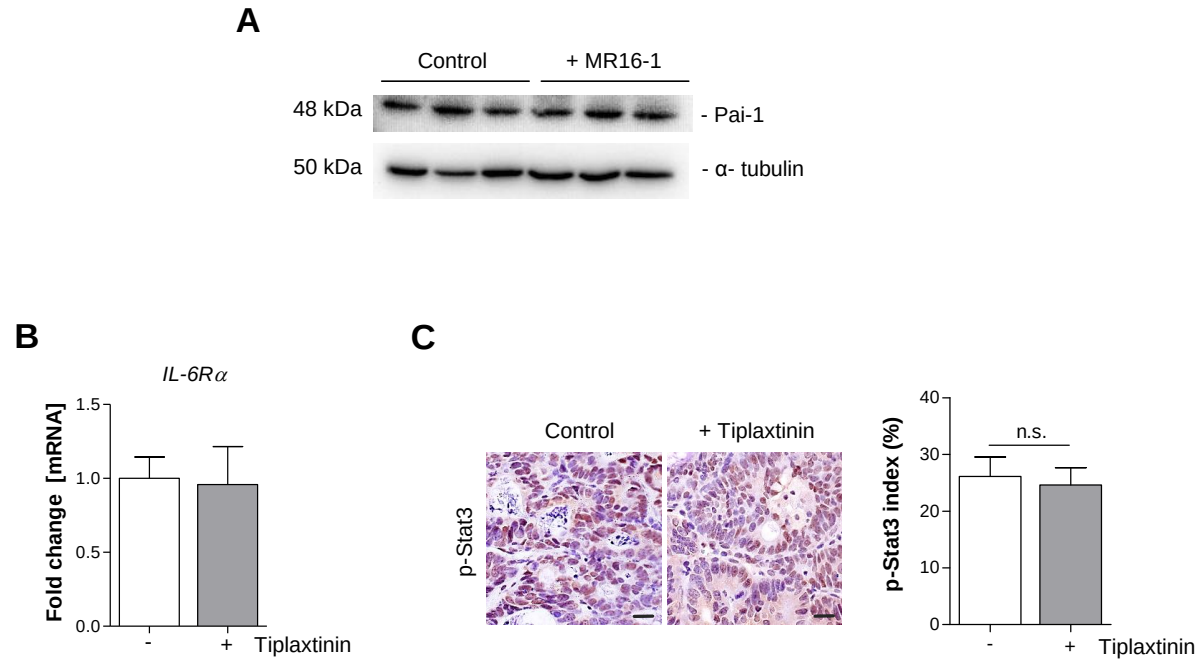

Figure 28. Treatment with MR16-1 does not affect the Pai-1 pathway and Tiplaxtinin does not affect the IL-6/Stat3 pathway in *Mir34a*$^{\Delta IEC}$*Tp53*$^{\Delta IEC}$ mice.
(A) Western-blot analysis of Pai-1 from colonic tumors of *Mir34a*$^{\Delta IEC}$*Tp53*$^{\Delta IEC}$ mice treated with MR16-1 or IgG (control) (n=3 tumors per genotype). **(B)** qPCR analysis of *IL6Rα* mRNA from tumors of *Mir34a*$^{\Delta IEC}$*Tp53*$^{\Delta IEC}$ mice treated with Tiplaxtinin supplemented chow or normal chow (control). **(C)** (left) IHC detection of p-Stat3 in tumors of *Mir34a*$^{\Delta IEC}$*Tp53*$^{\Delta IEC}$ mice with indicated treatments. Scale bars represent 20 µm. (right) Quantification of p-Stat3-positive cells in tumors. Mean values ±SEM are provided, n.s. not-significant by Student´s t-test.

5 Discussion

In the first part of this study, the role of *Mir34a* in mouse models of a CAC was investigated. As it was demonstrated *in vitro* , miR-34a functions in the context of a feedback-loop consisting of IL6R, STAT3 and miR-34a (Rokavec et al., 2014b). Repression of miR-34a induces IL6R/STAT3 signaling and SNAIL expression which contributes to EMT. To determine the relevance of these results *in vivo*, *Mir34a*$^{F/F}$ and *Mir34a*$^{-/-}$ mice were generated and the AOM/DSS model was used to induce colitis-associated colorectal cancer. In line with the *in vitro* evidence, the first part of the study demonstrated the relevance of the IL6-triggered IL6Ra/Stat3/Mir34a feedback loop that controls EMT for the formation of invasive colon tumors in *Mir34a*-deficient mice. Therefore, this study provided the first *in vivo* proof for a tumor suppressive function of *Mir34a* in a genetic mouse model of CAC.

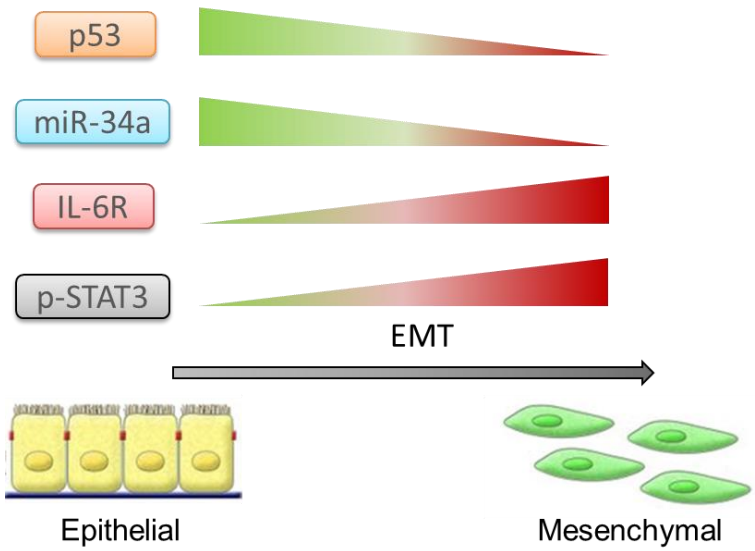

Figure 29. Altered expression of the IL6R/STAT3/miR-34a feedback loop components during EMT progression. During CRC progression, expression of miR-34a is down-regulated by CpG methylation and p53 is inactivated by mutation.

Results from this part of my study pointed out, that the activation of IL6R/Stat3 signaling leads to EMT and invasion of colitis-associated tumors upon *Mir34a*-loss. However, the role of EMT in invasion and metastasis was challenged by recent publications: Zheng et al. demonstrated that deletion of the *SNAIL1* and *TWIST1* genes in a pancreatic cancer mouse model does not attenuate metastasis (Zheng et al., 2015) and Fischer et al. showed by employing multiple transgenic mouse models

and establishing a cell lineage tracing approach together with characterization of epithelial and mesenchymal markers that EMT is not required in lung metastasis (Fischer et al., 2015). On the contrary, when *ZEB1* was deleted in an identical pancreatic cancer model as used in Zheng et al., 40% reduction in metastasis was observed without an evidence for compensation by other EMT-transcription factors (Krebs et al., 2017). Therefore, these studies show that, there is a context-dependency in the role and function of different EMT-transcription factors.

Since the first part of this study focused on *Mir34*-deficiency in germ-line knock-out mice, it is still unclear whether these observed effects were cell autonomous or if there was a contribution from the tumor stroma. To clarify that point, it would be useful to determine whether there are differences in abundance or function of stromal cell types in *Mir34a*$^{-/-}$ colon tumors compared to their *Mir34a*$^{F/F}$ controls. Tissue-specific knock-out mouse models could be useful to clarify the role of Mir34a in stromal cells in CAC in the future.

In the second part of this study, a cooperative role of *Mir34a* and *Tp53* in the suppression of tumor initiation, invasion and metastasis was shown in a mouse model of sporadic CRC. These findings explain why colonic tumors with combined inactivation of both genes display the worst prognosis and poorest survival when compared to those with singular deletions of these genes. Interestingly, *MIR34A* is silenced by CpG methylation in late stage colorectal tumors (Wang et al., 2016). Since this is similar to the timing of mutational inactivation of *TP53*, the simultaneity of these events would allow their cooperation in CRC progression.

Notably, *Mir34a*$^{\Delta IEC}$*Tp53*$^{\Delta IEC}$ mice displayed more tumor growth compared to single knockouts of *Mir34a*$^{\Delta IEC}$ and *Tp53*$^{\Delta IEC}$. In addition, *Mir34a*$^{\Delta IEC}$*Tp53*$^{\Delta IEC}$ mice demonstrated enhanced proliferation in the presence of DNA damage in *Mir34a/Tp53*-deficient IECs compared to other genotypes. Since, recent publications highlighted the role of miR-34a also in stemness (Bu et al., 2016; Park et al., 2014), it might be useful to further investigate whether combined inactivation of *Mir34a* and *Tp53* also influences the stemness.

Although *Mir34a* represents a direct Tp53 target, its loss further enhanced the effect of *Tp53* deficiency in early and late stages of CRC formation and progression. This indicates that *Mir34a* may mediate tumor suppression downstream of other factors and pathways besides Tp53 and its upstream activating pathways. Interestingly, a previous study showed that activation of BRAF may cause a Tp53-

independent induction of Mir34a expression via up-regulation of the transcription factor ELK1, which directly induces *Mir34a* (Bahrami et al., 2018; Christoffersen et al., 2010).

Expression profiling revealed the activation of key oncogenic factors and pathways, such as c-Myc, EMT, hypoxia, and an inflammatory response in CRCs of *Mir34a*$^{\Delta IEC}$*Tp53*$^{\Delta IEC}$ mice. Recently Li et al., could show that the *TP53* and *MIR34a* status are important determinants of the response to hypoxia (Li et al., 2017): only in colon cancer cells with inactivated *TP53*, *MIR34a* was directly repressed by hypoxia-mediated activation of HIF-1α. The down-regulation of miR-34a was necessary for hypoxia-induced STAT3 activation and EMT, which may ultimately promote invasion and metastasis. Interestingly, the profiles of the tumors studied here also revealed a hypoxia-related signature in *Mir34a/Tp53*-deficient mice. In addition, we had previously described that *miR-34a* is directly repressed by STAT3 after IL6 exposure (Rokavec et al., 2014b). Indeed, the common epigenetic silencing of *MIR34a* observed in human CRCs may occur after prolonged HIF-1α- or STAT3-mediated repression of *MIR34a*.

As *miR-34a* and *Tp53* are commonly inactivated in human colorectal tumors, the genetic evidence for the cooperation between simultaneous loss of *miR-34a* and *Tp53* provided here may have broad clinical implications. Since the restauration of wt TP53 or reactivation of mutant TP53 is hard to accomplish, tumors with inactivation of both *TP53* and *MIR34a* may benefit from the treatment with MiR34a mimetics. Notably, MRX34, a liposome-formulated mimic of miR-34a, developed by Mirna Therapeutics, has been shown to have ability to reduce proliferation of various types of cancer cells, cause significant tumor regression in multiple mouse models, and to reduce the tumor forming capacity of cancer stem cells (Bader, 2012; Beg et al., 2017). However, a multi-center, open label Phase 1 clinical trial to evaluate MRX34 as a single agent in multiple advanced solid tumors and various hematological malignancies was stopped due to immune-related serious adverse events in some patients (Clinical trial information: NCT01829971). Therefore, more research has to be performed to clarify the contributions of carriers and miRNA mimics to the inflammatory responses (Reid et al., 2016). Additionally, miR-34a has recently been shown to target PDL1 and thereby antagonize the immune escape of cancer cells (Cortez et al., 2016; Wang et al., 2015). Therefore, this therapeutic approach may also harness the patient's adaptive immune system against aggressive CRC.

Alternatively, as shown in this study, *Mir34a*-/*Tp53*-deficient CRCs may be treated with inhibitors directed towards miR-34a targets, which are up-regulated in these cancers. The up-regulation of these targets suggests that they are relevant for the etiology of the tumor. In addition, their up-regulation may result in a selective sensitivity of *Mir34a*-/*Tp53*-deficient colorectal tumors towards the respective inhibitors of these targets.

Inhibition of the Mir34a targets IL6R and PAI-1 by using antibodies or small drug inhibitors may represent promising approaches to treat CRCs that display combined *Tp53* and *miR-34a* loss: Here, we first focused on targeting IL6R since it represents a *bona fide* Mir34a target that activates the oncogenic transcription factor Stat3 (Rokavec et al., 2014b). Interestingly, treatment with an IL6R-neutralizing antibody was also shown to be effective in preventing metastasis in a lung colonization model (Lin et al., 2017). Furthermore, the IL6R-neutralizing antibody Tocillizumab was approved by the FDA for the treatment of chronic inflammatory diseases, such as rheumatoid and systemic juvenile idiopathic arthritis, Castleman disease, cytokine release syndrome and giant cell arteritis (Garbers et al., 2018; Johnson et al., 2018; Tanaka et al., 2012; Waldner et al., 2012). Therefore, IL6R targeting antibodies are well tolerated by the majority of patients and may therefore be employed to treat late stage CRC patients.

In colonic tumors of $Mir34a^{\Delta IEC}Tp53^{\Delta IEC}$ mice, *Pai-1* was one of the most significantly up-regulated genes. PAI-1 is a serine protease inhibitor (serpin) and the main regulator of the plasminogen activation system (Placencio and DeClerck, 2015). It inhibits tissue-type plasminogen activator (tPA) and urokinase-type plasminogen activator (uPA). Roles of PAI-1 in tumorigenesis are: (1) Leading to angiogenesis or intracellular apoptotic signaling by inhibition of uPA action to prevent the cleavage of plasminogen into plasmin and subsequent substrates on the cell surface; (2) it leads to intracellular signaling and cell migration by its ability to bind lipoprotein receptor-related protein (LRP1); and (3) promotes endothelial cell migration and angiogenesis by binding to vitronectin in the extracellular matrix (Placencio and DeClerck, 2015). PAI-1 can be produced by tumor cells and non-malignant cells, including endothelial cells (EC), macrophages or adipocytes in the tumor microenvironment and it can have paracrine or autocrine effects within the tumor microenvironment (Giacoia et al., 2014; Placencio and DeClerck, 2015). In this study, the most pronounced PAI1 expression was detected in tumor cells in the center and at the invasion front of

colorectal tumors with simultaneous inactivation of *MIR34A* and *TP53*. At the invasion front of these tumors PAI-1 may promote the budding of cancer cells by enhancing invasion-related processes, such as remodeling of the extracellular matrix. Notably, detection of PAI-1 is used as a prognostic marker for node-negative breast cancer since 2007 (Harbeck et al., 2013; Harris et al., 2007). Therefore, up-regulation of PAI-1 might represent not only a new therapeutic target but also an attractive prognostic marker for *MIR34A*/*TP53*-deficient colorectal tumors.

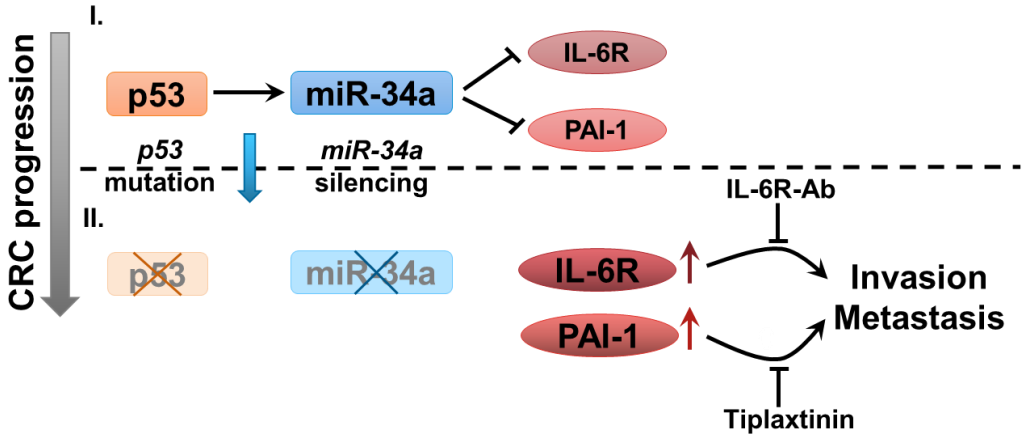

Figure 30. Graphical summary of combined inactivation of *Tp53* and *Mir34a* in CRC. *Tp53* and *Mir34a* cooperatively promote colorectal cancer development and progression via increasing levels of IL6R and PAI-1.

Tumor volume of human T24 bladder and HeLa cervical cancer xenotransplants in mice was reduced after oral administration of Tiplaxtinin (Gomes-Giacoia et al., 2013). In addition, the Pai1-inhibitors SK-116 and SK-216 were able to decrease the number of small intestinal polyps in Apc/Apc1638N mice (Mutoh et al., 2008). Although, others and we showed that targeting Pai-1 in cancer is an attractive therapeutic approach, limitations, such as the short half-live of these inhibitors, indicate that alternative Pai-1 inhibitors with improved pharmacologic profiles should be developed.

As previously shown, carcinogen challenge inducing activating mutations in the *Ctnnb* gene in $Tp53^{\Delta IEC}$ mice promotes invasive and metastatic colorectal tumors (Schwitalla et al., 2013). Tumorigenesis in the $Tp53^{\Delta IEC}$ mice model was also accompanied by formation of NF-κB dependent inflammatory microenvironment, which could also be detected in human colorectal cancer (Schwitalla et al., 2013).

Therefore, we chose the well-established *Tp53*$^{\Delta IEC}$ mice model to generate *Mir34a*$^{\Delta IEC}$*Tp53*$^{\Delta IEC}$ mice. As it was described in the second part of this study, tumor initiation and progression in *Mir34a*$^{\Delta IEC}$*Tp53*$^{\Delta IEC}$ mice were further enhanced compared to *Tp53*$^{\Delta IEC}$ mice and metastasis formation was accelerated by 8 weeks. Therefore, this model may be useful for testing metastasis targeting strategies. In fact, experiments employing the IL6Ra neutralizing antibody and Tiplaxtinin were only applied to *Mir34a*$^{\Delta IEC}$*Tp53*$^{\Delta IEC}$ mice, since only those developed lymph node metastasis in 16 weeks.

The consequence of deleting exons 2 to 10, that was employed here to inactivate *Tp53*, corresponds to the effects of loss-of-function mutations of *Tp53* that occur in ~50% of all CRCs (Bouaoun et al., 2016). Whether gain-of-function *Tp53* mutations, which occur at a lower frequency, have divergent effects in combination with the inactivation of *miR-34a* remains to be determined in the future.

In conclusion, this study provides genetic evidence for a role of the combined inactivation of *Mir34a* and *Tp53* in the initiation and progression of CRC. In addition, the up-regulated Mir34a-targets identified in *Mir34a*- and *p53*-deficient colonic tumors in this study provide a valuable resource for the future identification and characterization of therapeutic targets, as shown by the example of *IL6R* and *Pai-1*.

Taken together, this study demonstrated the role of *Mir34a* as a tumor suppressor in *in vivo* models of colorectal cancer and highlighted the importance of Mir34a targets for colorectal cancer treatment.

6 Summary

In this study, the potential role of miR-34a as a tumor suppressor in mouse models of carcinogen-induced colorectal cancer and colitis-associated cancer was investigated.

In the first part, I demonstrated that germline deletion of *Mir34a* promotes inflammation-induced colorectal carcinogenesis in mice. In a colitis-associated cancer model *Mir34a*-deficiency was associated with an increase in the frequency and size of colon tumors, and enhanced invasion into surrounding tissue. *Mir34a*-deficient colon tumors displayed IL6R/Stat3 pathway activation with elevated expression of EMT markers, such as Snail and Zeb1, which might explain the observed invasive characteristics of these colon tumors. Therefore, this study provided first *in vivo* proof for a tumor suppressive function of Mir34a in a genetic mouse model of CAC.

It was previously shown that *miR-34a* is a down-stream target of tumor suppressor Tp53. Inactivation of both *TP53* (by mutation) and *MIR34A* (by CpG methylation) occurs in late stages of colorectal carcinogenesis. In the second part of this study we found that *TP53* and the *MIR34A* were inactivated in 50% of CRCs which developed distant metastases. To trace the consequences of this combined inactivation, I deleted these genes in a mouse model of colorectal cancer, and characterized the CRC initiation and progression. RNA expression profiling of colon tumors revealed the activation of key oncogenic factors and pathways, such as c-Myc, EMT, hypoxia, and an inflammatory response in $Mir34a^{\Delta IEC}Tp53^{\Delta IEC}$ mice. Treatment of $Mir34a^{\Delta IEC}Tp53^{\Delta IEC}$ mice with inhibitors of up-regulated Mir34a targets, as exemplarily demonstrated here for IL6R and Pai-1, reduced tumor progression and inhibited the lymph-node metastasis. Analysis of 628 colon cancer cases represented in online databases and 61 primary tissue samples obtained from patients demonstrated that the findings made in a preclinical mouse model can be transferred to humans.

Taken together, the results obtained within this study improved the understanding of the role of *miR-34a* in colorectal cancer and underlined the therapeutic potential of miR-34a targets as an alternative approach for the treatment of colorectal cancer.

7 Zusammenfassung

In dieser Arbeit wurde die potentielle Wirkung von miR-34a als Tumorsuppressor in einem karzinogen-induzierten und einem Kolitis-assoziierten Mausmodell für das Kolorektale Karzinom untersucht.

Im ersten Teil der Arbeit zeigte ich, dass die Deletion von *Mir34a* in der Keimbahn von Mäusen die Entstehung von Entzündungs-induzierten Darmkrebs verstärkt. Verlust von *Mir34a* führte im Modell für Kolitis-assoziierten Krebs zu erhöhter Zahl und Größe von Tumoren und förderte deren Invasion in benachbarte Strukturen. In *Mir34a*-defizienten Darmtumoren zeigte sich eine Aktivierung des IL6R/Stat3-Signalwegs mit verstärkter Expression von EMT Genen, wie z.B. Snail und Zeb1, was die beobachteten invasiven Eigenschaften dieser Darmtumoren erklären könnte. Diese Arbeit stellt den ersten *in vivo* Beweis für eine tumorsuppressive Wirkung von Mir34a in einem genetischen Modell für Kolitis-assoziiertem Krebs dar.

Es war bereits bekannt, dass *miR-34a* ein nachgeschaltetes Zielgen des Tumorsuppressors p53 (TP53) ist. Im fortgeschrittenen Stadium von Kolorektal-karzinomen (KRK) kommt es zur Inaktivierung von *TP53* (durch Mutation) und von *MIR34A* (durch CpG Methylierung). Im zweiten Teil der Studie beschreiben wir, dass in jedem zweiten KRK mit Fernmetastasen sowohl TP53, als auch MIR-34A inaktiviert waren. Um die Folgen dieser kombinierten Inaktivierung aufzuspüren habe ich diese Gene in einem Modell für sporadisches Kolorektales Karzinom simultan deletiert und die frühe und fortgeschrittene Phase der Tumorentwicklung untersucht. Untersuchungen des Expressionsprofils von RNA in Darmtumoren zeigte die Aktivierung von zentralen onkogenen Faktoren und Signalwegen wie c-Myc, EMT, Hypoxie und Tumor-assoziierte Entzündung in *Mir34a*$^{\Delta IEC}$*Tp53*$^{\Delta IEC}$ Mäusen. Die Behandlung dieser Mäuse mit Inhibitoren aktivierter Mir34a Zielgene, wie hier exemplarisch für IL6R und Pai-1 gezeigt, reduzierte die Tumorentwicklung und blockierte die Entstehung von Lymphknotenmetastasen. Die Analyse von 628 Darmkrebsfällen aus Datenbanken und von 61 Gewebeproben von Patienten zeigte die Übertragbarkeit der Ergebnisse aus dem präklinischen Mausmodell auf den Menschen.

Zusammengefasst vertiefen die Ergebnisse dieser Arbeit unser Verständnis der Folgen einer *Mir34a*-Inaktivierung in Krebszellen und unterstreichen das

therapeutisches Potential von miR-34a-Zielgenen als alternativen Ansatz in der Behandlung von Darmkrebs.

8 References

Ashton-Rickardt, P. G., Dunlop, M. G., Nakamura, Y., Morris, R. G., Purdie, C. A., Steel, C. M., Evans, H. J., Bird, C. C., and Wyllie, A. H. (1989). High frequency of APC loss in sporadic colorectal carcinoma due to breaks clustered in 5q21-22. Oncogene *4*, 1169-1174.

Aust, D. E., Terdiman, J. P., Willenbucher, R. F., Chew, K., Ferrell, L., Florendo, C., Molinaro-Clark, A., Baretton, G. B., Lohrs, U., and Waldman, F. M. (2001). Altered distribution of beta-catenin, and its binding proteins E-cadherin and APC, in ulcerative colitis-related colorectal cancers. Mod Pathol *14*, 29-39.

Bader, A. G. (2012). miR-34 - a microRNA replacement therapy is headed to the clinic. Front Genet *3*, 120.

Bahrami, A., Hesari, A., Khazaei, M., Hassanian, S. M., Ferns, G. A., and Avan, A. (2018). The therapeutic potential of targeting the BRAF mutation in patients with colorectal cancer. J Cell Physiol *233*, 2162-2169.

Baker, S. J., Fearon, E. R., Nigro, J. M., Hamilton, S. R., Preisinger, A. C., Jessup, J. M., vanTuinen, P., Ledbetter, D. H., Barker, D. F., Nakamura, Y.*, et al.* (1989). Chromosome 17 deletions and p53 gene mutations in colorectal carcinomas. Science *244*, 217-221.

Bartel, D. P. (2009). MicroRNAs: target recognition and regulatory functions. Cell *136*, 215-233.

Becker, C., Fantini, M. C., Schramm, C., Lehr, H. A., Wirtz, S., Nikolaev, A., Burg, J., Strand, S., Kiesslich, R., Huber, S.*, et al.* (2004a). TGF-beta suppresses tumor progression in colon cancer by inhibition of IL-6 trans-signaling. Immunity *21*, 491-501.

Beg, M. S., Brenner, A. J., Sachdev, J., Borad, M., Kang, Y. K., Stoudemire, J., Smith, S., Bader, A. G., Kim, S., and Hong, D. S. (2017). Phase I study of MRX34, a liposomal miR-34a mimic, administered twice weekly in patients with advanced solid tumors. Invest New Drugs *35*, 180-188.

Bensaad, K., Tsuruta, A., Selak, M. A., Vidal, M. N., Nakano, K., Bartrons, R., Gottlieb, E., and Vousden, K. H. (2006). TIGAR, a p53-inducible regulator of glycolysis and apoptosis. Cell *126*, 107-120.

Bieging, K. T., Mello, S. S., and Attardi, L. D. (2014). Unravelling mechanisms of p53-mediated tumour suppression. Nat Rev Cancer *14*, 359-370.

Bollrath, J., and Greten, F. R. (2009). IKK/NF-kappaB and STAT3 pathways: central signalling hubs in inflammation-mediated tumour promotion and metastasis. EMBO Rep *10*, 1314-1319.

Bollrath, J., Phesse, T. J., von Burstin, V. a., Putoczki, T., Bennecke, M., Bateman, T., Nebelsiek, T., Lundgren-May, T., Canli, Ö., Schwitalla, S.*, et al.* (2009). gp130-Mediated Stat3 Activation in Enterocytes Regulates Cell Survival and Cell-Cycle Progression during Colitis-Associated Tumorigenesis. Cancer Cell *15*, 91-102.

Bommer, G. T., Gerin, I., Feng, Y., Kaczorowski, A. J., Kuick, R., Love, R. E., Zhai, Y., Giordano, T. J., Qin, Z. S., Moore, B. B.*, et al.* (2007). p53-mediated activation of miRNA34 candidate tumor-suppressor genes. Curr Biol *17*, 1298-1307.

Bouaoun, L., Sonkin, D., Ardin, M., Hollstein, M., Byrnes, G., Zavadil, J., and Olivier, M. (2016). TP53 Variations in Human Cancers: New Lessons from the IARC TP53 Database and Genomics Data. Hum Mutat *37*, 865-876.

Brosh, R., and Rotter, V. (2009). When mutants gain new powers: news from the mutant p53 field. Nat Rev Cancer *9*, 701-713.

Brownawell, A. M., and Macara, I. G. (2002). Exportin-5, a novel karyopherin, mediates nuclear export of double-stranded RNA binding proteins. J Cell Biol *156*, 53-64.

Bu, P., Wang, L., Chen, K. Y., Srinivasan, T., Murthy, P. K., Tung, K. L., Varanko, A. K., Chen, H. J., Ai, Y., King, S.*, et al.* (2016). A miR-34a-Numb Feedforward Loop Triggered by Inflammation Regulates Asymmetric Stem Cell Division in Intestine and Colon Cancer. Cell Stem Cell *18*, 189-202.

Calin, G. A., Sevignani, C., Dumitru, C. D., Hyslop, T., Noch, E., Yendamuri, S., Shimizu, M., Rattan, S., Bullrich, F., Negrini, M., and Croce, C. M. (2004). Human microRNA genes are frequently located at fragile sites and genomic regions involved in cancers. Proc Natl Acad Sci U S A *101*, 2999-3004.

Canavan, C., Abrams, K. R., and Mayberry, J. (2006). Meta-analysis: colorectal and small bowel cancer risk in patients with Crohn's disease. Aliment Pharmacol Ther *23*, 1097-1104.

Chakraborty, D., Sumova, B., Mallano, T., Chen, C. W., Distler, A., Bergmann, C., Ludolph, I., Horch, R. E., Gelse, K., Ramming, A.*, et al.* (2017). Activation of STAT3 integrates common profibrotic pathways to promote fibroblast activation and tissue fibrosis. Nat Commun *8*, 1130.

Chalaris, A., Schmidt-Arras, D., Yamamoto, K., and Rose-John, S. (2012). Interleukin-6 trans-signaling and colonic cancer associated with inflammatory bowel disease. Dig Dis *30*, 492-499.

Chendrimada, T. P., Gregory, R. I., Kumaraswamy, E., Norman, J., Cooch, N., Nishikura, K., and Shiekhattar, R. (2005). TRBP recruits the Dicer complex to Ago2 for microRNA processing and gene silencing. Nature *436*, 740-744.

Cheng, C. Y., Hwang, C. I., Corney, D. C., Flesken-Nikitin, A., Jiang, L., Öner, G. M., Munroe, R. J., Schimenti, J. C., Hermeking, H., and Nikitin, A. Y. (2014). MiR-34 Cooperates with p53 in Suppression of Prostate Cancer by Joint Regulation of Stem Cell Compartment. Cell Reports *6*, 1000-1007.

Cherry, L. M. (2011). The genetic etiology of familial and nonfamilial colorectal cancer. Proc (Bayl Univ Med Cent) *24*, 139-141.

Christoffersen, N. R., Shalgi, R., Frankel, L. B., Leucci, E., Lees, M., Klausen, M., Pilpel, Y., Nielsen, F. C., Oren, M., and Lund, A. H. (2010). p53-independent upregulation of miR-34a during oncogene-induced senescence represses MYC. Cell Death Differ *17*, 236-245.

Clapper, M. L., Cooper, H. S., and Chang, W. C. (2007). Dextran sulfate sodium-induced colitis-associated neoplasia: a promising model for the development of chemopreventive interventions. Acta Pharmacol Sin *28*, 1450-1459.

Concepcion, C., Han, Y., Mu P, Bonetti C, Yao E, D'Andrea A, Vidigal JA, Maughan WP, Ogrodowski P, and A., V. (2012). Intact p53-Dependent Responses in miR-34–Deficient Mice. Plos Genetics *8*.

Cortez, M. A., Ivan, C., Valdecanas, D., Wang, X., Peltier, H. J., Ye, Y., Araujo, L., Carbone, D. P., Shilo, K., Giri, D. K.*, et al.* (2016). PDL1 Regulation by p53 via miR-34. J Natl Cancer Inst *108*.

Crighton, D., Wilkinson, S., O'Prey, J., Syed, N., Smith, P., Harrison, P. R., Gasco, M., Garrone, O., Crook, T., and Ryan, K. M. (2006). DRAM, a p53-induced modulator of autophagy, is critical for apoptosis. Cell *126*, 121-134.

Dienstmann, R., Vermeulen, L., Guinney, J., Kopetz, S., Tejpar, S., and Tabernero, J. (2017). Consensus molecular subtypes and the evolution of precision medicine in colorectal cancer. Nat Rev Cancer *17*, 79-92.

Eaden, J. A., Abrams, K. R., and Mayberry, J. F. (2001). The risk of colorectal cancer in ulcerative colitis: a meta-analysis. Gut *48*, 526-535.

Elinav, E., Nowarski, R., Thaiss, C. A., Hu, B., Jin, C., and Flavell, R. A. (2013). Inflammation-induced cancer: crosstalk between tumours, immune cells and microorganisms. Nat Rev Cancer *13*, 759-771.

Elokdah, H. (2004). Tiplaxtinin, a Novel, Orally Efficacious Inhibitor of Plasminogen Activator Inhibitor-1: Design, Synthesis, and Preclinical Characterization. Journal of Medicinal Chemistry *47*.

Fearon, E. R., and Vogelstein, B. (1990). A genetic model for colorectal tumorigenesis. Cell *61*, 759-767.

Fenton, J. I., Hursting, S. D., Perkins, S. N., and Hord, N. G. (2006). Interleukin-6 production induced by leptin treatment promotes cell proliferation in an Apc (Min/+) colon epithelial cell line. Carcinogenesis *27*, 1507-1515.

Finlay, C. A., Hinds, P. W., and Levine, A. J. (1989). The p53 proto-oncogene can act as a suppressor of transformation. Cell *57*, 1083-1093.

Fischer, K. R., Durrans, A., Lee, S., Sheng, J., Li, F., Wong, S. T., Choi, H., El Rayes, T., Ryu, S., Troeger, J.*, et al.* (2015). Epithelial-to-mesenchymal transition is not required for lung metastasis but contributes to chemoresistance. Nature *527*, 472-476.

Francescone, R., Hou, V., and Grivennikov, S. I. (2015). Cytokines, IBD, and colitis-associated cancer. Inflamm Bowel Dis *21*, 409-418.

Garbers, C., Heink, S., Korn, T., and Rose-John, S. (2018). Interleukin-6: designing specific therapeutics for a complex cytokine. Nat Rev Drug Discov *17*, 395-412.

Giacoia, E. G., Miyake, M., Lawton, A., Goodison, S., and Rosser, C. J. (2014). PAI-1 leads to G1-phase cell-cycle progression through cyclin D3/cdk4/6 upregulation. Mol Cancer Res *12*, 322-334.

Gomes-Giacoia, E., Miyake, M., Goodison, S., and Rosser, C. J. (2013). Targeting plasminogen activator inhibitor-1 inhibits angiogenesis and tumor growth in a human cancer xenograft model. Mol Cancer Ther *12*, 2697-2708.

Gregory, R. I., Yan, K. P., Amuthan, G., Chendrimada, T., Doratotaj, B., Cooch, N., and Shiekhattar, R. (2004). The Microprocessor complex mediates the genesis of microRNAs. Nature *432*, 235-240.

Grivennikov, S., Karin, E., Terzic, J., Mucida, D., Yu, G. Y., Vallabhapurapu, S., Scheller, J., Rose-John, S., Cheroutre, H., Eckmann, L., and Karin, M. (2009). IL-6 and Stat3 Are Required for Survival of Intestinal Epithelial Cells and Development of Colitis-Associated Cancer. Cancer Cell *15*, 103-113.

Grivennikov, S. I. (2013). Inflammation and colorectal cancer: colitis-associated neoplasia. Semin Immunopathol *35*, 229-244.

Grivennikov, S. I., Greten, F. R., and Karin, M. (2010). Immunity, Inflammation, and Cancer. Cell *140*, 883-899.

Guinney, J., Dienstmann, R., Wang, X., de Reynies, A., Schlicker, A., Soneson, C., Marisa, L., Roepman, P., Nyamundanda, G., Angelino, P.*, et al.* (2015). The consensus molecular subtypes of colorectal cancer. Nat Med *21*, 1350-1356.

Ha, M., and Kim, V. N. (2014). Regulation of microRNA biogenesis. Nat Rev Mol Cell Biol *15*, 509-524.

Hammond, S. M. (2015). An overview of microRNAs. Adv Drug Deliv Rev *87*, 3-14.

Hanahan, D., and Weinberg, R. A. (2011). Hallmarks of cancer: the next generation. Cell *144*, 646-674.

Harbeck, N., Schmitt, M., Meisner, C., Friedel, C., Untch, M., Schmidt, M., Sweep, C. G., Lisboa, B. W., Lux, M. P., Beck, T.*, et al.* (2013). Ten-year analysis of the prospective multicentre Chemo-N0 trial validates American Society of Clinical Oncology (ASCO)-recommended biomarkers uPA and PAI-1 for therapy decision making in node-negative breast cancer patients. Eur J Cancer *49*, 1825-1835.

Harris, L., Fritsche, H., Mennel, R., Norton, L., Ravdin, P., Taube, S., Somerfield, M. R., Hayes, D. F., Bast, R. C., Jr., and American Society of Clinical, O. (2007). American Society of Clinical Oncology 2007 update of recommendations for the use of tumor markers in breast cancer. J Clin Oncol *25*, 5287-5312.

Heink, S., Yogev, N., Garbers, C., Herwerth, M., Aly, L., Gasperi, C., Husterer, V., Croxford, A. L., Moller-Hackbarth, K., Bartsch, H. S.*, et al.* (2017). Trans-presentation of IL-6 by dendritic cells is required for the priming of pathogenic TH17 cells. Nat Immunol *18*, 74-85.

Hermeking, H. (2007). p53 Enters the MicroRNA World. Cancer Cell *12*, 414-418.

Hermeking, H. (2012). MicroRNAs in the p53 network: micromanagement of tumour suppression. Nature Reviews Cancer *12*, 613-626.

Huntzinger, E., and Izaurralde, E. (2011). Gene silencing by microRNAs: contributions of translational repression and mRNA decay. Nat Rev Genet *12*, 99-110.

Hutchins, A. P., Diez, D., and Miranda-Saavedra, D. (2013). The IL-10/STAT3-mediated anti-inflammatory response: recent developments and future challenges. Brief Funct Genomics *12*, 489-498.

Hutvagner, G., McLachlan, J., Pasquinelli, A. E., Balint, E., Tuschl, T., and Zamore, P. D. (2001). A cellular function for the RNA-interference enzyme Dicer in the maturation of the let-7 small temporal RNA. Science *293*, 834-838.

Iacopetta, B. (2003). TP53 mutation in colorectal cancer. Hum Mutat *21*, 271-276.

Jiang, L., and Hermeking, H. (2017). miR-34a and miR-34b/c Suppress Intestinal Tumorigenesis. Cancer Res *77*, 2746-2758.

Johnson, D. E., O'Keefe, R. A., and Grandis, J. R. (2018). Targeting the IL-6/JAK/STAT3 signalling axis in cancer. Nat Rev Clin Oncol.

Jones, S., Chen, W. D., Parmigiani, G., Diehl, F., Beerenwinkel, N., Antal, T., Traulsen, A., Nowak, M. A., Siegel, C., Velculescu, V. E.*, et al.* (2008). Comparative lesion sequencing provides insights into tumor evolution. Proc Natl Acad Sci U S A *105*, 4283-4288.

Kanneganti, M., Mino-Kenudson, M., and Mizoguchi, E. (2011). Animal models of colitis-associated carcinogenesis. J Biomed Biotechnol *2011*, 342637.

Kastenhuber, E. R., and Lowe, S. W. (2017). Putting p53 in Context. Cell *170*, 1062-1078.

Kenzelmann Broz, D., and Attardi, L. D. (2010). In vivo analysis of p53 tumor suppressor function using genetically engineered mouse models. Carcinogenesis *31*, 1311-1318.

Ketting, R. F., Fischer, S. E., Bernstein, E., Sijen, T., Hannon, G. J., and Plasterk, R. H. (2001). Dicer functions in RNA interference and in synthesis of small RNA involved in developmental timing in C. elegans. Genes Dev *15*, 2654-2659.

Kim, M. P., and Lozano, G. (2018). Mutant p53 partners in crime. Cell Death Differ *25*, 161-168.

Kim, N. H., Kim, H. S., Li, X. Y., Lee, I., Choi, H. S., Kang, S. E., Cha, S. Y., Ryu, J. K., Yoon, D., Fearon, E. R.*, et al.* (2011). A p53/miRNA-34 axis regulates Snail1-dependent cancer cell epithelial-mesenchymal transition. J Cell Biol *195*, 417-433.

Kohlhapp, F. J., Mitra, A. K., Lengyel, E., and Peter, M. E. (2015). MicroRNAs as mediators and communicators between cancer cells and the tumor microenvironment. Oncogene *34*, 5857-5868.

Kopf, M., Baumann, H., Freer, G., Freudenberg, M., Lamers, M., Kishimoto, T., Zinkernagel, R., Bluethmann, H., and Kohler, G. (1994). Impaired immune and acute-phase responses in interleukin-6-deficient mice. Nature *368*, 339-342.

Krebs, A. M., Mitschke, J., Lasierra Losada, M., Schmalhofer, O., Boerries, M., Busch, H., Boettcher, M., Mougiakakos, D., Reichardt, W., Bronsert, P.*, et al.* (2017). The EMT-activator Zeb1 is a key factor for cell plasticity and promotes metastasis in pancreatic cancer. Nat Cell Biol *19*, 518-529.

Kruiswijk, F., Labuschagne, C. F., and Vousden, K. H. (2015). p53 in survival, death and metabolic health: a lifeguard with a licence to kill. Nat Rev Mol Cell Biol *16*, 393-405.

Lambert, A. W., Pattabiraman, D. R., and Weinberg, R. A. (2017). Emerging Biological Principles of Metastasis. Cell *168*, 670-691.

Lane, D. P. (1992). Cancer. p53, guardian of the genome. Nature *358*, 15-16.

Lee, R. C., Feinbaum, R. L., and Ambros, V. (1993). The C. elegans heterochronic gene lin-4 encodes small RNAs with antisense complementarity to lin-14. Cell *75*, 843-854.

Lee, Y., Kim, M., Han, J., Yeom, K. H., Lee, S., Baek, S. H., and Kim, V. N. (2004). MicroRNA genes are transcribed by RNA polymerase II. EMBO J *23*, 4051-4060.

Lesina, M., Kurkowski, M. U., Ludes, K., Rose-John, S., Treiber, M., Kloppel, G., Yoshimura, A., Reindl, W., Sipos, B., Akira, S.*, et al.* (2011). Stat3/Socs3 activation by IL-6 transsignaling promotes progression of pancreatic intraepithelial neoplasia and development of pancreatic cancer. Cancer Cell *19*, 456-469.

Levine, A. J., and Oren, M. (2009). The first 30 years of p53: growing ever more complex. Nat Rev Cancer *9*, 749-758.

Li, H., Rokavec, M., Jiang, L., Horst, D., and Hermeking, H. (2017). Antagonistic Effects of p53 and HIF1A on microRNA-34a Regulation of PPP1R11 and STAT3 and Hypoxia-induced Epithelial to Mesenchymal Transition in Colorectal Cancer Cells. Gastroenterology *153*, 505-520.

Lin, C., Liao, W., Jian, Y., Peng, Y., Zhang, X., Ye, L., Cui, Y., Wang, B., Wu, X., Xiong, Z.*, et al.* (2017). CGI-99 promotes breast cancer metastasis via autocrine interleukin-6 signaling. Oncogene *36*, 3695-3705.

Lugli, A., Zlobec, I., Baker, K., Minoo, P., Tornillo, L., Terracciano, L., and Jass, J. R. (2007). Prognostic significance of mucins in colorectal cancer with different DNA mismatch-repair status. J Clin Pathol *60*, 534-539.

Matoba, S., Kang, J. G., Patino, W. D., Wragg, A., Boehm, M., Gavrilova, O., Hurley, P. J., Bunz, F., and Hwang, P. M. (2006). p53 regulates mitochondrial respiration. Science *312*, 1650-1653.

McGuire, S. (2016). World Cancer Report 2014. Geneva, Switzerland: World Health Organization, International Agency for Research on Cancer, WHO Press, 2015. Adv Nutr *7*, 418-419.

Morin, P. J., Sparks, A. B., Korinek, V., Barker, N., Clevers, H., Vogelstein, B., and Kinzler, K. W. (1997). Activation of beta-catenin-Tcf signaling in colon cancer by mutations in beta-catenin or APC. Science *275*, 1787-1790.

Mutoh, M., Niho, N., Komiya, M., Takahashi, M., Ohtsubo, R., Nakatogawa, K., Ueda, K., Sugimura, T., and Wakabayashi, K. (2008). Plasminogen activator inhibitor-1 (Pai-1) blockers suppress intestinal polyp formation in Min mice. Carcinogenesis *29*, 824-829.

Naugler, W. E., Sakurai, T., Kim, S., Maeda, S., Kim, K., Elsharkawy, A. M., and Karin, M. (2007). Gender disparity in liver cancer due to sex differences in MyD88-dependent IL-6 production. Science *317*, 121-124.

Neufert, C., Becker, C., and Neurath, M. F. (2007). An inducible mouse model of colon carcinogenesis for the analysis of sporadic and inflammation-driven tumor progression. Nature protocols *2*, 1998-2004.

O'Brien, J., Hayder, H., Zayed, Y., and Peng, C. (2018). Overview of MicroRNA Biogenesis, Mechanisms of Actions, and Circulation. Front Endocrinol (Lausanne) *9*, 402.

Okada, N., Lin, C. P., Ribeiro, M. C., Biton, A., Lai, G., He, X., Bu, P., Vogel, H., Jablons, D. M., Keller, A. C.*, et al.* (2014). A positive feedback between p53 and miR-34 miRNAs mediates tumor suppression. Genes Dev *28*, 438-450.

Park, E. Y., Chang, E., Lee, E. J., Lee, H. W., Kang, H. G., Chun, K. H., Woo, Y. M., Kong, H. K., Ko, J. Y., Suzuki, H.*, et al.* (2014). Targeting of miR34a-NOTCH1 axis reduced breast cancer stemness and chemoresistance. Cancer Res *74*, 7573-7582.

Peller, S., and Rotter, V. (2003). TP53 in hematological cancer: low incidence of mutations with significant clinical relevance. Hum Mutat *21*, 277-284.

Peng, Y., and Croce, C. M. (2016). The role of MicroRNAs in human cancer. Signal Transduct Target Ther *1*, 15004.

Placencio, V. R., and DeClerck, Y. A. (2015). Plasminogen Activator Inhibitor-1 in Cancer: Rationale and Insight for Future Therapeutic Testing. Cancer Res *75*, 2969-2974.

Powell, E., Piwnica-Worms, D., and Piwnica-Worms, H. (2014). Contribution of p53 to metastasis. Cancer Discov *4*, 405-414.

Pratt, A. J., and MacRae, I. J. (2009). The RNA-induced silencing complex: a versatile gene-silencing machine. J Biol Chem *284*, 17897-17901.

Putoczki, T. L., Thiem, S., Loving, A., Busuttil, R. A., Wilson, N. J., Ziegler, P. K., Nguyen, P. M., Preaudet, A., Farid, R., Edwards, K. M.*, et al.* (2013). Interleukin-11 is the dominant IL-6 family cytokine during gastrointestinal tumorigenesis and can be targeted therapeutically. Cancer Cell *24*, 257-271.

Rabe, B., Chalaris, A., May, U., Waetzig, G. H., Seegert, D., Williams, A. S., Jones, S. A., Rose-John, S., and Scheller, J. (2008). Transgenic blockade of interleukin 6 transsignaling abrogates inflammation. Blood *111*, 1021-1028.

Reid, G., Kao, S. C., Pavlakis, N., Brahmbhatt, H., MacDiarmid, J., Clarke, S., Boyer, M., and van Zandwijk, N. (2016). Clinical development of TargomiRs, a miRNA mimic-based treatment for patients with recurrent thoracic cancer. Epigenomics *8*, 1079-1085.

Rigby, R. J., Simmons, J. G., Greenhalgh, C. J., Alexander, W. S., and Lund, P. K. (2007). Suppressor of cytokine signaling 3 (SOCS3) limits damage-induced crypt hyper-proliferation and inflammation-associated tumorigenesis in the colon. Oncogene *26*, 4833-4841.

Rivlin, N., Brosh, R., Oren, M., and Rotter, V. (2011). Mutations in the p53 Tumor Suppressor Gene: Important Milestones at the Various Steps of Tumorigenesis. Genes Cancer *2*, 466-474.

Rokavec, M., Li, H., Jiang, L., and Hermeking, H. (2014a). The p53/miR-34 axis in development and disease. J Mol Cell Biol *6*, 214-230.

Rokavec, M., Öner, M. G., Li, H., Jackstadt, R., Jiang, L., Lodygin, D., Kaller, M., Horst, D., Ziegler, P. K., Schwitalla, S.*, et al.* (2014b). IL-6R/STAT3/miR-34a feedback loop promotes EMT-mediated colorectal cancer invasion and metastasis. Journal of Clinical Investigation *124*, 1853-1867.

Rose-John, S. (2018). Interleukin-6 Family Cytokines. Cold Spring Harb Perspect Biol *10*.

Rubin, D. C., Shaker, A., and Levin, M. S. (2012). Chronic intestinal inflammation: inflammatory bowel disease and colitis-associated colon cancer. Front Immunol *3*, 107.

Sablina, A. A., Budanov, A. V., Ilyinskaya, G. V., Agapova, L. S., Kravchenko, J. E., and Chumakov, P. M. (2005). The antioxidant function of the p53 tumor suppressor. Nat Med *11*, 1306-1313.

Saitoh, M., Endo, K., Furuya, S., Minami, M., Fukasawa, A., Imamura, T., and Miyazawa, K. (2016). STAT3 integrates cooperative Ras and TGF-beta signals that induce Snail expression. Oncogene *35*, 1049-1057.

Schaper, F., and Rose-John, S. (2015). Interleukin-6: Biology, signaling and strategies of blockade. Cytokine Growth Factor Rev *26*, 475-487.

Scheller, J., Chalaris, A., Schmidt-Arras, D., and Rose-John, S. (2011). The pro- and anti-inflammatory properties of the cytokine interleukin-6. Biochim Biophys Acta *1813*, 878-888.

Schwitalla, S., Ziegler, P. K., Horst, D., Becker, V., Kerle, I., Begus-Nahrmann, Y., Lechel, A., Rudolph, K. L., Langer, R., Slotta-Huspenina, J.*, et al.* (2013). Loss of p53 in Enterocytes Generates an Inflammatory Microenvironment Enabling Invasion and Lymph Node Metastasis of Carcinogen-Induced Colorectal Tumors. Cancer Cell *23*, 93-106.

Siegel, R. L., Miller, K. D., and Jemal, A. (2018). Cancer statistics, 2018. CA Cancer J Clin *68*, 7-30.

Siemens, H., Jackstadt, R., Hünten, S., Kaller, M., Menssen, A., Götz, U., and Hermeking, H. (2011). miR-34 and SNAIL form a double-negative feedback loop to regulate epithelial-mesenchymal transitions. Cell Cycle *10*, 4256-4271.

Siemens, H., Neumann, J., Jackstadt, R., Mansmann, U., Horst, D., Kirchner, T., and Hermeking, H. (2013). Detection of miR-34a promoter methylation in combination with elevated expression of c-Met and β-catenin predicts distant metastasis of colon cancer. Clinical Cancer Research *19*, 710-720.

Sontheimer, E. J. (2005). Assembly and function of RNA silencing complexes. Nat Rev Mol Cell Biol *6*, 127-138.

Sullivan, N. J., Sasser, A. K., Axel, A. E., Vesuna, F., Raman, V., Ramirez, N., Oberyszyn, T. M., and Hall, B. M. (2009). Interleukin-6 induces an epithelial-mesenchymal transition phenotype in human breast cancer cells. Oncogene *28*, 2940-2947.

Takahashi, M., Nakatsugi, S., Sugimura, T., and Wakabayashi, K. (2000). Frequent mutations of the beta-catenin gene in mouse colon tumors induced by azoxymethane. Carcinogenesis *21*, 1117-1120.

Tanaka, T., Narazaki, M., and Kishimoto, T. (2012). Therapeutic targeting of the interleukin-6 receptor. Annu Rev Pharmacol Toxicol *52*, 199-219.

Toft, N. J., Winton, D. J., Kelly, J., Howard, L. A., Dekker, M., te Riele, H., Arends, M. J., Wyllie, A. H., Margison, G. P., and Clarke, A. R. (1999). Msh2 status modulates both apoptosis and mutation frequency in the murine small intestine. Proc Natl Acad Sci U S A *96*, 3911-3915.

Valastyan, S., and Weinberg, R. A. (2011). Tumor metastasis: molecular insights and evolving paradigms. Cell *147*, 275-292.

Vogelstein, B., and Kinzler, K. W. (1999). Digital PCR. Proc Natl Acad Sci U S A *96*, 9236-9241.

Waldner, M. J., Foersch, S., and Neurath, M. F. (2012). Interleukin-6--a key regulator of colorectal cancer development. Int J Biol Sci *8*, 1248-1253.

Wang, L., Bu, P., Ai, Y., Srinivasan, T., Chen, H. J., Xiang, K., Lipkin, S. M., and Shen, X. (2016). A long non-coding RNA targets microRNA miR-34a to regulate colon cancer stem cell asymmetric division. Elife *5*.

Wang, X., Li, J., Dong, K., Lin, F., Long, M., Ouyang, Y., Wei, J., Chen, X., Weng, Y., He, T., and Zhang, H. (2015). Tumor suppressor miR-34a targets PD-L1 and functions as a potential immunotherapeutic target in acute myeloid leukemia. Cell Signal *27*, 443-452.

West, N. R., McCuaig, S., Franchini, F., and Powrie, F. (2015). Emerging cytokine networks in colorectal cancer. Nat Rev Immunol *15*, 615-629.

Wu, Y., Deng, J., Rychahou, P. G., Qiu, S., Evers, B. M., and Zhou, B. P. (2009). Stabilization of snail by NF-kappaB is required for inflammation-induced cell migration and invasion. Cancer Cell *15*, 416-428.

Yang, S., Li, Y., Gao, J., Zhang, T., Li, S., Luo, A., Chen, H., Ding, F., Wang, X., and Liu, Z. (2013). MicroRNA-34 suppresses breast cancer invasion and metastasis by directly targeting Fra-1. Oncogene *32*, 4294-4303.

Yu, H., Kortylewski, M., and Pardoll, D. (2007). Crosstalk between cancer and immune cells: role of STAT3 in the tumour microenvironment. Nat Rev Immunol *7*, 41-51.

Zheng, X., Carstens, J. L., Kim, J., Scheible, M., Kaye, J., Sugimoto, H., Wu, C. C., LeBleu, V. S., and Kalluri, R. (2015). Epithelial-to-mesenchymal transition is dispensable for metastasis but induces chemoresistance in pancreatic cancer. Nature *527*, 525-530.

9 Supplementary Tables

9.1 50 mRNAs most significantly, positively associated with increased tumor aggressiveness

mRNA	p-value (t-test for trend) [A]	Correl.with tumor agressiveness [B]	Fold change $Mir34a^{\Delta IEC}$ / $Mir34a^{Fl/Fl}$ $Tp53^{Fl/Fl}$	Fold change $Tp53^{\Delta IEC}$ / $Mir34a^{Fl/Fl}$ $Tp53^{Fl/Fl}$	Fold change $Mir34a^{\Delta IEC}$ $Tp53^{\Delta IEC}$ / $Mir34a^{Fl/Fl}$ $Tp53^{Fl/Fl}$	Fold change $Tp53^{\Delta IEC}$ /$Mir34a^{\Delta IEC}$	Fold change $Mir34a^{\Delta IEC}$ $Tp53^{\Delta IEC}$ / $Mir34a^{\Delta IEC}$	Fold change $Mir34a^{\Delta IEC}$ $Tp53^{\Delta IEC}$ / $Tp53^{\Delta IEC}$
RP23-352D14.1	0.00002	0.92500	10.00	9.00	19.00	0.90	1.90	2.11
Ctla2a	0.00002	0.92176	1.77	1.99	4.07	1.13	2.30	2.04
Lrrc8d	0.00002	0.92176	1.16	1.08	1.29	0.93	1.12	1.20
Gm5466	0.00006	0.90327	2.37	2.47	5.23	1.04	2.21	2.12
Gpihbp1	0.00007	0.89801	2.19	2.25	5.56	1.03	2.54	2.47
Egf	0.00011	0.88940	1.60	1.56	1.68	0.98	1.05	1.08
2700062C07Rik	0.00012	0.88763	1.13	1.21	1.40	1.07	1.23	1.15
Cdh5	0.00012	0.88763	2.41	2.16	3.72	0.90	1.54	1.72
Flt1	0.00012	0.88763	1.86	1.54	3.71	0.83	1.99	2.40
Ftsj1	0.00012	0.88763	1.07	1.14	1.48	1.07	1.38	1.30
Scd1	0.00012	0.88763	1.98	1.41	2.74	0.71	1.39	1.95
Sox7	0.00012	0.88763	1.79	2.17	3.76	1.21	2.11	1.74
Ovgp1	0.00019	0.87623	1.12	1.51	2.04	1.35	1.82	1.35
Serpina10	0.00023	0.87074	0.00	0.00	0.00	0.40	2.80	7.00
Gng11	0.00034	0.85977	1.92	1.45	3.11	0.75	1.62	2.15
Gm5913	0.00041	0.85349	2.17	1.86	3.21	0.86	1.48	1.72
Abcf3	0.00041	0.85349	1.08	1.09	1.32	1.01	1.23	1.22
Atp5s	0.00041	0.85349	1.24	1.18	1.51	0.95	1.22	1.28
Eno1	0.00041	0.85349	1.90	1.20	2.15	0.63	1.13	1.79
Hist3h2ba	0.00041	0.85349	1.97	1.81	2.91	0.92	1.48	1.61
Pus7l	0.00041	0.85349	1.33	1.39	1.83	1.05	1.37	1.31
Rars	0.00041	0.85349	1.10	1.27	1.46	1.15	1.32	1.15
Trak2	0.00041	0.85349	1.14	1.14	1.30	1.00	1.14	1.13
AU021092	0.00056	0.84395	1.89	1.18	2.54	0.62	1.34	2.15
Ctla2b	0.00056	0.84395	2.22	2.56	4.00	1.15	1.80	1.57
RP23-415E17.1	0.00068	0.83735	1.36	2.46	3.20	1.81	2.36	1.30
Evc	0.00070	0.83643	1.20	0.93	2.47	0.78	2.06	2.64
Gm14295	0.00070	0.83636	2.68	1.43	20.64	0.53	7.71	14.45
Gm4609	0.00083	0.83028	0.00	0.00	0.00	1.00	2.00	2.00
Slc10a6	0.00086	0.82874	3.00	3.00	8.00	1.00	2.67	2.67
Cfhr3	0.00089	0.82783	1.45	1.36	2.27	0.94	1.56	1.67
Pcdhb7	0.00093	0.82602	2.15	1.77	3.31	0.82	1.54	1.87
Gm13722	0.00098	0.82407	1.33	1.83	40.00	1.38	30.00	21.82
Peg10	0.00099	0.82353	2.40	2.80	4.40	1.17	1.83	1.57
Lingo1	0.00106	0.82103	1.86	3.00	3.71	1.62	2.00	1.24
Pai-1	0.00111	0.81935	1.97	3.34	4.29	1.69	2.17	1.29
9430016H08Rik	0.00111	0.81935	1.09	1.27	1.41	1.17	1.29	1.10
Apobec3	0.00111	0.81935	1.53	1.08	3.81	0.71	2.50	3.53
Fabp4	0.00111	0.81935	1.88	1.40	3.57	0.75	1.90	2.55
Fam132b	0.00111	0.81935	1.17	1.21	1.65	1.04	1.41	1.36
Gm5883	0.00111	0.81935	2.14	2.24	3.10	1.05	1.45	1.38
Hspa4	0.00111	0.81935	0.99	1.06	1.20	1.07	1.21	1.13
Iba57	0.00111	0.81935	1.18	1.24	1.47	1.05	1.24	1.19
Kcnj8	0.00111	0.81935	1.39	2.15	3.02	1.55	2.18	1.41
Msto1	0.00111	0.81935	1.17	1.30	1.77	1.11	1.51	1.36
Plcg2	0.00111	0.81935	1.26	1.07	1.78	0.85	1.41	1.66
Sparcl1	0.00111	0.81935	1.77	1.41	2.44	0.80	1.38	1.74
Tanc2	0.00111	0.81935	1.71	1.20	2.48	0.70	1.45	2.07
Tmem97	0.00111	0.81935	1.50	1.53	1.96	1.02	1.31	1.28
Zscan25	0.00111	0.81935	1.10	1.28	1.52	1.16	1.38	1.19

mRNAs were ranked according to t-test for trend **(A)** based on Spearman correlation **(B)** between mRNA expression as determined by RNA-Seq and genotypes ranked in the order: $Mir34a^{Fl/Fl}/Tp53^{Fl/Fl}$, $Mir34a^{\Delta IEC}$, $Tp53^{\Delta IEC}$, $Mir34a^{\Delta IEC}Tp53^{\Delta IEC}$, since the degree of tumor aggressiveness (tumor number/size/invasiveness) increased in this order. Differential expression between tumors with the 4 different genotypes is indicated in columns 4-10. Fold changes were calculated by dividing normalized RNAseq counts between indicated genotypes.

9.2 50 mRNAs most significantly, negatively associated with increased tumor aggressiveness

mRNA	p-value (t-test for trend) [A]	Correl.with tumor agressiveness [B]	Fold change $Mir34a^{\Delta IEC}$ / $Mir34a^{Fl/Fl}Tp53^{Fl/Fl}$	Fold change $Tp53^{\Delta IEC}$ / $Mir34a^{Fl/Fl}Tp53^{Fl/Fl}$	Fold change $Mir34a^{\Delta IEC}Tp53^{\Delta IEC}$ / $Mir34a^{Fl/Fl}Tp53^{Fl/Fl}$	Fold change $Tp53^{\Delta IEC}$ /$Mir34a^{\Delta IEC}$	Fold change $Mir34a^{\Delta IEC}Tp53^{\Delta IEC}$ / $Mir34a^{\Delta IEC}$	Fold change $Mir34a^{\Delta IEC}Tp53^{\Delta IEC}$ / $Tp53^{\Delta IEC}$
Cyp2d11	0.00002	-0.92300	0.59	0.54	0.14	0.92	0.24	0.26
Acvr1b	0.00002	-0.92176	0.90	0.83	0.58	0.93	0.65	0.70
Aqp8	0.00002	-0.92176	0.51	0.34	0.01	0.67	0.03	0.04
Kcnmb2	0.00008	-0.89629	0.79	0.83	0.59	1.05	0.75	0.72
Mgat4c	0.00009	-0.89416	0.77	0.65	0.26	0.84	0.34	0.41
Clca6	0.00012	-0.88763	0.60	0.26	0.09	0.44	0.14	0.33
Dnal4	0.00012	-0.88763	0.79	0.75	0.60	0.95	0.76	0.80
Ggh	0.00012	-0.88763	0.69	0.53	0.18	0.77	0.26	0.34
H2-Q1	0.00012	-0.88763	0.59	0.53	0.25	0.89	0.43	0.48
Khnyn	0.00012	-0.88763	0.97	0.92	0.58	0.94	0.59	0.63
Lzic	0.00012	-0.88763	0.85	0.73	0.54	0.85	0.63	0.74
Mcl1	0.00012	-0.88763	0.89	0.83	0.62	0.94	0.69	0.74
Siva1	0.00012	-0.88763	0.80	0.85	0.57	1.06	0.72	0.68
Stk35	0.00012	-0.88763	0.95	0.93	0.81	0.99	0.85	0.86
Tmigd1	0.00016	-0.87950	0.45	0.31	0.14	0.68	0.30	0.44
Ube2a	0.00019	-0.87571	0.93	0.78	0.75	0.83	0.81	0.97
Pnldc1	0.00023	-0.86992	0.61	0.53	0.47	0.87	0.77	0.89
Rnf39	0.00027	-0.86594	0.67	0.73	0.31	1.10	0.46	0.42
Srsf4	0.00029	-0.86403	0.90	0.93	0.77	1.03	0.86	0.83
Nlrp9b	0.00029	-0.86403	0.70	0.42	0.31	0.60	0.44	0.74
Lrrc69	0.00041	-0.85373	0.93	0.79	0.68	0.86	0.73	0.85
Agrn	0.00041	-0.85349	0.82	0.77	0.58	0.94	0.71	0.75
BC022687	0.00041	-0.85349	0.83	0.88	0.56	1.06	0.68	0.64
Ces2c	0.00041	-0.85349	0.63	0.56	0.28	0.88	0.44	0.51
Dnase1l1	0.00041	-0.85349	0.85	0.77	0.72	0.91	0.85	0.94
Gnb1	0.00041	-0.85349	0.93	0.90	0.80	0.97	0.86	0.89
Grm8	0.00041	-0.85349	0.73	0.64	0.16	0.88	0.22	0.25
Mboat1	0.00041	-0.85349	0.76	0.88	0.34	1.15	0.45	0.39
Mfsd7a	0.00041	-0.85349	0.70	0.51	0.20	0.73	0.28	0.39
Mtfr1l	0.00041	-0.85349	0.83	0.86	0.63	1.04	0.77	0.74
Nmnat1	0.00041	-0.85349	0.70	0.67	0.52	0.95	0.75	0.79
Rab3b	0.00041	-0.85349	0.51	0.33	0.15	0.65	0.28	0.44
Rassf3	0.00041	-0.85349	0.87	0.79	0.63	0.91	0.72	0.80
Rsrp1	0.00041	-0.85349	0.86	0.47	0.39	0.54	0.46	0.84
Smim19	0.00041	-0.85349	0.82	0.86	0.76	1.04	0.92	0.88
Tmem139	0.00041	-0.85349	0.72	0.50	0.29	0.70	0.40	0.58
Ttc22	0.00041	-0.85349	0.85	0.69	0.38	0.81	0.45	0.55
Upk1a	0.00041	-0.85349	0.66	0.32	0.21	0.48	0.32	0.66
Zdhhc1	0.00041	-0.85349	0.81	0.73	0.65	0.90	0.80	0.90
Slc5a12	0.00044	-0.85127	0.87	0.50	0.33	0.58	0.38	0.67
Gm12648	0.00046	-0.84986	0.92	0.67	0.57	0.72	0.61	0.85
D330041H03Rik	0.00049	-0.84782	0.68	0.65	0.54	0.95	0.78	0.83
Cyp2d34	0.00056	-0.84353	0.71	0.65	0.16	0.91	0.23	0.25
Tmem240	0.00068	-0.83735	0.93	0.69	0.34	0.74	0.37	0.50
1700031M16Rik	0.00069	-0.83675	0.54	0.49	0.38	0.90	0.70	0.78
Rbp2	0.00070	-0.83636	0.85	0.39	0.17	0.46	0.20	0.43
RP24-492O4.4	0.00070	-0.83636	0.71	0.77	0.47	1.08	0.67	0.62
Krt27	0.00082	-0.83080	0.29	1.41	0.11	4.83	0.37	0.08
5730422E09Rik	0.00095	-0.82538	0.79	0.76	0.62	0.96	0.78	0.81
Olfr165	0.00095	-0.82535	0.33	0.14	0.02	0.42	0.05	0.13
Cyp2b13	0.00095	-0.82535	0.55	0.48	0.26	0.86	0.47	0.54

mRNAs were ranked according a t-test for trend **(A)** based on Spearman correlation **(B)** between mRNA expression as determined by RNA-Seq and genotypes ranked in the order: $Mir34a^{Fl/Fl}/Tp53^{Fl/Fl}$, $Mir34a^{\Delta IEC}$, $Tp53^{\Delta IEC}$, $Mir34a^{\Delta IEC}Tp53^{\Delta IEC}$, since the degree of tumor aggressiveness (tumor number/size/invasiveness) increased in this order. Differential expression between tumors with the 4 different genotypes is indicated in columns 4-10. Fold changes were calculated by dividing normalized RNAseq counts between indicated genotypes.

9.3 List of up-regulated mRNAs in *Mir34a*$^{\Delta IEC}$ and/or *Tp53*$^{\Delta IEC}$- deficient colonic tumors enriched in the Hallmark Myc targets V2 gene set

Hallmark Myc Targets V2			
mRNA	Description	p-value [A]	Correlation [B]
TMEM97	transmembrane protein 97	0.00111	0.81935
FARSA	phenylalanyl-tRNA synthetase, alpha subunit	0.00869	0.71693
WDR74	WD repeat domain 74	0.00869	0.71693
LAS1L	LAS1-like (S. cerevisiae)	0.00869	0.71693
AIMP2	aminoacyl tRNA synthetase complex-interacting multifunctional protein 2	0.01440	0.68279
DDX18	DEAD (Asp-Glu-Ala-Asp) box polypeptide 18	0.01440	0.68279
SLC19A1	solute carrier family 19 (folate transporter), member 1	0.01440	0.68279
IMP4	IMP4, U3 small nucleolar ribonucleoprotein, homolog (yeast)	0.01440	0.68279
RRP9	ribosomal RNA processing 9, small subunit (SSU) processome component, homolog (yeast)	0.02250	0.64865
PA2G4	proliferation-associated 2G4, 38kDa	0.02250	0.64865
MYBBP1A	MYB binding protein (P160) 1a	0.02250	0.64865
RCL1	RNA terminal phosphate cyclase-like 1	0.02250	0.64865
SRM	spermidine synthase	0.03349	0.61451
NOC4L	nucleolar complex associated 4 homolog (S. cerevisiae)	0.03349	0.61451
RRP12	ribosomal RNA processing 12 homolog (S. cerevisiae)	0.04788	0.58037
NOP2	NOP2 nucleolar protein homolog (yeast)	0.04788	0.58037
SUPV3L1	suppressor of var1, 3-like 1 (S. cerevisiae)	0.04788	0.58037
NIP7	nuclear import 7 homolog (S. cerevisiae)	0.04788	0.58037
IPO4	importin 4	0.04788	0.58037
GRWD1	glutamate-rich WD repeat containing 1	0.04788	0.58037

mRNAs were ranked according a t-test for trend **(A)** based on Spearman correlation **(B)** between mRNA expression as determined by RNA-Seq and genotypes ranked in the order: *Mir34a*$^{Fl/Fl}$/*Tp53*$^{Fl/Fl}$, *Mir34a*$^{\Delta IEC}$, *Tp53*$^{\Delta IEC}$, *Mir34a*$^{\Delta IEC}$*Tp53*$^{\Delta IEC}$, since the degree of tumor aggressiveness (tumor number/size/invasiveness) increased in this order.

9.4 List of up-regulated mRNAs in *Mir34a*$^{\Delta IEC}$ and/or *Tp53*$^{\Delta IEC}$- deficient colonic tumors enriched in the Hallmark Myc targets V1 gene set

Hallmark Myc Targets V1			
mRNA	Description	p-value [A]	Correlation [B]
HDDC2	HD domain containing 2	0.00487	0.75107
ABCE1	ATP-binding cassette, sub-family E (OABP), member 1	0.00869	0.71693
SF3A1	splicing factor 3a, subunit 1, 120kDa	0.00869	0.71693
PRPF31	PRP31 pre-mRNA processing factor 31 homolog (S. cerevisiae)	0.00869	0.71693
CCT3	chaperonin containing TCP1, subunit 3 (gamma)	0.00869	0.71693
AIMP2	aminoacyl tRNA synthetase complex-interacting multifunctional protein 2	0.01440	0.68279
DDX18	DEAD (Asp-Glu-Ala-Asp) box polypeptide 18	0.01440	0.68279
PWP1	PWP1 homolog (S. cerevisiae)	0.01440	0.68279
EIF3B	eukaryotic translation initiation factor 3, subunit B	0.01440	0.68279
NME1	non-metastatic cells 1, protein (NM23A) expressed in	0.01764	0.66780
RRP9	ribosomal RNA processing 9, small subunit (SSU) processome component, homolog (yeast)	0.02250	0.64865
PA2G4	proliferation-associated 2G4, 38kDa	0.02250	0.64865
SRM	spermidine synthase	0.03349	0.61451
G3BP1	GTPase activating protein (SH3 domain) binding protein 1	0.03349	0.61451
EIF1AX	eukaryotic translation initiation factor 1A, X-linked	0.03349	0.61451
CCT5	chaperonin containing TCP1, subunit 5 (epsilon)	0.03349	0.61451
ILF2	interleukin enhancer binding factor 2, 45kDa	0.03349	0.61451
TCP1	t-complex 1	0.03349	0.61451
TUFM	Tu translation elongation factor, mitochondrial	0.03349	0.61451
EIF3D	eukaryotic translation initiation factor 3, subunit D	0.04788	0.58037
KARS	lysyl-tRNA synthetase	0.04788	0.58037
EIF4A1	eukaryotic translation initiation factor 4A1	0.04788	0.58037
GSPT1	G1 to S phase transition 1	0.04788	0.58037
POLD2	polymerase (DNA directed), delta 2, regulatory subunit 50kDa	0.04788	0.58037
PSMB2	proteasome (prosome, macropain) subunit, beta type, 2	0.04788	0.58037
FBL	fibrillarin	0.04788	0.58037
UBE2L3	ubiquitin-conjugating enzyme E2L 3	0.04788	0.58037
CAD	carbamoyl-phosphate synthetase 2, aspartate transcarbamylase, and dihydroorotase	0.04788	0.58037

mRNAs were ranked according a t-test for trend **(A)** based on Spearman correlation **(B)** between mRNA expression as determined by RNA-Seq and genotypes ranked in the order: *Mir34a*$^{Fl/Fl}$/*Tp53*$^{Fl/Fl}$, *Mir34a*$^{\Delta IEC}$, *Tp53*$^{\Delta IEC}$, *Mir34a*$^{\Delta IEC}$*Tp53*$^{\Delta IEC}$, since the degree of tumor aggressiveness (tumor number/size/invasiveness) increased in this order.

9.5 List of up-regulated mRNAs in *Mir34a*$^{\Delta IEC}$ and/or *Tp53*$^{\Delta IEC}$- deficient colonic tumors enriched in the Hallmark Hypoxia gene set

Hallmark Hypoxia			
mRNA	Description	p-value [A]	Correlation [B]
ENO1	enolase 1, (alpha)	0.00041	0.85349
PAI-1	plasminogen activator inhibitor 1	0.00111	0.81935
GAA	glucosidase, alpha; acid	0.00247	0.78544
CAV1	caveolin 1, caveolae protein, 22kDa	0.00248	0.78521
PYGM	phosphorylase, glycogen, muscle	0.00866	0.71714
TGM2	transglutaminase 2 (C polypeptide, protein-glutamine-gamma-glutamyltransferase)	0.00869	0.71693
CTGF	connective tissue growth factor	0.00869	0.71693
LOX	lysyl oxidase	0.00869	0.71693
CP	ceruloplasmin (ferroxidase)	0.00869	0.71693
IGFBP3	insulin-like growth factor binding protein 3	0.01440	0.68279
TPI1	triosephosphate isomerase 1	0.01440	0.68279
IL6	interleukin 6 (interferon, beta 2)	0.01440	0.68279
ETS1	v-ets erythroblastosis virus E26 oncogene homolog 1 (avian)	0.01440	0.68279
GRHPR	glyoxylate reductase/hydroxypyruvate reductase	0.01440	0.68279
ALDOC	aldolase C, fructose-bisphosphate	0.01440	0.68279
CHST3	carbohydrate (chondroitin 6) sulfotransferase 3	0.02250	0.64865
GAPDH	glyceraldehyde-3-phosphate dehydrogenase	0.03349	0.61451
PFKFB3	6-phosphofructo-2-kinase/fructose-2,6-biphosphatase 3	0.03349	0.61451
ATP7A	ATPase, Cu++ transporting, alpha polypeptide	0.03349	0.61451
ANGPTL4	angiopoietin-like 4	0.04208	0.59312
PGM1	phosphoglucomutase 1	0.04788	0.58037
SCARB1	scavenger receptor class B, member 1	0.04788	0.58037

mRNAs were ranked according a t-test for trend **(A)** based on Spearman correlation **(B)** between mRNA expression as determined by RNA-Seq and genotypes ranked in the order: *Mir34a*$^{Fl/Fl}$/*Tp53*$^{Fl/Fl}$, *Mir34a*$^{\Delta IEC}$, *Tp53*$^{\Delta IEC}$, *Mir34a*$^{\Delta IEC}$*Tp53*$^{\Delta IEC}$, since the degree of tumor aggressiveness (tumor number/size/invasiveness) increased in this order.

9.6 List of up-regulated mRNAs in *Mir34a*$^{\Delta IEC}$ and/or *Tp53*$^{\Delta IEC}$- deficient colonic tumors enriched in the Hallmark Epithelial Mesenchymal Transition gene set

Hallmark Epithelial Mesenchymal Transition			
mRNA	Description	p-value [A]	Correlation [B]
PAI-1	plasminogen activator inhibitor 1	0.00111	0.81935
TFPI2	tissue factor pathway inhibitor 2	0.00248	0.78521
MEST	mesoderm specific transcript homolog (mouse)	0.00487	0.75107
PRRX1	paired related homeobox 1	0.00866	0.71714
TGM2	transglutaminase 2 (C polypeptide, protein-glutamine-gamma-glutamyltransferase)	0.00869	0.71693
CTGF	connective tissue growth factor	0.00869	0.71693
LOX	lysyl oxidase	0.00869	0.71693
IGFBP3	insulin-like growth factor binding protein 3	0.01440	0.68279
CD44	CD44 molecule (Indian blood group)	0.01440	0.68279
IL6	interleukin 6 (interferon, beta 2)	0.01440	0.68279
NOTCH2	notch 2	0.01440	0.68279
PLOD2	procollagen-lysine, 2-oxoglutarate 5-dioxygenase 2	0.01527	0.67857
MMP14	matrix metallopeptidase 14 (membrane-inserted)	0.02250	0.64865
COL4A1	collagen, type IV, alpha 1	0.02250	0.64865
TNFRSF11B	tumor necrosis factor receptor superfamily, member 11b	0.02250	0.64865
RGS4	regulator of G-protein signaling 4	0.02250	0.64865
FBN2	fibrillin 2	0.02250	0.64865
MMP3	matrix metallopeptidase 3 (stromelysin 1, progelatinase)	0.03827	0.60218
CXCL12	chemokine (C-X-C motif) ligand 12	0.04788	0.58037
COL4A2	collagen, type IV, alpha 2	0.04788	0.58037
COL5A3	collagen, type V, alpha 3	0.04788	0.58037

mRNAs were ranked according a t-test for trend **(A)** based on Spearman correlation **(B)** between mRNA expression as determined by RNA-Seq and genotypes ranked in the order: *Mir34a*$^{Fl/Fl}$/*Tp53*$^{Fl/Fl}$, *Mir34a*$^{\Delta IEC}$, *Tp53*$^{\Delta IEC}$, *Mir34a*$^{\Delta IEC}$*Tp53*$^{\Delta IEC}$, since the degree of tumor aggressiveness (tumor number/size/invasiveness) increased in this order.

9.7 List of up-regulated mRNAs in *Mir34a*$^{\Delta IEC}$ and/or *Tp53*$^{\Delta IEC}$- deficient colonic tumors enriched in the Hallmark Inflammatory Response gene set

Hallmark Inflammatory Response			
mRNA	Description	p-value [A]	Correlation [B]
PAI-1	plasminogen activator inhibitor 1	0.00111	0.81935
TNFRSF9	tumor necrosis factor receptor superfamily, member 9	0.00433	0.75746
SLC28A2	solute carrier family 28 (sodium-coupled nucleoside transporter), member 2	0.00672	0.73272
CCL5	chemokine (C-C motif) ligand 5	0.00690	0.73110
IL6	interleukin 6 (interferon, beta 2)	0.01440	0.68279
PROK2	prokineticin 2	0.02123	0.65332
MMP14	matrix metallopeptidase 14 (membrane-inserted)	0.02250	0.64865
SLC11A2	solute carrier family 11 (proton-coupled divalent metal ion transporters), member 2	0.02250	0.64865
CSF3	colony stimulating factor 3 (granulocyte)	0.02616	0.63617
SELL	selectin L	0.02616	0.63617
CXCL9	chemokine (C-X-C motif) ligand 9	0.03030	0.62348
FPR1	formyl peptide receptor 1	0.03827	0.60218
GP1BA	glycoprotein Ib (platelet), alpha polypeptide	0.04780	0.58054
IL18RAP	interleukin 18 receptor accessory protein	0.04788	0.58037
CCL20	chemokine (C-C motif) ligand 20	0.04788	0.58037
CD14	CD14 molecule	0.04788	0.58037
MARCO	macrophage receptor with collagenous structure	0.04788	0.58037
SLC7A2	solute carrier family 7 (cationic amino acid transporter, y+ system), member 2	0.04949	0.57702

mRNAs were ranked according a t-test for trend **(A)** based on Spearman correlation **(B)** between mRNA expression as determined by RNA-Seq and genotypes ranked in the order: *Mir34a*$^{Fl/Fl}$/*Tp53*$^{Fl/Fl}$, *Mir34a*$^{\Delta IEC}$, *Tp53*$^{\Delta IEC}$, *Mir34a*$^{\Delta IEC}$*Tp53*$^{\Delta IEC}$, since the degree of tumor aggressiveness (tumor number/size/invasiveness) increased in this order.

10 Acknowledgment

First of all, I would like to thank Prof. Heiko Hermeking for providing this research position in which I have found plenty of opportunity to develop my technical skills, my theoretical background on various subjects and my scientific approach to different issues. He helped me a lot to be able to look subjects from different angles, in developing skeptic-thinking abilities and in finding way out when I was hindered by certain experimentation. The experience I gained from his supervision will be one of the most powerful earnings to build up my future academic career. For this reason and many others, it was a great pleasure for me to have the chance to perform research together with him.

I am also grateful to Prof. David Horst for his collaboration for the human cohort samples and his help, guidance through their analysis. I also would like to thank Dr. Peter Jung for his ideas, discussions and support through my study.

I am especially thankful to Dr. Matjaz Rokavec for his guidance in the lab especially when I started in this group and his help, support, collaboration for the bioinformatics analysis of my projects. I also appreciate for his trustful friendship through the years. I also acknowledge to Dr. Markus Kaller for his initial support with the bioinformatics and to Dr. Nassim Bouznad for providing me his samples and his friendly advices.

My other lab mates Dr. Markus Winter, Xiaolong Shi, Dr. Winny, Dr. Longchang Jiang, I am also thankful for your help and good times in the lab. I especially thank our “all-in-one” technician Ursula Götz for her golden heart, her support and countless help in the lab.

Very special thanks to Paul Ziegler and Dr. Tiago De Oliveira for teaching me all the experimental methods with mice, answering all my questions and for being there.

Besides, I would like to thank my dear friends Dr. Çigdem Atay, Marina Schmidt and Dr. Cira Garcia De Durango and for their help, support and faith. Also thanks to members of “girls club” who cheered up the lunch time and coffee breaks.

I would like to thank my family for their eternal love, support and encouragement. Especially I am so grateful to my dear husband Paul Ziegler who always for his encouragement, support and love.